Experimental modelling of lateral loads on large diameter mono-pile foundations in sand

Master of Science Thesis

by
Etienne A. Alderlieste

April 2011

Version: final

Experimental modelling of lateral loads on large diameter mono-pile foundations in sand

For obtaining the degree of M.Sc. in Civil Engineering at Delft University of Technology

by
Etienne A. Alderlieste

1313169

April 2011

Delft University of Technology
Faculty of Civil Engineering & Geosciences
Department of Geotechnical Engineering

Personal information:

Author	:	Etienne A. Alderlieste
Electronic mail	:	e.a.alderlieste@student.tudelft.nl etienne@alderlieste.org

Committee members:

Delft University of Technology, Geotechnical Engineering

Professor	:	Prof. ir. A.F. van Tol (chairman)
Supervisors	:	Dr. ir. W. Broere
	:	Dr. ir. J. Dijkstra
	:	Dr. ir. O. Heeres

Delft University of Technology, Offshore Engineering

Supervisor	:	Prof. ir. C.A. Willemse, MBA

Deltares

Supervisor	:	Ir. H.J. Luger

Gemeentewerken Rotterdam

Supervisor	:	Ing. H. Brassinga

General information:

Postal Address	:	Delft University of Technology Geo-Engineering Section P.O. Box 5048 2600 GA Delft The Netherlands
Telephone	:	(+31) 010-2182270 (+31) 015-2781880 (secretary)
Telefax	:	(+31) 015-2783328

Abstract

The last years several offshore wind farms have been completed. Such farms typically consist of a few dozen wind turbines. The majority of these wind turbines is founded on mono-piles with a diameter of 4–5 m and is designed according to standards that use the p-y method for lateral loading conditions. However, this p-y method is not validated for such diameter piles. Full-scale field tests and model pile tests with properly scaled stress conditions subjected to lateral loads are scarce.

This Thesis investigates the effect of a diameter increase on the lateral bearing capacity of 2.2 m and 4.4 m diameter mono-piles in dry sand. Static displacement controlled and one-way cyclic force controlled model pile load tests were performed using the Delft University of Technology geotechnical centrifuge.

Results show that the smaller 2.2 m diameter pile has a lower secant and tangent soil-pile stiffness when compared to the 4.4 m diameter pile. In all cases the tangent stiffness is about 50% higher than the secant stiffness. Also, a force acting higher above soil surface yields a lower initial system stiffness. Results furthermore show that an increase in pile diameter with a constant slenderness or L/D-ratio, relative density I_d and load excentricity e, leads to a significant increase in static lateral capacity. The secant and tangent stiffness also significantly increase with increasing diameter.

The accumulation of lateral pile displacements as function of the number of applied one-way cyclic lateral loads has been investigated using 500 force controlled cycles. For an increasing number of load cycles the pile head displacements increase whilst the rate of accumulation decreases. However, additional loading cycles, up to e.g. 100000, are recommended.

For static loading conditions experimental results have been compared to the default API formulation for laterally loaded piles. This default formulation shows a significant overestimation of the initial stiffness. However, after incorporating a stress dependent secant stiffness E_{50}, which has been derived from triaxial compression tests on model sand, good agreement is found between the experimental results and the modified API formulation for pile displacements $<0.1D$. For displacements of about 0.05D the modified p-y method underestimates the lateral bearing capacity of the 4.4 m diameter pile by up to 25

Further research with loading conditions that mimic field loading conditions and a sample with a higher initial density are recommended. It is also recommended to improve the current set-up using better load control and a larger strongbox and to perform additional model pile tests on saturated samples.

Samenvatting

De laatste jaren zijn er verschillende offshore windmolen parken voltooid. De windmolens van deze parken worden meestal gefundeerd op holle stalen buispalen met een diameter van 4–5 m, welke worden ontworpen aan de hand van standaarden die de zogeheten p-y methode hanteren voor laterale belastingscondities. Echter, deze p-y methode is niet gevalideerd voor palen met deze diameter afmeting. Verder zijn veld proeven en modelpaal proeven met correct geschaalde spanningscondities en laterale belastingen schaars.

Deze Thesis onderzoekt het effect van een diameter toename op de laterale grond draagkracht van 2.2 m en 4.4 m diameter monopalen met een constant lengte/diameter ratio in droog zand. Verplaatsingsgestuurde statische en krachtgestuurde enkelzijdig belaste cyclisch modelpaal proeven zijn uitgevoerd gebruik makende van de Technische Universiteit Delft geotechnische centrifuge.

De resultaten laten zien dat de kleinere 2.2 m diameter paal een lagere secant en tangent stijfheid heeft in vergelijking tot de 4.4 m diameter paal. In alle proeven is de tangent stijfheid ongeveer 50% hoger dan de secant stijfheid en een toename van belastingsexcentriciteit leidt tot een reductie van de grond-paal stijfheid. Verder is gevonden dat bij een constant lengte/diameter ratio van de paal, gelijke relatieve dichtheid van de grond en ongewijzigde belastingsexcentriciteit, een diameter toename van de paal leidt tot een significante toename van de laterale capaciteit voor cyclische belaste model palen. Ook de secant en tangent stijfheid nemen aanzienlijk toe wanneer de paal diameter toeneemt.

De accumulatie van de horizontale paal verplaatsingen als functie van het aantal opgelegde enkelzijdige belastingen is onderzocht voor 500 belastingscycli. Een toename van aantal belastingen leidt tot een toename van de paal verplaatsing, terwijl het increment van de verplaatsing afneemt. Een aanzienlijk groter aantal belastingswisselingen is aanbevolen, bijvoorbeeld 100000.

De resultaten van de statische model paal proeven zijn vergeleken met een veelgebruikte ontwerprichtlijn, namelijk de p-y methode. Gebruik van de standaard waarden zoals voorgeschreven door de API voor een bepaalde hoek van inwendige wrijving en relatieve dichtheid van de grond leidt tot een aanzienlijke overschatting van de initiële stijfheid. Wanneer daarentegen een spanningsafhankelijke secant stijfheid E_{50}, welke afkomstig is van triaxiaal compressie proeven, wordt gebruikt, wordt een acceptabele overeenkomst tussen p-y methode en experimentele resultaten gevonden voor paal verplaatsingen $<0.1D$.

Vervolg onderzoek met belastingscondities die de offshore condities beter representeren en een hogere relatieve dichtheid van het grondpakket worden aanbevolen. Verder wordt aanbevolen de huidige experimentele configuratie, met name de belastingsregulering, te verbeteren en vervolg modelpaal proeven te doen op verzadigde grond en in een grote bak.

Those who sacrifice liberty for security, deserve neither.

Benjamin Franklin

Contents

List of Figures

List of Tables

Abbreviations and Symbols

Abbreviations

API	American Petroleum Institute
BEF	Beam on Elastic Foundation
BSI	British Standard Institution
CPT	Cone Penetration Test(s)
DNV	*Det Norske Veritas*
DSS	Direct Simple Shear
DUT	Delft University of Technology
FE	Finite Element
FEA	Finite Element Analysis
FEM	Finite Element Method
GL	*Germanischer Lloyd*
JGS	Japanese Geotechnical Society
MP	Mega Pixel
NEN	*Nederlands Normalisatie-instituut*
OWEZ	Offshore Wind farm *Egmond aan Zee*
SSD	Solid State Disk
SW(-model)	Soil-Wedge (model)
TC	Triaxial Compression
TE	Triaxial Extension
WEC(s)	Wind Energy Convertor(s)

Symbols

A	Factor to account for loading type	[-]
	Area	[m^2]
a	Acceleration	[$m\,s^{-2}$]
b	Pile width perpendicular to loading direction	[m]
C_1	Constant	[-]
C_2	Constant	[-]
C_3	Constant	[-]
c_u	Uniformity coefficient	[-]
D	Diameter	[m]
D_l	Diameter of the large 27.36 mm model pile	[m]
D_s	Diameter of the small 13.68 mm model pile	[m]
D_{10}	10% smallest particle size	[μm]
D_{50}	50% smallest particle size	[μm]
D_{60}	60% smallest particle size	[μm]
D_p	Prototype scale pile diameter	[m]
E	Young's modulus (or elasticity modulus)	[$kN\,m^{-2}$]
E_{50}	Secant stiffness at 50% of the peak load	[kN m]
E_{sec}	Secant stiffness	[kN m]
E_{tan}	Tangent stiffness	[kN m]
EA	Axial stiffness	[kN]
EI	Flexural stiffness	[$kN\,m^2$]
e	Void ratio	[-]
	Excentricity of applied load	[m]
F	Force	[kN]
F_{bc}	Total axial bearing capacity	[kN]
$F_{bc,shaft}$	Axial shaft bearing capacity	[kN]
$F_{bc,tip}$	Axial tip bearing capacity	[kN]
F_h	Force (horizontal)	[kN]
$F_{r,1}$	Passive soil resistance	[kN]
$F_{r,2}$	Passive soil resistance	[kN]
F_v	Force (vertical)	[kN]
f	Frequency	[Hz]
g	Gravitational acceleration	[$m\,s^{-2}$]
I	Moment of inertia	[m^4]
I_d	(Initial) relative density	[%]
k	Soil resistance	[$kN\,m^{-3}$]
K_0	Lateral earth pressure coefficient	[-]
L	Length	[m]
L_{emb}	Embedded length	[m]
L_p	Prototype embedded pile length	[m]
M_b	Bending moment	[kNm]
M_t	Torsional moment	[kNm]
m	Mass	[kg]

n	Porosity	[-]
p	Soil resistance	[kN m^{-1}]
p_{ult}	Ultimate bearing capacity	[kN]
p_{ud}	Lateral soil resistance, deep	[kN m^{-1}]
p_{us}	Lateral soil resistance, shallow	[kN m^{-1}]
r	Radius	[m]
t	Wall thickness	[m]
	Time	[s]
V	Volume	[m^3]
V_{pores}	Volume of pores	[cm^3]
V_{solid}	Volume of solids	[cm^3]
V_{total}	Total volume ($= V_{pores} + V_{solid}$)	[cm^3]
v	Velocity	[m s^{-1}]
y	Deflection	[m]
z	Depth	[m]
γ	Specific weight	[kN m^{-3}]
ε	Strain	[%]
φ	Angle of internal friction	[°]
ω	Angular velocity	[rad s^{-1}]
σ	Stress	[kN m^{-2}]
σ_1	Principal stress direction	[kN m^{-2}]
σ_3	Secondary stress direction	[kN m^{-2}]

Chapter 1

Introduction

1.1 Offshore wind energy

In Western Europe the amount of energy generated from renewable sources such as wind and solar energy increased dramatically over the last decade, e.g. [89; 96; 97]. For wind energy this results from an increased number of installed wind energy convertors (WECs) or wind turbines at onshore as well as offshore locations. The main components of WECs are shown in Figure 1.1. Several WECs together form a so-called wind farm. In comparison to onshore, offshore sites offer favourable wind conditions as well as limited regulations, for instance for noise produced during installation and operation.

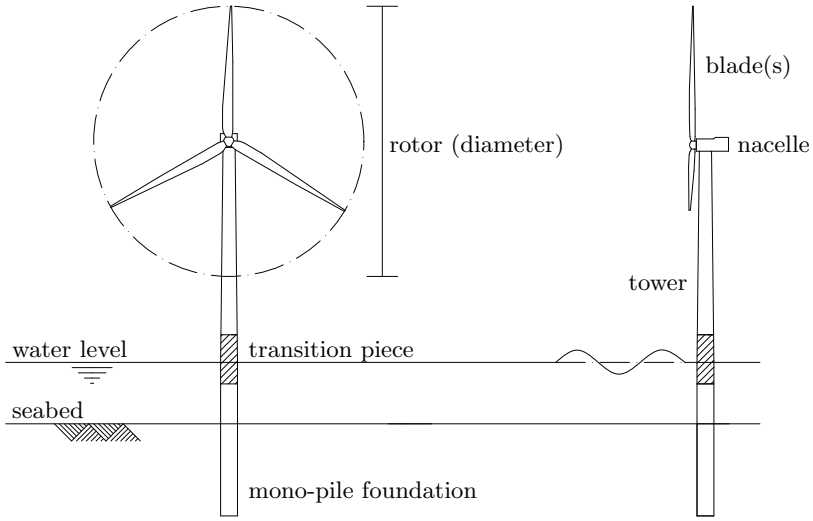

Figure 1.1 Main wind turbine components

In the coming decade more turbines will be installed offshore. The Dutch government has planned a total installed generator capacity of 6000 MW for offshore sites in year 2020 [4]. Currently (2011), the total capacity is only about 200 MW. In several other countries next to the North Sea (e.g. the United Kingdom, Belgium, Denmark and Germany) new

offshore wind farms will also be constructed. Wind farms require large areas, O(40 km^2), and may not block shipping routes. Also, free space close to shore is limited. Large areas of the North Sea are characterized by sandy soil conditions and a limited water depth. This limited water depth allows for the construction of offshore wind farms further offshore.

Offshore generator capacity trails onshore generator capacity. In November 2010 a 7.5 MW turbine has been installed onshore in Germany by Enercon [30] whilst 5 MW turbines are installed offshore at the Beatrice wind farm in Scotland. The Offshore Prinses Amalia wind farm [64] consist of 60 Vestas V80-2.0 MW turbines that are founded on 4.0 m mono-piles. The water depth is 19–24 m and the total power output is 120 MW. This wind farm was completed in 2007 and became operational in 2008. Offshore Wind farm *Egmond aan Zee* (OWEZ) [98], completed in 2006, consists of 36 Vestas V90-3.0 MW turbines located 10 to 18 km from the Dutch coast. More recently (2009), wind farms are constructed as far as 46–52 km from shore, i.e. the Belwind [13] wind farm, comprising of 55 Vestas V90-3.0 MW turbines situated on Bligh Bank. This farm has been completed in 2010 and is operational. The typical water depth at Belwind and OWEZ sites ranges from 15 to 37 m.

1.2 Wind turbine foundations

Wind turbines can be constructed using several foundation types. Onshore wind turbine towers are commonly bolted to a concrete slab at soil surface level. For soft soil conditions this slab is founded on long slender piles. Offshore foundations not only transfer wind loads, but also marine loads to the subsoil. Possible foundation solutions are shown in Figure 1.2.

A jacket or tripod foundation can be built with a specific wall thickness for different parts of the structure and thus be more optimal by design in terms of stress, strain and material usage compared to a mono-pile. A mono-pile requires a large wall thickness to resist bending moments, but is relatively easy to construct and transport. Compared to jacket or tripod foundations, mono-pile foundations have a limited lateral bearing capacity.

In general the water depth increases further from shore. In water with greater depth higher waves can occur. Higher waves and an increasing height between seabed and water

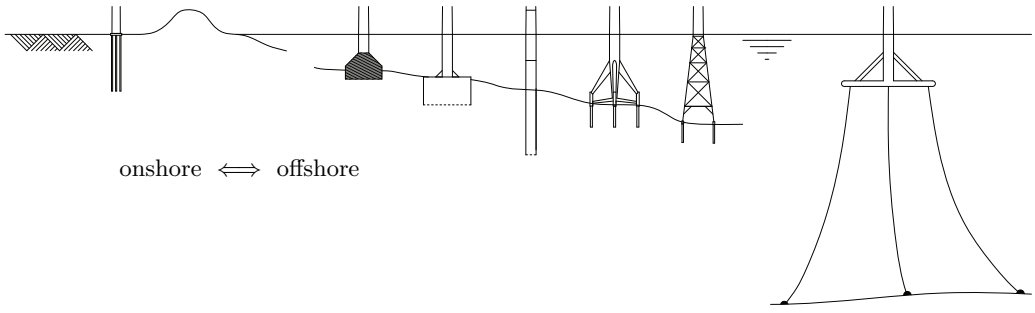

Figure 1.2 Overview of foundation types for wind turbines; from left to right: onshore piled foundation, offshore gravity base, suction caisson, mono-pile, tripod, jacket and floating platform foundation

level, at which the waves are loading the structure, lead to larger marine based loads. Increasing turbine generator capacity generally requires a larger rotor, which leads to higher towers and larger forces acting on the foundation. In order to build wind farms with higher capacity generators further offshore, i.e. with foundations having to cope with increasing lateral and vertical loads, the foundation dimensions have to be adapted. A mono-pile with a larger diameter is the result.

The limited water depth and sandy soil conditions at many sites of the North Sea allow for the construction of mono-pile foundations. An overview of some soil profiles at the OWEZ wind farm is presented in Appendix A. The mono-pile foundation is designed for water depths of less than 30 m. Water depths of 30 – 40 m are considered the transition depth. For water depths >40 m jacket foundations become more economical ([1; 25; 78]). For OWEZ and Belwind wind farms mono-piles with an approximate outside diameter of 4.4 and 5.5 m respectively have been used.

1.3 Mono-pile foundation loads and soil response

Offshore wind turbines are built to last >20 years. During this period the structure is loaded many times, O(10^8), from varying directions and with different magnitude. Marine based loads act at a different height compared to wind based loads and both can load the structure from different angles simultaneously. This large number of loading cycles and the direction of the loads are important for the design of a foundation. When loaded repeatedly the steel structure will show fatigue, i.e. loss of strength. Soil behaviour is also rather sensitive for loading history [3; 48; 65; 66; 84; 93; 94]. Cyclic loading will, therefore, impact soil properties. An overview of the axial load F_v, lateral load F_h and bending and torsional moments, M_b and M_t respectively, acting on the mono-pile foundation is given in Figure 1.3.

In sands an increasing number of load cycles N generally leads to an accumulated displacement or strain at mud line level. However, the effect of the number of cycles N and the load magnitude on the failure mode of the mono-pile is still a research topic. Research investigating the effect of a prescribed force (spectrum) on the rate of displacement accumulation of large diameter mono-piles is scarce.

1.4 Design of large diameter mono-piles

Standards for designing laterally loaded piles, e.g. the American Petroleum Institute (API) [6], Det Norske Veritas (DNV) [26] or Germanischer Lloyd (GL) [34] are based on the p-y curves method [21; 74]. The p-y method describes the non-linear relation between pile deflection y and soil resistance p. With increasing depth z the soil response becomes stiffer. In these codes the soil resistance p depends on the soil type and its properties such as (relative) density and angle of internal friction φ.

Although the p-y method is specifically developed for foundation solutions in the oil and gas sector, it is nevertheless frequently applied for the design of mono-pile foundations with a diameter up to e.g. 5.5 m that are subjected to static and cyclic loading conditions. In this Thesis mono-piles with a diameter >2.0 m are considered *large diameter* mono-piles.

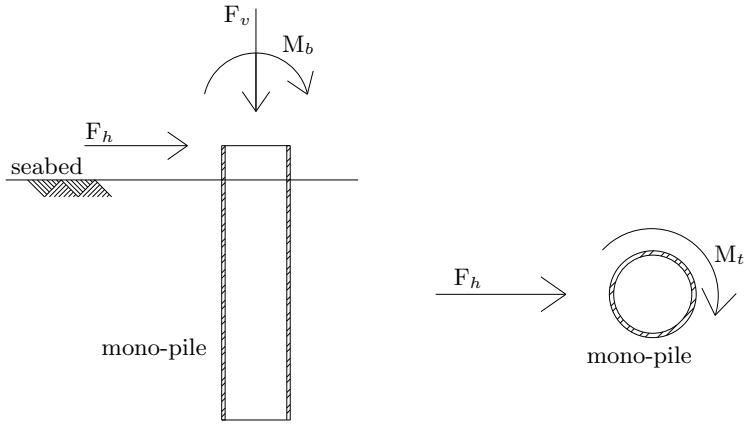

(a) Side view **(b)** Top view

Figure 1.3 Schematic overview of forces (horizontal and vertical) and moments (bending and torsional) acting on a mono-pile foundation

Current large diameter offshore mono-piles have a slenderness ratio or embedded length over outer diameter L/D-ratio of 5 – 7 and are considered to behave rigid. This L/D-ratio differs significantly from the piles from which the p-y method is calibrated (L/D = 34.4) [21; 74]. For large diameter piles the initial soil stiffness response of the pile-soil interaction will be higher compared to slender piles [8; 49; 50; 95] and the p-y method does not explicitly take pile stiffness into account. Therefore, determination of the validity of the p-y method for large diameter piles is necessary.

1.5 Objectives

The current research will investigate soil-pile behaviour for large diameter mono-piles subjected to one-way cyclic lateral loading in medium dense sand with a consistent relative density I_d of approximately 60%. Model pile tests will be performed in a geotechnical centrifuge and referred to as ng tests. Prototype pile diameters of 2.2 m and 4.4 m are examined.

Primary objective:

- Experimental investigation into the accumulation of horizontal displacements for piles with different diameters as function of applied one-way cyclic lateral loading schemes by means of several ng model pile tests.

Secondary objectives:

- Determination of validity of the p-y method for static loading of large diameter steel piles by means of several ng model pile tests.

- Identification of loading conditions and model scaling for ng-tests and determination of physical boundary conditions for model piles.

1.6 Limitations of this research

Field soil and loading conditions cannot be exactly reproduced in scaled down model pile tests. Several aspects are simplified.

- The North Sea subsoil is built-up of multiple saturated soil layers that generally consist of medium dense to dense sand with an I_d of e.g. 70–95%. Layers of clay and peat can be present as well. The model pile tests will be performed in a homogeneous single layer of dry sand with a consistent relative density I_d of 60%. This will result in a lower lateral bearing capacity compared to denser sand.
- Offshore wind turbines are founded in saturated soil. The use of dry sand for model pile tests results in higher effective stresses and will result in a higher lateral bearing capacity.
- Multi-directional loads acting at different positions are simplified as a force acting in one direction and at a single height for each experiment. Geotechnical centrifuge scaling laws dictate that a 0.1 Hz prototype frequency requires a 10 Hz frequency at $100g$. The load frame has a maximum velocity of 0.5 mm/sec. Therefore, for displacements O(mm) the system is not fast enough to mimic field loading frequencies.

1.7 Outline of this Thesis

Chapter 2 presents the background of available methods for calculating lateral bearing capacity and displacements of laterally loaded piles and in particular the p-y method. Field tests, $1g$ and ng experiments as well as the behaviour of soil subjected to cyclic loading will be discussed. In Chapter 3 the (ultimate) lateral load for different prototype pile diameters is calculated for static and cyclic loading conditions with varying load excentricity based on North Sea soil conditions. Scaling laws, model piles, results of laboratory soil experiments and the experimental programme are then presented. The geotechnical centrifuge set-up of Delft University of Technology is introduced and possibilities and limitations of geotechnical centrifuge experiments are discussed. The results of the performed tests and analyses of the results are presented in Chapter 4. The experimental results are then compared to the default and a modified p-y method in Chapter 5. Chapter 6 presents results of analysed field data and compares the field pile displacements at seabed level with model pile test displacements. The concluding Chapter 7 contains a brief summary of objectives and conclusions based on this research and recommendations.

Chapter 2

Laterally Loaded Piles

2.1 Failure of rigid piles

Piles with low slenderness ratios behave more rigid and rotate rather than bend. The centre of rotation is located at a depth of about 0.8 times the embedded pile length L_{emb} [16; 20]. Figure 2.1 shows a schematic pile rotation and corresponding soil resistance distribution. Based on equilibrium of forces (Eq. 2.1) and moments (around the pile toe; Eq. 2.2) the resistance to rotation can be determined [16],

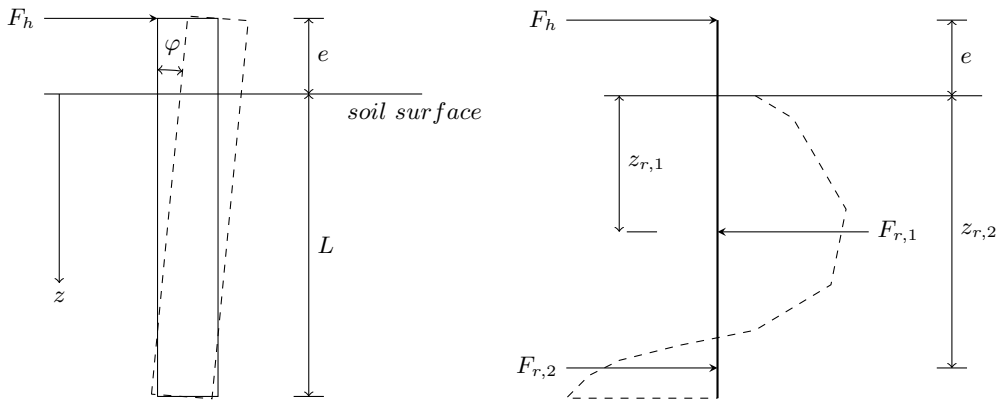

(a) Schematic pile rotation **(b)** Schematic soil resistance

Figure 2.1 Behaviour of laterally loaded rigid pile

$$F_h = F_{r,1} + F_{r,2}, \tag{2.1}$$

$$F_h = \frac{-F_{r,1}\,(L - z_{r,1}) + F_{r,2}\,(L - z_{r,2})}{L + e}. \tag{2.2}$$

When a pile rotates a shear resistance can be mobilized at the pile toe. The presence of this shear resistance is indicated by numerical calculations and it is suggested to be taken into account designing large diameter mono-piles [12; 50]. According to the German design standard GL the rotation of a laterally loaded mono-pile foundation should be minimized in order to guarantee system operation. A maximum pile rotation of 0.5° at mud line is allowed [34]. For a pile with an L/D-ratio of 5 and a diameter of 4.4 m this leads to a deflection restriction of 15.4 cm, i.e. $0.035D$. This standard, however, does not allow a lateral displacement of the pile toe. Satisfying this latter criterion requires deep installed mono-piles, e.g. up to 43 m for pile diameters of 5.0 m (i.e. with an L/D-ratio of 8.6) [3], which would make this type of foundation less economical. An increase in embedded length of a cyclic laterally loaded pile leads to a smaller rate of accumulated displacement and therefore, piles with a higher L/D-ratio can cope better with a large number of cyclic lateral loads [2; 3]. Mono-piles with an L/D-ratio of 5–6 have been installed offshore, which suggests that in practice a small pile toe displacement is nevertheless accepted when designing a laterally loaded mono-pile foundation.

2.2 Design methods for laterally loaded piles

Wind turbine structures are subjected to variable lateral wind and marine loads which lead to bending moments in the tower and mono-pile foundation. Due to the asymmetric 3-bladed shape of the rotor also torsional moments are generated. These lateral loads, bending and torsional moments are transferred to the soil by the mono-pile foundation. The behaviour of mono-pile foundations is a non-linear three-dimensional soil-pile interaction problem. Numerous methods for the analysis of laterally loaded single piles have been created. These methods are generally based on simplifications. A brief overview of 4 different methods is given below.

Elasticity method The elasticity method takes soil continuity into account, but the soil modulus is assumed elastic and varies with stress level [10; 70; 72]. As soil behaviour is more accurately described in a non-linear manner, this method is limited to small strains (i.e. smaller than 1%) and not suitable to determine ultimate lateral pile loads.

Limit state method The limit state method can determine the ultimate lateral pile capacity p_{ult} [19]. This method, also known as Broms' method, assumes a rigid pile and a linear relation between pile diameter and ultimate lateral soil capacity. Finite Element (FE) calculations indicate this limit state method underestimates the p_{ult} for sand [32].

Finite Element Method (FEM) Finite Element Analysis (FEA) is a useful tool capable of modelling soil continuity, nonlinearities, complex pile-soil interaction and 3D boundary conditions. Large diameter mono-piles with typical wall thickness and flexural stiffness embedded in a sandy soil can nowadays be modelled, see e.g. [3; 12; 50]. However, FE analysis is still mainly used for research purposes using simplified soil models. FEA can nevertheless help improve understanding of pile-soil interaction.

Subgrade reaction method This method, which includes the p-y method, is based on a beam on elastic foundation (BEF) and is widely used for its simplicity and reasonable accuracy [16; 57; 75; 87]. The soil resistance is assumed to be linear. The p-y method does take the non-linear relation between load F and pile deflection y into account using so-called p-y curves. This subgrade reaction method is limited by the fact that soil resistance is modelled as a finite number of springs, whilst soil properties should be considered continuous. Also, the horizontal subgrade modulus is a model parameter rather than a fundamental soil property.

The p-y method has been applied for many years and almost all large diameter offshore mono-pile foundation dimensions are based on current design standards [6; 26; 34] which incorporate the p-y method, despite several known limitations and uncertainties. These limitations will be discussed in Section 2.3.

Plans for new wind farms already exist and currently mono-piles are the recommended foundation type. Due to this increase of application of mono-piles for offshore wind farms the research topic of soil resistance-pile deflection (p-y) is revived, especially for application of large diameter piles with low slenderness ratios.

2.3 Details of the p-y method

The p-y method is a method for determining the pile deflection and (ultimate) lateral bearing capacity as result of a lateral load acting on a foundation. Soil resistance is modelled using non-linear springs. The applied force F is related to the lateral pile deflection y by p-y curves. These curves depend on soil type, depth and loading type. At greater depth soil reacts stiffer and a stiffer soil response leads to a steeper curve, see e.g. Figure 2.3. The lateral load F is based on the spring stiffness of the soil k at the corresponding depth and the deflection y,

$$F(z) = k(z) \cdot y(z). \tag{2.3}$$

For sand this p-y method was derived from field tests on Mustang Island (USA) [21; 74]. These field tests consisted of 2 static and 5 cyclic load tests applied to two 0.61 m (24 inch) diameter D piles with wall thickness t of 95 mm (3/8 inch), length L of 21 m (69 feet) and an L/D-ratio of 34.4. The wall thickness over diameter t/D-ratio equated to about 64. Based on the same data it has been concluded that a hyperbolic curve is an improvement over the originally formulated expression [60]. This adapted formulation has been accepted by several design standards e.g. [6; 26; 34]. However, in both variants multiple soil layers and non-constant pile diameters are not accounted for. The soil-wedge (SW) model [9; 62], which is used to predict the response of a laterally loaded flexible pile, does incorporate the pile properties and is able to handle multiple soil layers. For sand the lateral soil resistance versus deflection relationship at depth z is approximated by the expression,

$$p_{us}(z) = (C_1 z + C_2 D)\,\gamma z, \tag{2.4}$$

$$p_{ud}(z) = C_3 D \gamma z. \tag{2.5}$$

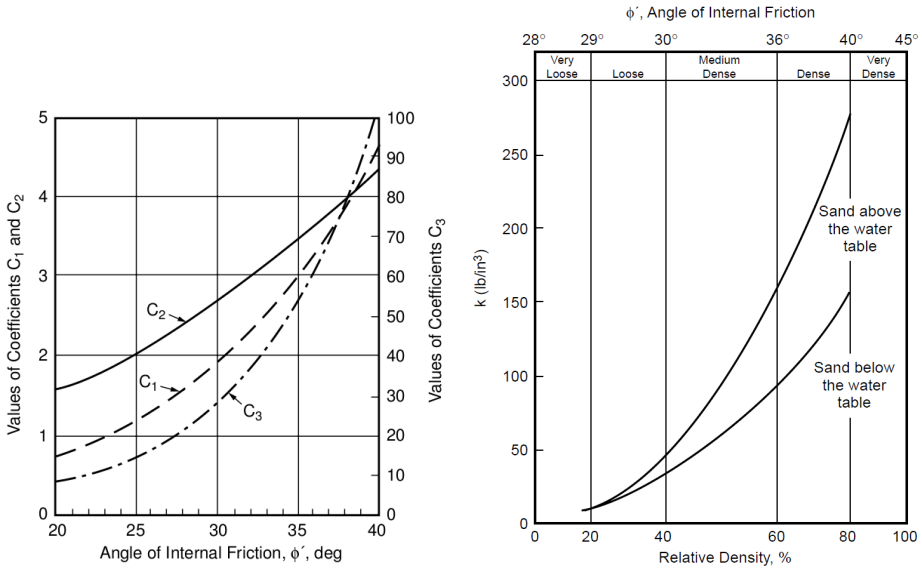

(a) Constants C_1, C_2 and C_3 **(b)** Relative density and friction angle

Figure 2.2 Parameter determination based on soil state [6]

The ultimate lateral resistance p_u (addition s = shallow, d = deep) is based on the effective unit weight γ in kN/m^3, depth below ground surface z in m, pile diameter D in m and the friction angle of the material φ. The C_1, C_2 and C_3 coefficients are determined using Figure 2.2a. The parameter k depends on the internal friction angle (see Figure 2.2b). Multiplying a lb/in^3 value by 276.4 yields kN/m^3 values, i.e. 160 lb/in^3 equals about 44000 kN/m^3. For *deep* foundations there is a linear relation between pile diameter and p_{ud}. The p_{us} is also linearly dependent on the pile diameter D, but increases quadratic with depth z. The minimum value of either p_{us} or p_{ud} serves as input for Eq. 2.6. Several plots presented in Appendix B show p_{us} is decisive for large diameter piles up to 22 m depth. The p-y relationships for sand are non-linear and are approximated by Eq. 2.6. A correction factor A is used to account for loading type, $A(z) = 0.9$ for cyclic and $A(z) = 3.0 - 0.8z/D \geq 0.9$ for static loading. A diameter dependency of A is shown in Appendix B. The $p(z)$ in kN equals the (ultimate) lateral bearing capacity for a given deflection y and is based on the initial modulus of subgrade reaction $k(z)$,

$$p(z) = A \cdot \min\left(p_{us}(z), p_{ud}(z)\right) \tanh\left(\frac{kz}{A \cdot \min\left(p_{us}(z), p_{ud}(z)\right)} y\right). \tag{2.6}$$

The p-y method is known to have several limitations. For instance, this method is only suitable for constant pile diameters installed in single layered soils. Secondly, the pile (flexural) stiffness EI is not taken into account. During driving of a mono-pile the initial stress state and soil density are altered. For example, the ratio between the horizontal and vertical stress component, or the lateral earth pressure coefficient K_0, is likely to change. The API [6] assumes a constant $K_0 = 0.4$. Other values like $K_0 = 1 - \sin\varphi$ have also been used, e.g. [16]. For (medium) dense sand with a φ equal to 37° there is no difference.

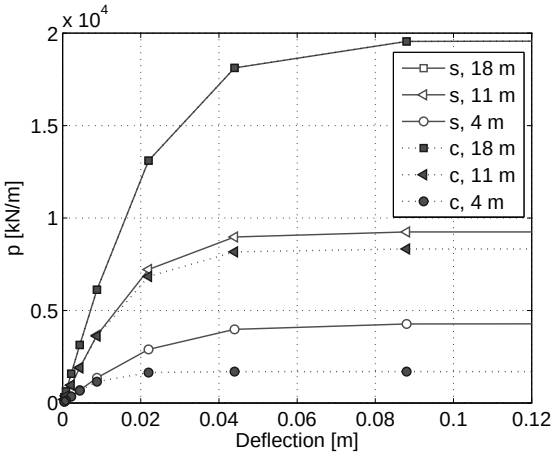

Figure 2.3 Static (s) and cyclic (c) p-y curves for sand at different depths

Numerical calculations show that application of p-y curves probably leads to an overestimation of the stiffness of large diameter mono-piles in sand with respect to horizontal loading. This may lead to insufficient pile design lengths [3; 50; 95]. EI variations of the pile do not significantly influence p-y curves for sand [32]. 3D FEA using linear elastic soil models shows an influence of pile diameter on subgrade reaction modulus [8; 40]. This analysis also states this influence is expected to be negligible as pile stiffness increases with increasing diameter (the pile diameter used is 1.2 m). Non-linear behaviour of soil tends to increase the pile diameter effect in relation to the pile response and standard p-y curves show a tendency to overestimate soil resistance for large diameter piles for weakly cemented sands [8; 40]. In contrast, a linear dependency of pile diameter on soil resistance suggests no diameter dependency [51]. Applicability of the p-y method for large diameter mono-piles therefore requires additional investigation, e.g. into the diameter influence on the lateral bearing capacity.

2.4 Cyclic soil testing

The stress path occurring in the soil adjacent to the mono-pile foundation can be simulated using a triaxial apparatus with triaxial compression (TC) or triaxial extension (TE) or using a direct simple shear (DSS) apparatus (see Figure 2.4). However, the exact stress path formulation remains unknown. Using a DSS apparatus a normal force is applied and the resistance to shear is measured. Although different stress conditions can be simulated, the failure plane is rather fixed. Cyclic loading of sand samples is often done using a triaxial apparatus. Results of several tests are presented in Section 2.4.

For many different engineering situations cyclic soil loading is relevant, e.g. for railways and bridge foundations. From cyclic triaxial tests a strain accumulation rate proportional to the logarithm of the number of cycles N was found [48]. Using load controlled cyclic triaxial tests on gravel and sand at 5 Hz a relation between the strain accumulation rate and N proportional to $1/N$ with parameters c_1 for $N < 1000$ and c_2 for $N > 1000$

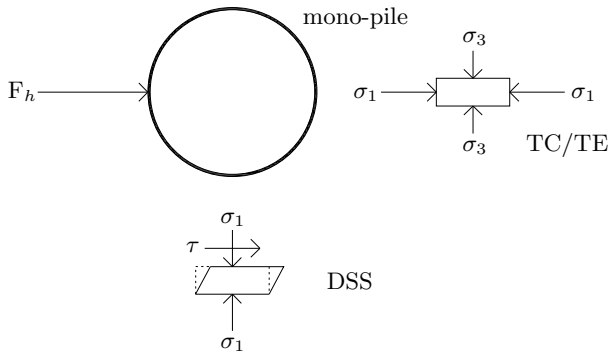

Figure 2.4 Schematic view of laterally loaded mono-pile and soil tests: triaxial compression/extension (TC/TE) and direct (simple) shear (DSS)

and $c_1 > c_2$ was found [85]. A $c_2 > c_1$ was found investigating medium coarse and fine sands using triaxial tests [36]. A near-logarithmic relation for up to 10^4 cycles and an over-proportional logarithmic relation for a larger number of loading cycles N was found using saturated drained triaxial tests and multi-axial direct simple shear tests [93]. Work from latter authors also states the strain accumulation rate is not dependent on the applied frequency (for the tested range of 0.05 – 2 Hz) and there is no significant difference between dry and saturated drained triaxial test results. Soil type and soil density influence the strain accumulation rate, although an increase in number of cycles N leads to an accumulation of displacements nevertheless.

Hettler (Eq. 2.7) performed triaxial tests on dry sand and model pile tests using sand and suggested a relation between displacement for 1 cycle w_1 and the displacement for N cycles w_n depending on a material parameter C_n (for sand equal to approximately 0.2) [37]. Little and Briaud (Eq. 2.8) suggested a power relation based on the number of cycles N [55]. Experimental investigation into the influence of regular and irregular cyclic loading on dry granular material yields a displacement curve versus the logarithmic number of cycles N also according to an N^m relation [66].

$$w_n = w_1 + (1 + C_n \ln N)\,, \tag{2.7}$$

$$w_n = w_1 N^{0.136}. \tag{2.8}$$

Undisturbed fine grained soil samples subjected to cyclic excitations show a reduction of stiffness [65], which corresponds to the p-y method. This contradicts with results showing a stiffness increase with increasing number of loading cycles [42; 53]. Although soil behaviour depends on the stress state and e.g. the followed stress path for triaxial tests with cyclic soil loading, nevertheless the p-y method and other soil-pile related topics require further investigation.

2.5 Pile load tests

Although numerical calculations nowadays are more often applied, validation of analytical design methods or the more advanced FE methods requires reliable field data or proper laboratory data. Only a limited amount of research on (cyclic) laterally loaded mono-piles has been published. Additionally, the number of full-scale field tests on laterally loaded single tubular pipe piles is very limited, as is the diameter of the piles tested (i.e. a maximum of 1.2 m). The number of centrifuge tests conducted on >2 m diameter prototype pipe piles is also limited. Sections 2.5.1, 2.5.2 and 2.5.3 discuss results from laterally loaded pile foundations on field test scale, model pile tests at $1g$ and ng respectively.

2.5.1 Field tests

For laterally loaded single piles in sand overviews of conducted field tests consisting of up to 34 pile tests [54; 56] are given. Besides drilled shafts with L/D-ratios of 3–8 both overviews mainly contain rather slender piles with an L/D-ratio >15 and only a limited number of steel pile tests is presented. In fact, only two field tests conducted on steel pipe piles are presented that already include the test series from which the p-y method is derived [21; 60; 74]. The amount of loading cycles for both tests is 100. In occasional cases in which large diameter piles are tested no particular influence of the diameter is revealed for sandy conditions [76].

Although there are instrumented wind turbines where e.g. accelerations are measured, no full-scale large diameter mono-pile field test with lateral loads up to a prescribed failure criterion are found. However, field data from instrumented offshore wind turbines is available. In Chapter 6 the results of analysed field data will be presented. Model pile tests at $1g$ are affordable and often considered a decent alternative to gain information about soil-pile interaction.

2.5.2 Physical model pile tests at $1g$

To better understand soil-pile interaction, often scaled down model pile tests are performed at $1g$. Such experiments often have (lateral) pile load-displacement analysis as aim. However, $1g$ experiments lack properly scaled pore fluid properties and stress conditions.

Model pile tests on a 90 mm diameter pile with up to 50000 multi-directional lateral loading cycles does not show generation of (excess) pore water pressures [27]. Variation of loading direction leads to 2–3 times the pile head displacement for dense sand compared to unidirectional loading. The importance of two-way loading direction is underlined [45], as waves load a structure in a two-way manner, although mainly unidirectional. Furthermore, tests on a rigid 1:50 scale model pile show one-way cyclic loading increases the soil stiffness and that this increase is not dependent on relative soil density [46]. This is in contradiction with degradation of static p-y curves to account for cyclic loading.

These experiments indicate that lateral loads acting on a foundation from different angles can lead to larger lateral deformations than one-way loading conditions. Further research investigating the soil-pile response, e.g. for a multi-directional loading situation or different pile diameters and with properly scaled soil stresses, is needed to better understand offshore mono-pile behaviour over time.

2.5.3 Physical model pile tests at ng

Another way of modelling soil-pile interaction or other foundation related topics is by means of a geotechnical centrifuge. Using a higher level of acceleration a stress distribution comparable to prototype scale is obtained. Several topics, mainly concerning pile diameter and lateral bearing capacity, are discussed next.

Geotechnical centrifuge experiments on laterally loaded single piles with a prototype diameter of 1.0 m for both static as well as cyclic (100 cycles) loading in dense (90 to 95% relative density) sand show an increase in pile-soil stiffness whilst the conventional p-y method suggests a degradation of soil-pile stiffness [42]. The cyclic loading resulted in an increase of lateral bearing capacity and small variations in initial density only led to small variations of the lateral bearing capacity.

Different $40g$ up to $120g$ centrifuge tests have been performed with 16 mm model piles (i.e. up to 1.9 m prototype scale) to validate p-y curves [11]. Fine sand (D_{50} of 100–120 μm) packed to 80 % relative density has been used. These tests confirm that the p-y method overestimates the initial stiffness and its variation with depth and underestimates the ultimate soil resistance near the pile head.

Model pile tests have been performed in a displacement controlled manner for dynamic (0.8 m/s) and static loading ($1.7{\cdot}10^{-5}$ m/s) of dry and saturated soil sand. The tests were performed at $1g$ and $40g$, leading to a prototype diameter of 80 cm [15]. Results indicate that rate and manner of loading significantly influence lateral bearing capacity for Nevada sand with 80% relative density. An increased lateral loading rate resulted in a 10% and 35% increase in lateral resistance for dry respectively saturated soil.

Recently (2010), $200g$ experiments have been conducted to better quantify the effect of a larger cross-sectional area by adding wings to a mono-pile foundation [28]. Such wings, added to the pile near seabed level, effectively widen the pile and mobilize a larger soil mass, thereby limiting lateral deflection of the pile head. Tests were performed on dry medium dense sand and one-way cyclic loads were applied at 0.25 Hz (model frequency). The prototype diameter of the pile tested was 2.4 m and with wings the width equals 5.6 m. The addition of wings for the same loading conditions resulted in a 50% higher lateral bearing capacity or a reduction of about 40% in pile head displacement. These results indicate that a larger area limits horizontal deformations for typical loading conditions, suggesting a larger diameter pile will be able to withstand larger lateral loads.

Investigation into behaviour of large diameter mono-piles has been presented for $100g$ tests with a prototype diameter of 5.0 m, subjected to 1000 loading cycles for dense (95% relative density) dry sand [53]. Unidirectional force-controlled loads have been applied with a loading frequency in the range from 0.02 – 0.4 Hz. Significant accumulated permanent displacements are found which evolve approximately linear on a logarithmic scale.

The quantity of ng experiments remains limited. Furthermore, validity and applicability of the p-y method for large diameter piles remain a topic of research. For many situations adapted (FE) models are created to help understand experimental data. Especially, since full-scale tests, particularly with marine loading conditions, are expensive and complex.

2.6 Summary and conclusions

The p-y method is not specifically formulated for large diameter mono-pile foundations. Numerical methods as well as experimental research show limitations of using the p-y design methods for large mono-piles. However, it remains unclear for which pile diameter and loading conditions the p-y curves start to deviate from existing measurements. Furthermore, experimental evidence for the validation of this design method is scarce.

Cyclic soil loading and the soil-pile response require further research in order to arrive at a more reliable design method. Before a new series of improved soil tests can be performed more information on the cyclic lateral pile-soil response needs to be gathered from (model) pile tests.

The next Chapter 3 will introduce the prototype piles and model piles. The ultimate lateral load for different pile diameters is calculated. Next, the Delft University of Technology geotechnical centrifuge and the experimental programme which will investigate soil behaviour when subjected to lateral static and one-way cyclic loads is introduced.

Chapter 3

Experimental Test Set-up

In order to determine the validity of the p-y method for large diameter mono-piles and the effect of diameter increase on the lateral bearing capacity, reference piles are introduced. Based on the reference piles two model piles are made that will be tested using the geotechnical centrifuge of Delft University of Technology. These *ng* experiments are introduced in Section 3.9.

3.1 Reference offshore mono-pile foundation

Several offshore wind farms have been completed. About 65% of the foundations are mono-piles [96]. The Danish *Horns Rev* wind farm consists of 80 Vestas V80-2MW MW turbines that are founded on 4.0 m diameter mono-piles in water up to 15 m deep. The embedded length of these piles is about 25 m, i.e. the L/D-ratio is 6.25, and this farm was completed in 2002. *Horns Rev 2*, completed in 2008, consists of 91 Siemens Wind Power SWP 2.3-93 turbines with a total capacity of 209 MW. All towers are founded on mono-piles with a diameter of approximately of 3.9 m. The L/D-ratio and water depth are 6–7 and 9–17 m respectively. The English *Lynn and Inner Dowsing Wind Farm*, completed in 2008, is constructed using 4.7 m diameter mono-piles with an embedded length of 22 m, leading to an L/D-ratio of 4.7. The total generated power output equals 209 MW and is generated by 54 Siemens 3.6-107 turbines.

The reference mono-pile foundation is based on the mono-pile foundation installed at *Offshore Wind farm Egmond aan Zee*. This reference pile has a diameter of 4.4 m and is made from steel with an Young's modulus of 210 GPa, has a wall thickness of $1/80D$ and embedded length L_{emb} of about $6D$.

There is a tendency to use shorter piles or piles with a larger diameter whilst maintaining a constant embedded length. This leads to a decrease in slenderness ratio. Piles with an L/D-ratio of 5 have already been installed and future farms will probably be constructed using piles with an L/D-ratio of 5 or even less, as already piles with an L/D-ratio of 4.7 have been used at the British *Lynn and Inner Dowsing Wind Farm*.

Therefore, this Thesis takes a pile with a diameter of 4.4 m and an embedded length of $5D$ as the reference. For *ng* experiments a second prototype pile of half the dimensions of the 4.4 m prototype pile is introduced. A detailed overview of properties of the reference

Table 3.1 Properties of two prototype piles

Property	Prototype pile 1	Prototype pile 2	Dimension
Diameter	4.4	2.2	m
Wall thickness	0.06	0.03	m
Embedded length	22	11	m
L/D ratio	5	5	-
Young's modulus	210	210	GPa
Area	0.818	0.205	m^2
Moment of inertia	1.926	0.120	m^4
Flexural stiffness, EI	$404 \cdot 10^9$	$43 \cdot 10^9$	Nm^2
Axial stiffness, EA	$173 \cdot 10^9$	$25 \cdot 10^9$	N

4.4 m and 2.2 m diameter mono-piles is given in Table 3.1. In Section 3.4 the scaling laws by which prototype diameter piles are converted to model piles are introduced. In Section 3.5 the model piles will be presented.

3.2 Vertical bearing capacity

The majority of foundation piles is primarily designed to carry a vertical load, i.e. transfer a vertical load to the subsoil. A decrease in embedded pile length is only possible if the vertical bearing capacity is maintained. The total vertical bearing capacity F_{bc} is built-up of shaft resistance $F_{bc,shaft}$ and pile tip resistance $F_{bc,tip}$. For unplugged piles both the inner and outer shaft surface area provide resistance. On the other hand, plugged piles derive their total vertical bearing capacity from outside shaft friction and entire cross-sectional base area,

$$F_{bc,tip} = \gamma L N_q A, \tag{3.1}$$

$$F_{bc,shaft} = \pi D \beta \gamma \frac{1}{2} L^2. \tag{3.2}$$

These Equations rely on the pile diameter D in m, soil density γ in kN/m^3, soil parameters N_q and β, as well as the embedded pile length L in m. The N_q value is based on medium dense to dense sand. According to the API [7] the maximum predicted shaft resistance and tip resistance for the reference piles respectively are 67 kPa and 3.0 MN.

The calculated total vertical bearing capacity F_{bc} for the 2.2 m and 4.4 m diameter piles is 2.5 MN and 17 MN respectively. An entire OWEZ wind turbine resembles a weight of approximately 600 ton, i.e. 6 MN, and is founded on a 4.4 m diameter mono-pile. Therefore, the vertical bearing capacity is not the limiting factor in the design of an offshore wind turbine mono-pile foundation.

3.3 Pile response due to lateral loading

Calculations with MPile [14] have been performed to get an understanding of the ultimate soil resistance p_{ult} of a laterally loaded pile and the corresponding lateral pile displacement in dry sand. The influence of the height above seabed at which the applied force acts is also quantified. This PC programme uses the p-y method to calculate the ultimate lateral capacity of piles. The calculation uses the cap interaction model. The input soil profile is a simplified representation of OWEZ CPTs (Appendix A) and shown in Appendix C. The maximum cone resistance is 20 MPa and as the API prescribes the $K_0 = 0.4$. Both cyclic and static load cases are calculated.

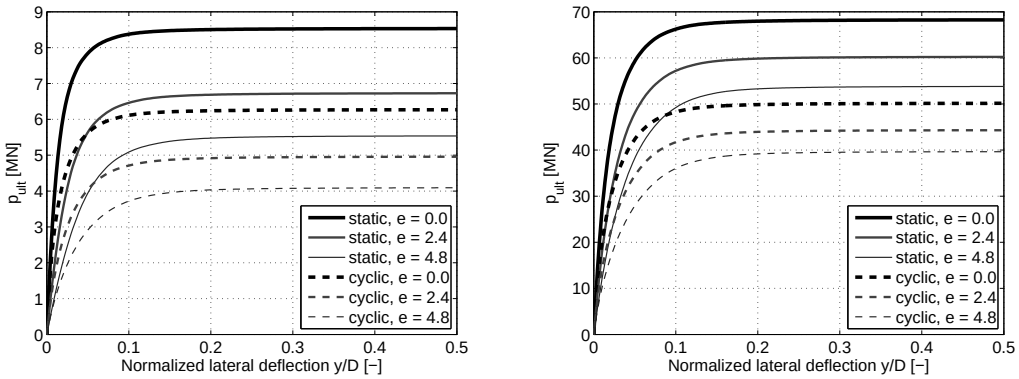

(a) $D = 2.2$ m **(b)** $D = 4.4$ m

Figure 3.1 p_{ult} and influence of load excentricity on p_{ult}

The ultimate lateral bearing capacity p_{ult} of the pile is referred to as the load cap. A high initial stiffness and plateau for $y \geq 0.1D$ are visible in the load-displacement results as shown e.g. in Figure 3.1 and Appendix D. The load-displacement results of 4.4 m and 2.2 m diameter piles embedded in dry sand are shown in Figure 3.1. The results indicate that the mono-pile behaves rigid, as only marginal bending of the pile occurs. The centre of rotation lies about $4D$ below soil surface level, which is in agreement with [16; 20]. The normalized lateral deflection is measured at 0.0 m, 2.4 m and 4.8 m. Detailed MPile results are included in Appendix D. As shown, an increase in load height to 2.4 m above seabed level leads to a decrease in p_{ult} of about 13% for the 4.4 m diameter pile. A load offset of 4.8 m above seabed level leads to an additional 11% decrease of the p_{ult}.

3.4 Scaling to model dimensions

The use of a geotechnical centrifuge in physical modelling makes it possible to simulate the mechanical response of full-scale (geotechnical) structures in scaled down physical models. In order to achieve a properly scaled model test it is necessary to replicate a materials' effective stress state at full scale conditions. This implies that a 1:100 model should be tested under an acceleration of $100g$. The most relevant parameters and scale factors for this Thesis are given in Table 3.2, e.g. [33; 80; 81; 83; 86].

Scaling to model space has to be done with care, for not all properties scale in a linear manner. For these tests the main objective for the model piles is a correctly scaled flexural stiffness. The aim is to scale the geometry as good as possible.

Table 3.2 Overview of centrifuge scaling factors

Quantity	Symbol	Prototype	Model
Acceleration	a	1	N
Length	L	1	1/N
Area	A	1	$1/N^2$
Force	F	1	$1/N^2$
Stress	σ	1	1
Strain	ε	1	1
Density	γ	1	1
Mass	m	1	$1/N^3$
Frequency	f	1	N
Time (dynamic)	t	1	1/N
Flexural stiffness	EI	1	$1/N^4$

3.5 Model piles

The primary prototype pile has a diameter of 4.4 m. The secondary prototype pile is chosen to be half the size of the 4.4 m diameter pile, resulting in a diameter of 2.2 m, an embedded pile length of 11 m and a wall thickness of 3 cm. The two model piles are based on these two large diameter piles and are scaled to corresponding stiffness whilst scaling the original geometry as close as possible. Model piles are constructed using brass with a Young's modulus of 110 GPa and about half the Young's modulus of steel (210 GPa). This means the model pile wall thickness can be increased by a factor of 2. A detailed cross-sectional view of both model piles is presented in Appendix E.

Table 3.3 Model pile dimensions and properties

Property	Model pile 1	Model pile 2	Dimension
Length (embedded + additional)	68.4 + 35.0	136.8 + 35.0	mm
Diameter, internal	13.00 ± 0.05	26.00 ± 0.05	mm
Diameter, outside	13.68 ± 0.05	27.36 ± 0.05	mm
Wall thickness	0.34	0.68	mm
Weight	14.5 ± 0.1	93.5 ± 0.1	g
Young's modulus (E)	110	110	GPa
Moment of inertia (I)	$0.32{\cdot}10^{-9}$	$5.07{\cdot}10^{-9}$	N^4
Flexural stiffness (EI)	34.9	558	Nm^2

3.6 Soil tests and parameters

North Sea conditions cannot be exactly reproduced in the laboratory using the currently available equipment. The samples have a lower initial density and a somewhat different grading. The properties of the used model sand are described in the following paragraphs.

Pycnometer The density of the sand particles is determined using a *MagnaChrome Ultrapycnometer 1000* and equals 2.6457 Mg/m^3. Additional information can be found in Appendix F.

Void ratio and porosity The extreme void ratios are determined according to the Japanese Geotechnical Society (JGS) [39]. To get the lowest void ratio or the highest soil density the specified volume is filled layer by layer and gently densified. The highest void ratio or lowest density is achieved by slowly and carefully pouring sand through a funnel into the specified volume.

Although effort is put into producing accurate and consistent results, it is assumed that the very extremes are not possible to be achieved in relative short amounts of time, i.e. up to 20 minutes. The average of the 3 peak values for either the lowest density and highest density are taken. The porosity n, void ratio e and relative density I_d are determined based on these two sets of three values. The n_{min} and n_{max} differ about 10% which is acceptable for fine grained sand. The desired I_d of 60% leads to a porosity and void ratio of 0.394 and 0.651 respectively. The particle density is 2.6457 Mg/m^3 and the specific density is 1.603 Mg/m^3.

$$n = \frac{V_{pores}}{V_{total}}, \tag{3.3}$$

$$e = \frac{V_{pores}}{V_{solid}} = \frac{n}{1-n}, \tag{3.4}$$

$$I_d = \frac{e_{max} - e}{e_{max} - e_{min}}. \tag{3.5}$$

Table 3.4 Limiting densities

	Highest density	Lowest density	Dimension
Volume	113.1	113.1	cm^3
Total serie of 10 tests			
Average mass	192.52	164.84	g
Mass standard deviation	1.31	0.53	g
Serie of 3 peak tests			
Average mass	194.68	164.12	g
Mass standard deviation	0.43	0.18	g
Average specific density	1.721	1.451	Mg/m^3
Porosity extremes	n_{min} 0.349	n_{max} 0.451	-
Void ratio extremes	e_{min} 0.537	e_{max} 0.823	-

Triaxial tests The soil particles in oven dry as well as saturated drained conditions have been tested using a triaxial apparatus according to the British Standard Institution (BSI) [17] and *Nederlands Normalisatie-instituut* (NEN) [61]. The effective confining pressure applied is 500 kPa, which is equal to about 31 m below soil surface. Since all tests have been performed at the same (effective) confining pressure it is not possible to determine the cohesion. The cohesion is assumed to be 0 kPa for this granular material. In Appendix H the deviatoric stress is plotted against the strain. Additionally, several Mohr circles are plotted. The peak angle of internal friction φ equals about 35°. The secant stiffness of the initial loading branch is 1400 ± 100 kN/m. The reloading stiffness is 2200 ± 100 kN/m.

Sieving The sand particles have been sieved in order to determine the particle size distribution and coefficient of uniformity. The D_{10}, D_{50} and D_{60} are equal to 170, 245 and 260 μm respectively, and as the coefficient of uniformity indicates, the soil is considered poorly graded,

$$C_u = \frac{D_{60}}{D_{10}} = \frac{260}{170} = 1.5 \leq 2.0. \tag{3.6}$$

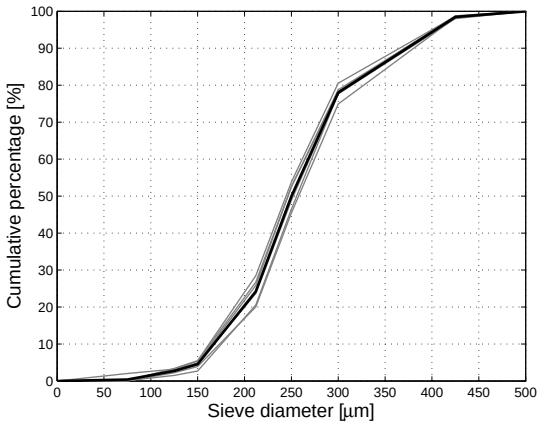

Figure 3.2 Grain size distribution

Sand in open air The sand does attract almost no water from the air. Oven dry sand that has been laying in the lab exposed for 48 hours and >480 hours resulted in a weight increase of about 0.02% ± 0.01% and 0.03% ± 0.01% respectively. These percentages are considered negligible and the sand is considered dry.

Several soil parameters have been determined and the experimental programme can now further be accommodated. The Delft University of Technology geotechnical centrifuge, in which the *ng* experiments will be performed, is introduced next. The sample preparation and experimental programme will be introduced respectively in Sections 3.8 and 3.9.

3.7 Geotechnical centrifuge

3.7.1 Brief history of centrifuge testing

In an 1869 paper Edouard Phillips [67] opted for the use of centrifuge models in engineering. He proposed to exploit centrifugal acceleration to generate increased body forces on models of reduced size. The first literature referring to applied centrifuge modelling appears to be by P. Bucky in 1931, New York (USA). At almost the same time N. N. Davidenkov and G. Y. Pokrovsky worked on centrifuge modelling in the USSR, publishing their work [23; 68; 69] in Russian and later on at the First International Conference of Soil Mechanics and Foundation Engineering (ICSMFE). In later decades e.g. Rowe and Schofield have contributed to the field of centrifuge research, see for instance [77; 80].

Using centrifuge modelling the understanding of complex soil-foundation interaction can be improved. This was underlined by an increase in research activities and increasing number geotechnical centrifuges worldwide. Especially in the last few decades the technology evolved due to technological advances (i.e. micro-electronics and miniature instrumentation).

3.7.2 General principle of a geotechnical centrifuge

An object travelling in a circular motion experiences a force F away from the centre of rotation. A force of similar magnitude is required to keep the object in orbit and is given below, see Eq. 3.8. The mass of the object m in kg, velocity v in m/s or angular velocity ω in rad/s and radius r in m determine the force F in N,

$$F = \frac{mv^2}{r} = m\omega^2 r, \tag{3.7}$$

$$v = \omega r. \tag{3.8}$$

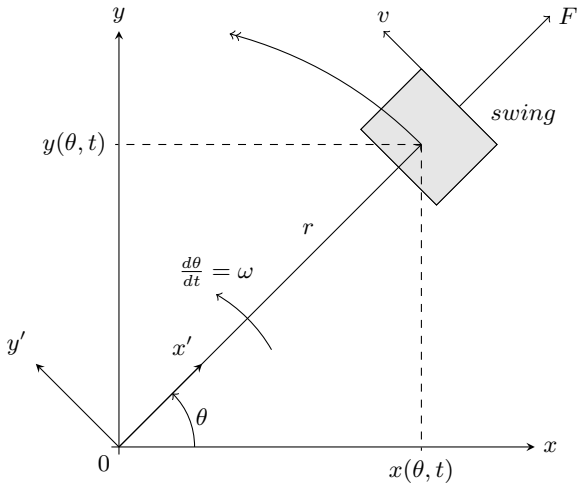

Figure 3.3 Global polar coordinates of the model and local coordinate system of the model

3.7.3 Geotechnical Centrifuge at Delft University of Technology

The centrifuge used for this research has been built-up by Allersma and co-workers in 1990 and is located at the Faculty of Civil Engineering of the Delft University of Technology (DUT) in Delft [5]. Several years ago it has been disassembled and moved to a new location. Not too long ago (2009), the system has been reassembled, tested and is now operational. Several modifications such as improved data sampling have been implemented.

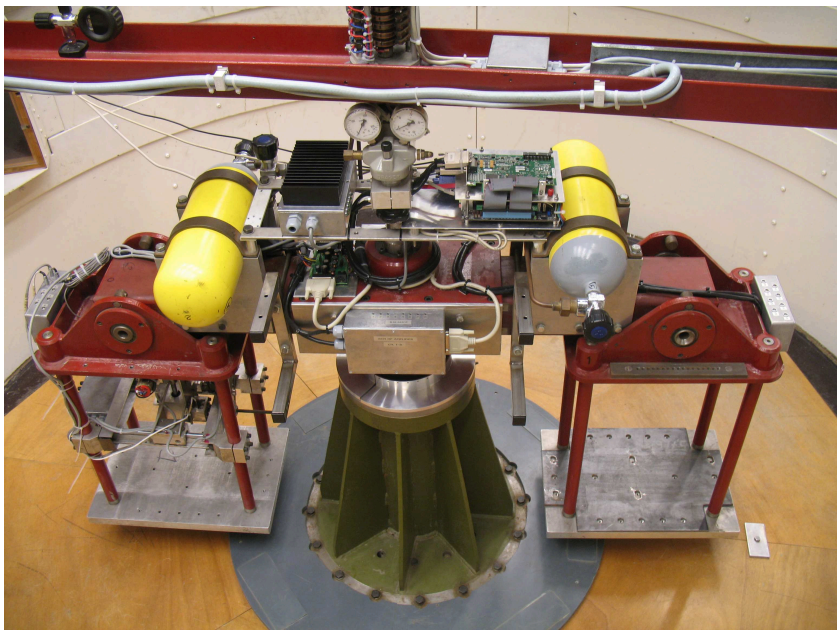

Figure 3.4 Photo of the DUT centrifuge

A control room housing 3 PCs is situated next to the room in which the centrifuge set-up is located. Using one of the PCs the tangential speed (i.e. the acceleration) can be set and controlled. The connection between the PC, motor and gearbox involves a controller. The revolutions of the beam and temperature of the bearings are monitored. During the tests performed for this Thesis the revolution monitoring was not operational.

A second PC is used to send data via slip rings to the mini-ITX PC system mounted on the beam of the centrifuge. This is also possible during full centrifuge operation. This connection consists of two times 100Mbit and is also used to transfer other data, e.g. from the 5 mega pixel (MP) camera mounted on the swing. An overview of the entire set-up is shown in Figure 3.6.

3.7.4 Data acquisition

There is a passively cooled mini-ITX PC and several controllers mounted on the centrifuge beam. Besides a revolution counter mounted close to the vertical axis an accelerometer is installed on the bottom of the swing. This accelerometer is functional up to $300g$ and accurate up to about 0.5% up to $200g$. The PC on the beam is also used to control load frame operation. Via an RS232 controller the motors and pulse counters for both

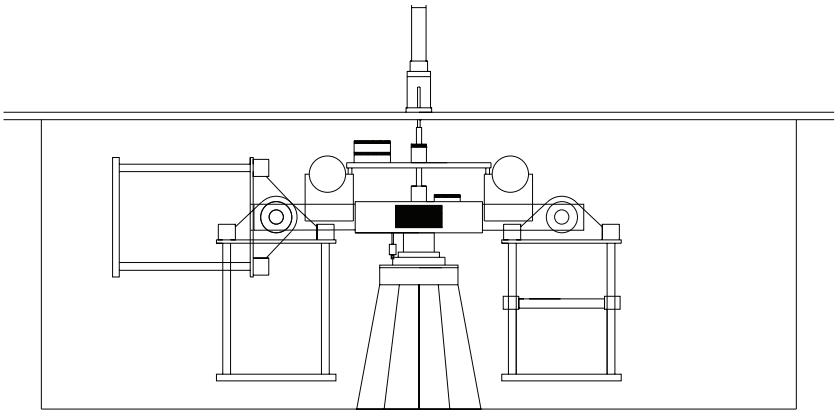

Figure 3.5 Schematic overview of the DUT centrifuge

Table 3.5 Summary of DUT centrifuge specifications

Property		Value	Dimension
Radius of the centrifuge arm		1195	mm
Maximum design acceleration		300·9.81	m/s^2
Maximum design payload (at $300g$)		0.04	ton
Swing dimensions	Height	420	mm
	Width	350	mm
	Length	450	mm
Maximum acceleration used		160·9.81	m/s^2
Maximum payload used		0.022	ton

horizontal and vertical movement are controlled. A National DAQ card is used to convert the analogue signal from load cells (for both vertical as well as horizontal loading) to a digital signal. Data is then stored on the 64 GB solid state disk (SSD) attached to the PC. If desired, this data is directly accessible using a PC connection via the slip rings. A more detailed overview of equipment is shown in Figure 3.6.

The horizontal movement of the load frame is measured at a rate of 5 Hz. Since the speed is 0.5 mm/sec this leads to an accuracy of approximately 0.1 mm. The load corresponding to the lateral movement of the load frame is registered at 16 Hz. The maximum available load on the load cell is 1500 N, which at $160g$ equates to 38 MN.

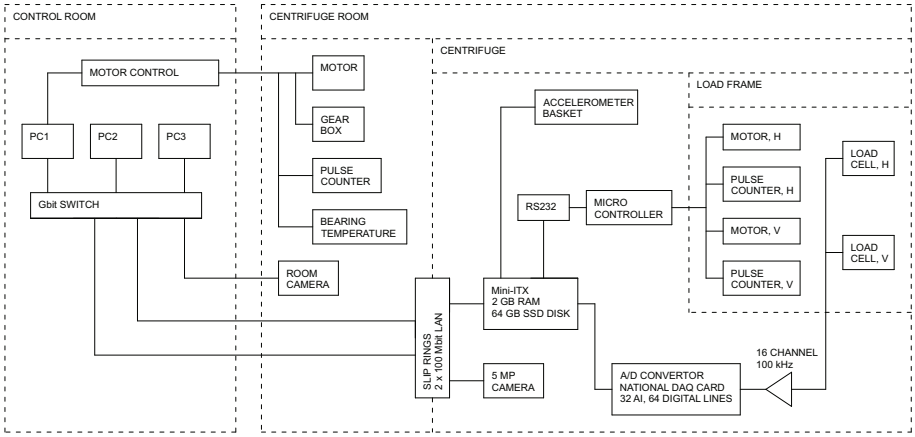

Figure 3.6 Schematic representation of centrifuge set-up

3.8 Strongbox properties and sample preparation

The centrifuge will be loaded on one side with the strongbox (including the sand and model pile). The other side is loaded with dead weights to counter balance the system.

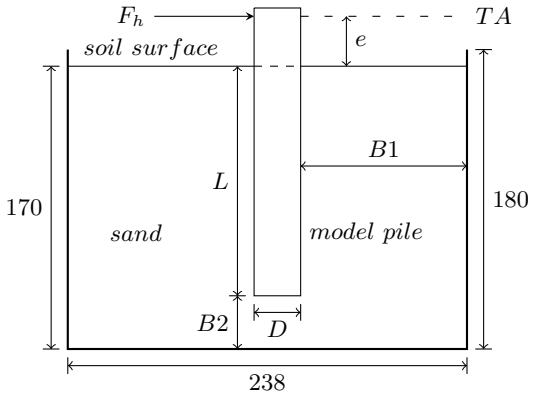

Figure 3.7 Schematic cross-section of the strongbox, dimensions in mm

Strongbox dimensions The strongbox is a metal box with internal length, width and height of 238, 222 and 180 mm respectively, and of which an overview is given in Figure 3.7. The weight of the empty box is 5401 g ± 1 g. In loading direction the total space is 238 mm. The pile with outer diameter D will be installed in the strongbox up to the required depth $L = 5D$. The space available between the horizontal boundary $B1$ and vertical boundary $B2$ is in the order of $3.7D$ and $1D$ respectively for the large model pile. For the small model pile $B1$ and $B2$ equal $9D$ and $6D$ respectively. The force F applied to the pile and measured at height e above soil level. The displacement of the pile is also measured at location TA, equal to e above the soil level.

Sample preparation For each test a new sample was prepared by pouring dry sand in the strongbox and subsequently vibrating the entire sample. This method resulted in consistent soil densities with relative densities I_d varying between 58–62% for all tests. After initial sample preparation the model pile was installed at $1g$ and the entire strongbox was again briefly vibrated to minimize pile installation effects. The total weight of the sample is determined and the sample is carefully transported to the centrifuge room. The total weight of about 20 kg does not require special tools for transportation. The initial pile positions before flight were measured and the sample is placed on one of the swings of the centrifuge.

3.9 Experimental programme

The experimental programme consists of static and cyclic pile load tests. The static tests are conducted to obtain understanding of soil-pile interaction for large displacements and a second set of static pile load tests is performed to determine boundary effects. Static tests are displacement controlled. At this point no field data is present. Therefore, the force for the force controlled cyclic tests is based on an arbitrary $0.1D$ pile displacement from the static model pile tests.

Tests will be conducted with varying load excentricity e of 0.0 m, 2.4 m or 4.8 m in prototype scale above soil surface level. An increase in excentricity should lead to a lower ultimate lateral resistance [42; 71] and e.g. shown by Figure 3.1. The number of load cycles is represented by N and the acceleration compared to $1g$ is represented by n. An overview of all tests is shown in Table 3.6.

Table 3.6 Overview of centrifuge tests (prototype dimensions)

Test	D_p	L_p/D_p	e	N	n	EI
	m	-	m	-	-	Nm^2
a	2.2	5	0	1	160	35
b	2.2	5	4.8	1	160	35
c	2.2	5	0	1	80	558
d	2.2	5	2.4	1	80	558
e	2.2	5	4.8	1	80	558
f	2.2	5	2.4	500	80	558
g	4.4	5	0	1	160	558
h	4.4	5	2.4	1	160	558
i	4.4	5	4.8	1	160	558
j	4.4	5	2.4	500	160	558
k	4.4	5	4.8	500	160	558

3.10 Loading schemes

The static load scheme can be represented as a linear time-displacement graph as the load frame speed is constant and equal to 0.5 mm/sec, see Figure 3.8a. The force applied as cyclic load is derived from the static load-displacement curve for y is about $0.1D$. The same excentricity e is used in both tests. The cyclic loads are applied in a force controlled way and the displacement is measured at the same time and e at which the force is applied.

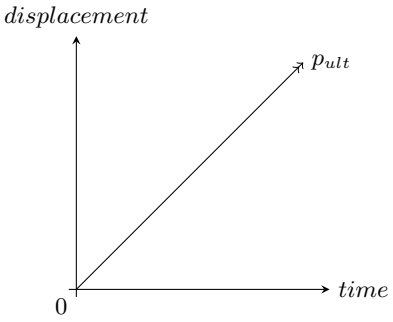

(a) Static loading scheme

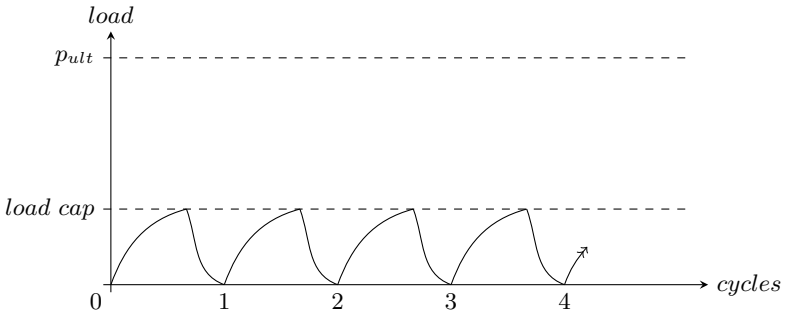

(b) Cyclic loading scheme

Figure 3.8 Schematic representation of static and cyclic loading schemes

3.10.1 Secant and tangent stiffness

A relation between secant or tangent stiffness and the number of load cycles N helps improve understanding of soil-pile behaviour. Figure 3.9 gives an overview of how the secant stiffness E_{sec} and tangent stiffness E_{tan} will be calculated based on obtained load displacement curves from cyclic pile load tests; E_{sec} is calculated using the highest point in the load curve and the lowest point after unloading and before reloading and E_{tan} is based on the tangent of the reloading curve,

$$E_{sec} = \frac{F_1 - F_2}{u_1 - u_2} = \frac{F_1}{u_1 - u_2}, \tag{3.9}$$

$$E_{tan} = \frac{F_4 - F_3}{u_4 - u_3}. \tag{3.10}$$

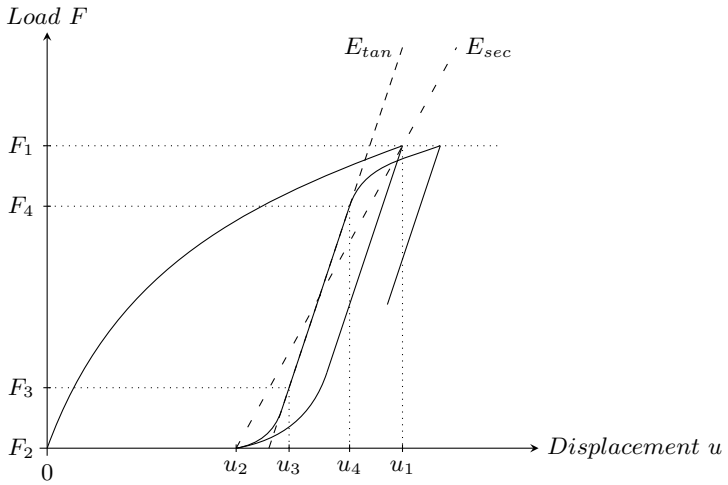

Figure 3.9 Schematic overview of secant and tangent stiffness

3.10.2 Pile displacement accumulation

An increasing number of load cycles generally leads to an increase in displacements, but with a decreasing amount for each additional cycle. Several equations to predict this reduction (e.g. Eqs. 2.7 and 2.8) exist and are used to predict pile displacements for a given cycle count N. The pile displacement will be plotted against the number of cycles and will be compared to these existing formulae.

3.11 Experimental limitations and boundary conditions

Physical boundary conditions The ratio between pile diameter and strongbox size (measured in loading direction, i.e. 238 mm) ideally is in the order of 40 [79]. Using the current strongbox, this ratio for the small diameter model pile is about 18 and it is only about 8 for the large model pile. According to [79] for both model piles the physical boundary can influence pile test results. Experiments testing the small 13.68 mm model pile at $160g$ and the large 27.36 mm model pile at $80g$, leading to a prototype 2.2 m diameter pile for both cases, will better identify possible boundary effects. The results of these tests will be discussed in Chapter 4.

Model pile installation The ratio between model pile wall thickness t and grain size D_{50} is limited, about two for the small diameter model pile and 4 for the large diameter model pile. Installing the model piles at $1g$ limits the build-up of high stresses below the pile tip compared to pile installation at ng. Also, since the model piles will not be loaded by forces other then the self-weight and the main force is acting laterally, the influence on the lateral pile response of this low t/D_{50} ratio is considered negligible.

Shear band width and particle size versus model wall thickness and diameter The shear band width is relevant for centrifuge experiments as often a low ratio between pile diameter and grain size is found. Shear band widths are about $16D_{50}$ [59; 83]. Furthermore a value of $> 100D_{50}$ is desired for the pile diameter. In this research a shear band width and suggested pile diameter of 3.9 mm and 24.5 mm respectively are found. Since the governing pile (failure) mechanism is rotation, which leads to shear below the pile toe, the clearance between pile toe and strongbox bottom of $>1D$ should be sufficient.

Void ratio decrease Due to the applied acceleration field the sample possible could densify. Tests with an initial porosity of 39.7% to 48.4% and acceleration of $120g$ indicate a decrease in overall sample porosity of approximately 1% [83]. The majority of this densification will have occurred before the tests started. The current set-up does not allow for measuring a porosity decrease during flight. Nevertheless, soil levels will be measured before and after flight and the results will be presented in Chapter 4.

Soil density The I_d of 60% is low compared to North Sea soil conditions for several locations, but makes the density of the sample better controllable and consistent and it should deliver reproducible results. This relative low density will lead to a lower (initial) stiffness of the soil.

Loading conditions The current set-up is designed for one-way loading of a model pile foundation at a single height. Different heights at which forces in the field act (i.e. wind loads act at a different height than marine loads) cannot be modelled using the current set-up. Neither is it possible to load the foundation from multiple directions.

All ng experiments are conducted on dry sand, using static or one-way cyclic loading conditions with a force at a fixed height for each experiment. In reality loading conditions are not that simple, as forces from different directions, with varying magnitude and at different heights load the wind turbine. Also, since pile tests are performed using dry sand, the effective stresses are higher compared to saturated sand.

3.12 Summary and discussion

The 4.4 m diameter prototype pile with a slenderness ratio of 5 is the basis for the experiments. A 2.2 m diameter pile with half the dimensions of the 4.4 m diameter pile is also investigated. Two model piles of 13.68 and 27.68 mm outside diameter are tested at $80g$ and $160g$, representing 2.2 m and 4.4 m prototype piles. All tests are performed at an I_d of 60% $\pm$ 2% using dry sand with an average particle size D_{50} and angle of internal friction φ of $245\mu m$ and 35° respectively.

Chapter 4

Test Results

4.1 Overview of the experimental programme

The results from model pile tests, of which an overview is given in Table 4.1, will be presented in Section 4.3. The load excentricity e, number of load cycles N and level of acceleration n are shown. The EI represents the flexural stiffness of the corresponding model pile, of which the prototype diameter is indicated by D_p.

Table 4.1 Overview of centrifuge tests

Test	D_p m	L_p/D_p -	e m	N -	n -	EI Nm^2
a	2.2	5	0	1	160	35
b	2.2	5	4.8	1	160	35
c	2.2	5	0	1	80	558
d	2.2	5	2.4	1	80	558
e	2.2	5	4.8	1	80	558
f	2.2	5	2.4	500	80	558
g	4.4	5	0	1	160	558
h	4.4	5	2.4	1	160	558
i	4.4	5	4.8	1	160	558
j	4.4	5	2.4	500	160	558
k	4.4	5	4.8	500	160	558

In order to better appreciate the results presented in this Chapter, first soil surface settlements and the mass difference of the sample before and after experiments are discussed. Thereafter, in Section 4.3 pile load-displacement results and the effect of load excentricity will be presented.

4.2 Surface settlement and sample weight loss

Surface settlement During two pile load tests of longer duration, i.e. up to 2 hours flight time, up to 25 positions have been measured at $1g$ before and after testing in the centrifuge. These positions are equally distributed over the surface and form a 5 by 5 grid. Table 4.2 summarizes the results of two tests. At locations where the soil has been disturbed because of pile displacement no valid post experiment measurements were taken.

Table 4.2 Overview of surface settlements (mm)

Test 1: 160g, 60 minutes					Test 2: 80g, 30 minutes				
-0.2	-0.3	-0.0	-0.2	-0.3	-0.1	-0.4	-0.6	-0.2	-0.2
-0.4	-0.7	-0.2	-0.1	-0.3	-0.0	-0.2	-0.1	-0.1	-0.5
-0.1	-0.6		-0.2	-0.2	-0.0	-0.1			-0.1
-0.4	-0.4	-0.2	-0.1	-0.4	-0.3	-0.5	-0.1	-0.2	-0.1
-0.1	-0.3	-0.0	-0.1	-0.5	-0.4	-0.0	-0.1	-0.2	-0.5

No additional measurements have been performed to quantify the rate of particle settlement. However, typically the major part of the settlements occurs within the first minutes of flight [83]. The limited number of measured points only gives an indication whilst e.g. laser scanning of the surface could create a more accurate view of the settlements. When measuring the surface settlement during flight also the settlement rate can be quantified.

The mean for test 1 and 2 is equal to surface settlement respectively of 0.26 $\pm$ 0.3 mm and 0.22 $\pm$ 0.3 mm. This relatively high uncertainty, which is in the same order of magnitude as the measured settlement, is the result of the manual measurement method. Nevertheless, a general trend is distinguished and no surface rise has been witnessed (obviously, except on the passive side of the laterally loaded pile).

A surface drop of 0.3 mm results in a volume decrease of 15.7 cm^3 or 0.2% and an I_d increase from the desired 60% to 60.7%. The influence of surface settlements on the pile load tests therefore is limited.

Sample weight loss Before and after each test the weight of the strongbox, including sand and model pile, has been measured. The strongbox and model pile will not loose mass during the experiments. Therefore, the weight difference is due to the loss of sand particles. The average amount of sand particles lost during flight is less than 1 gram, which makes the total mass loss negligible. The running time of tests has no effect on the total amount of mass loss.

4.3 Experimental test results

The experimental programme contains a non-instrumented model pile. Neither have measurements been performed in the soil sample. The cyclic (force controlled) and static (displacement controlled) model pile tests rely on load F_h applied at height e above the soil surface and pile displacements y are measured at the exact same height.

4.3.1 Pile rotation and translation

Large diameter piles rotate rather then bend when laterally loaded. For the current experiments several model piles have been displaced $>0.5D$. In front of the pile, on the passive side, heave occurred. To find out whether the pile purely rotates or also translates the distance between the pile and a fixed vertical beam was measured at 5 mm, 12 mm and 30 mm above soil level before and after several experiments. These measurements are in line with the load direction of the load frame. An overview is presented in Figure 4.1.

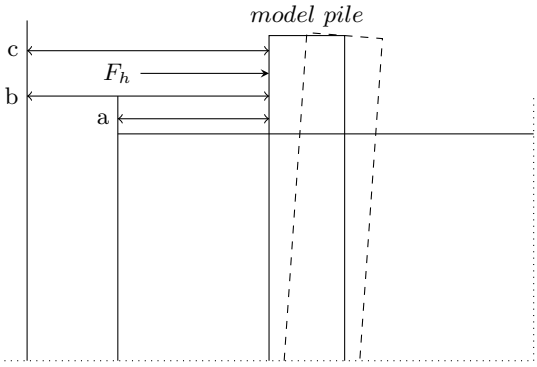

Figure 4.1 Schematic side view of initial pile position (continues line), displaced pile position (dashed line) and measurement locations a, b and c

To verify that no deviation of the pile from the loading direction occurs, at 5 mm and 12 mm above soil surface level the pile position before and after experiments is examined perpendicular to the loading direction. Sideways pile displacements are <0.6 mm $\pm$ 0.2 mm for all recorded cases. The pile thus displaces in line with the load frame, i.e. in the prescribed loading direction.

The initial and final model pile positions have been measured at $1g$. Therefore, the exact position of the model pile in the final state during flight remains unknown. More over, even when the load frame is stopped during lateral loading of the model pile and the system is spun down, the soil is unloaded, thereby influencing the pile position.

Table 4.3 Pile displacement, rotation and translation

						Dimension
Mean pile deflection y	6.7	12.3	5.8	24.1	9.6	mm
Deriving the point of rotation based on φ_{ab}, φ_{bc} and φ_{ac}:						
φ_{ab}	2.4	4.9	1.6	9.7	2.4	°
φ_{bc}	3.2	5.1	1.9	9.5	3.5	°
φ_{ac}	3.0	5.0	1.8	9.5	3.2	°
Average	2.9	5.0	1.8	9.6	3.1	°
Standard deviation	0.4	0.1	0.2	0.1	0.5	°
Point of rotation	$4.3D$	$4.5D$	$6.1D$	$4.6D$	$5.9D$	-
Taking the centre of rotation at $4D$, the following φ are found:						
φ_a	2.9	5.4	2.6	10.5	4.3	°
φ_b	2.9	5.4	2.6	10.4	4.2	°
φ_c	2.9	5.3	2.5	10.3	4.1	°
Average	2.9	5.4	2.6	10.4	4.2	°
Standard deviation	<0.1	<0.1	<0.1	0.1	0.1	°

Constructing the pile rotation angle from differences between the measured locations a–b, b–c and a–c, the centre of rotation is found to be between $4D$ and about $6D$. Any value $>5D$ suggests pile translation. Although the lateral pile displacement is measured sufficiently accurate, the distance between the positions a, b and c is too small to properly distinguish between rotation and translation. When taking the centre of rotation at $4D$ below soil surface, the average pile angle is consistent. However, measurement errors are smeared out over a length of approximately $4.5D$. In order to distinguish between pile translation and rotation and to better quantify the pile rotation, measurement of pile displacements have to be significantly improved.

4.3.2 Static load displacement curves

The results of the static displacement controlled pile load tests are presented in Figures 4.2a and 4.2b. In both Figures the lateral displacement normalized against the pile diameter at surface level is plotted against the prototype lateral load in MN. This is done for load excentricities e of 0.0 m, 2.4 m and 4.8 m.

As expected, an increase in excentricity results in a decrease of the stiffness response. These results are more pronounced in model tests with the large pile diameter. The initial stiffness variation can be caused by minor sample density inconsistencies. Results indicate that for displacements up to $1D$ no ultimate lateral bearing capacity p_{ult} was found in the current tests. The accumulation of sand in front of the pile leads to an increasing lateral resistance.

The prototype pile diameter of 2.2 m is obtained by the 13.68 mm pile at $160g$, but also using the 27.36 mm pile at $80g$. Comparing load-displacement curves of both piles the influence of the physical strongbox boundary can be quantified. These curves are shown in Figure 4.3.

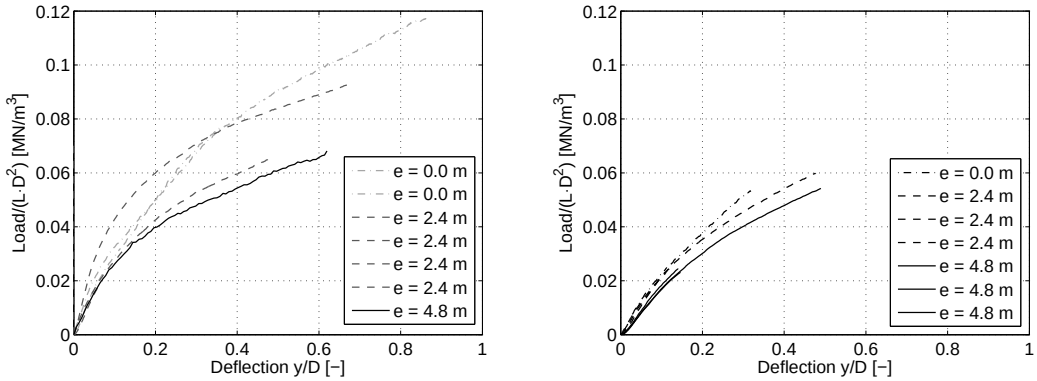

(a) 2.2 m diameter **(b)** 4.4 m diameter

Figure 4.2 Effect of load excentricity on load-displacement behaviour

It was not possible to perform two model pile test using the same sample. Therefore, minor inconsistencies in soil density between the two samples may be present. The small 13.68 mm and large 27.36 mm diameter model piles were located at respectively $8.5D_s$ and $3.7D_l$ from the strongbox boundary. However, ideally a much larger strongbox is required to be certain a negligible influence of strongbox boundary on the model pile test results is present. Also, a minimal pile diameter of 24.5 mm is recommended for the current D_{50} of 245 μm [59; 79; 83]. Nevertheless, good agreement between both piles is visible for pile displacements up to $0.25D$. For displacements up to $0.25D$ the influence of the strongbox boundary is limited and the use of the large 27.36 mm diameter model pile is acceptable.

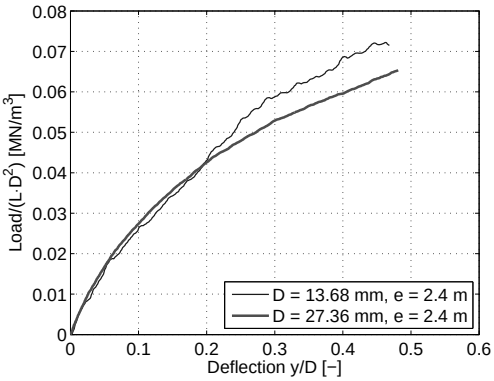

Figure 4.3 Quantification of the physical strongbox boundary

4.3.3 Cyclic load displacement curves

Cyclic lateral load tests with 500 cycles have been performed for both the 2.2 m as well as the 4.4 m pile. Also during these tests the excentricity has been varied. Figures 4.5a and 4.5b plot load against the displacement normalized against the pile diameter. In both tests the lateral displacement increased with an increasing number of load cycles N. Although a load cap has been applied, the recorded load nevertheless increases with a large cycle count. Although a clear cause for this load increase is unknown, it can partially be explained by a combination of several aspects:

- A stiffness increase during the first 10 cycles is visible. Later cycles show only minor fluctuations in secant and tangent stiffness, see Figures 4.8a and 4.8b.
- A 0.2 s time gap between the displacement measurement and force measurement is present. When the target load is reached the load frame continues movement for 0.2 s, thereby further displacing the pile, which results in a higher lateral load. However, as the secant and tangent stiffness do not significantly change for >50 cycles, this should lead to a constant loading level.
- During tests no airconditioning was present. As result, during longer tests of e.g. two hours the room temperature increased from about 20° to >30°, which may have had an effect on the response of the load cell. Eventhough the force plotted against the applied number of cycles shows only a marginal increase of the force for N>50 cycles, see Figure 4.6.

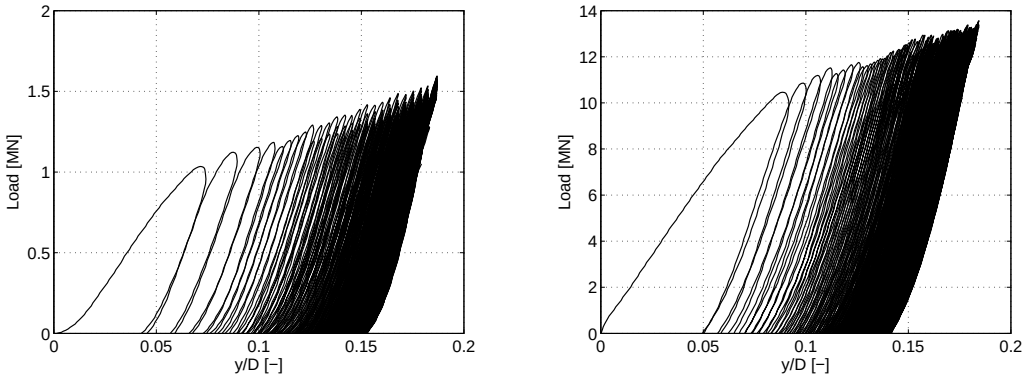

(a) 2.2 m diameter, $e = 2.4$ m **(b)** 4.4 m diameter, $e = 2.4$ m

Figure 4.4 Load-displacement curves for one-way cyclic laterally loaded piles

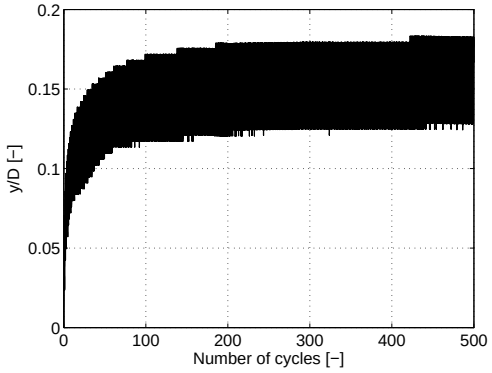

(a) 2.2 m diameter, $e = 2.4$ m

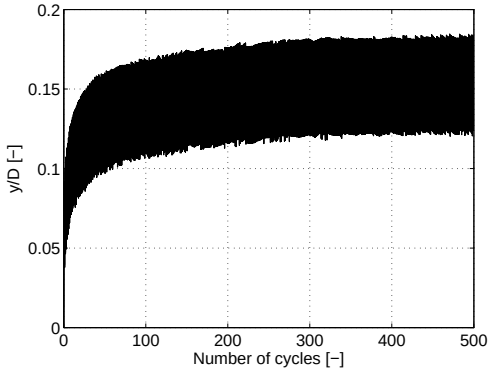

(b) 4.4 m diameter, $e = 2.4$ m

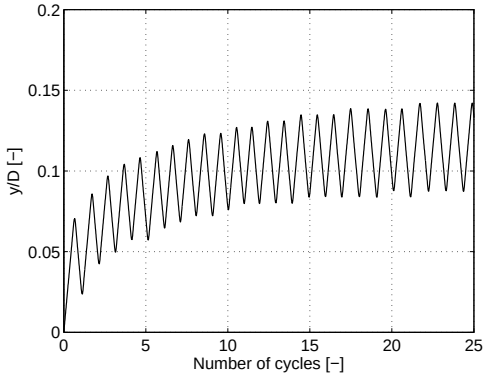

(c) 2.2 m diameter, $e = 2.4$ m, the first 25 cycles

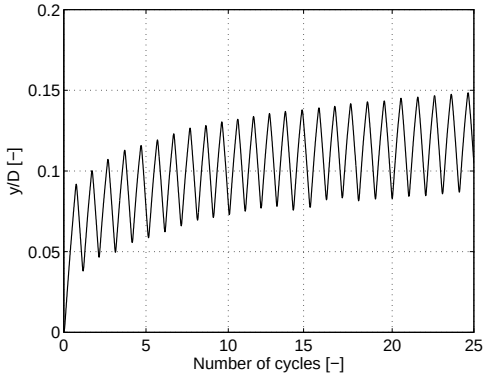

(d) 4.4 m diameter, $e = 2.4$ m, the first 25 cycles

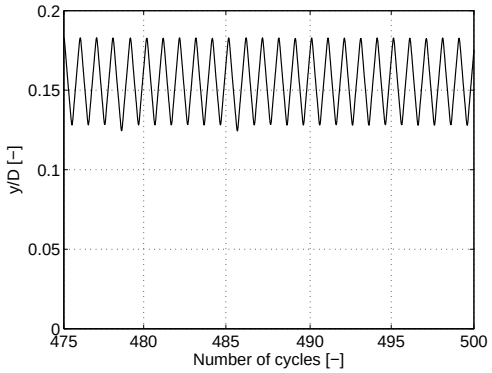

(e) 2.2 m diameter, $e = 2.4$ m, the last 25 cycles

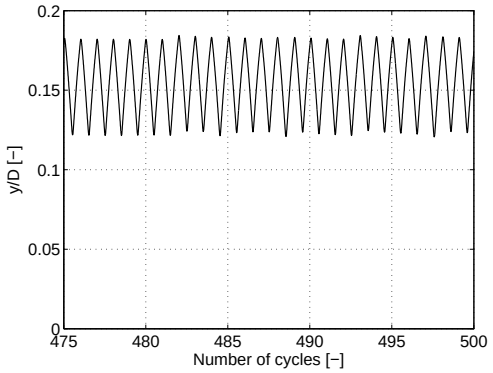

(f) 4.4 m diameter, $e = 2.4$ m, the last 25 cycles

Figure 4.5 Pile load-displacement behaviour with $e = 2.4$ m

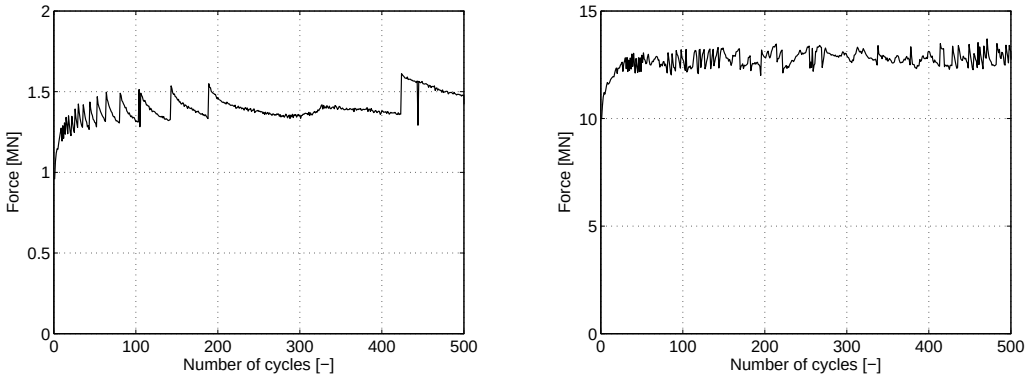

(a) 2.2 m diameter, $e = 2.4$ m, load $F(N)$ **(b)** 4.4 m diameter, $e = 2.4$ m, load $F(N)$

Figure 4.6 Force F plotted against number of cycles N

4.3.4 Secant and tangent stiffness

The secant and tangent stiffness (see Figure 4.7) improve the understanding of the soil-pile interaction. However, since the pile is rigid, the secant and tangent stiffness instead give information about the soil. Figures 4.8a and 4.8b present the results for cyclic force controlled pile tests.

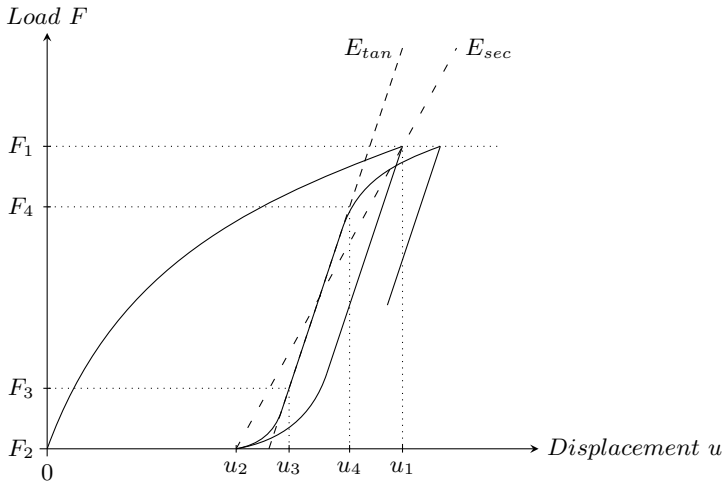

Figure 4.7 Schematic overview of secant and tangent stiffness

A smaller pile diameter shows a lower secant and tangent stiffness. In all cases the tangent stiffness is about 50 % higher than the secant stiffness. Also, larger excentricities e yield a lower stiffness. The results show that an increase in pile diameter with constant L/D, I_d and e, results in a significant increase in static lateral capacity and secant and tangent stiffness from cyclic load tests.

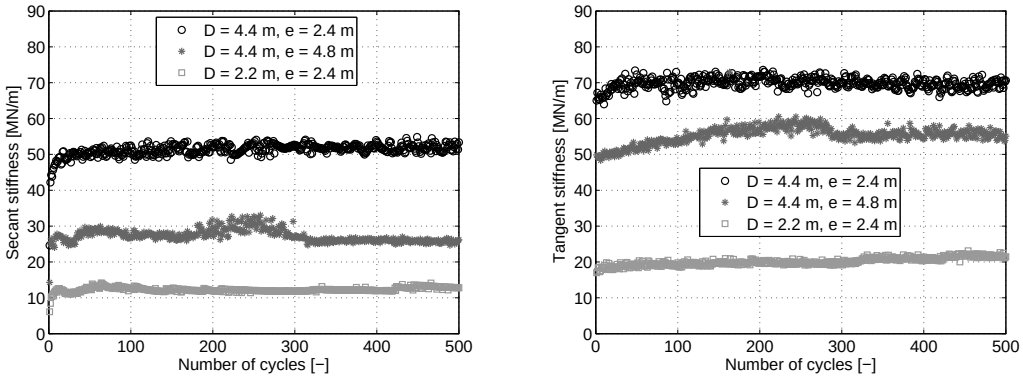

(a) Secant stiffness **(b)** Tangent stiffness

Figure 4.8 Secant and tangent stiffness versus number of cycles N

4.4 Pile displacement accumulation

An increasing number of load cycles results in a displacement accumulation with a decreasing rate. Figure 4.9 plots the formulae as suggested by Hettler (Eq. 2.7) and Little and Briaud (Eq. 2.8) as well as the displacement accumulation for three model pile tests.

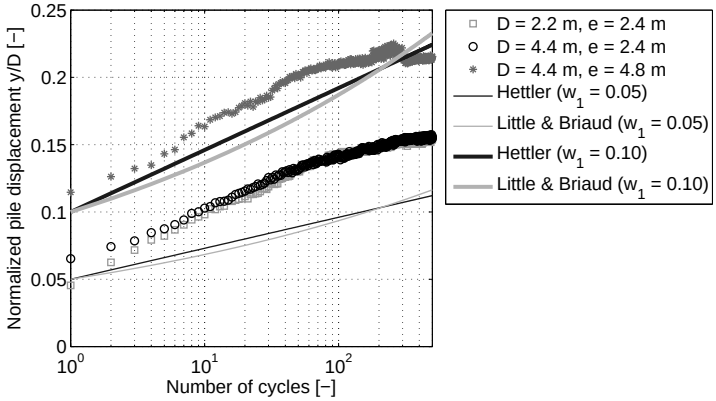

Figure 4.9 Pile displacement accumulation

The empirical formulae do not correspond well to the soil behaviour from the model pile test data. Model pile test results show an over-logarithmic rate of stiffness increase for the first 100 cycles and an under-logarithmic rate thereafter.

Two tests with an excentricity of 2.4 m show good agreement and the $e = 4.8$ test shows a similar accumulation trend, but with a higher initial offset. A higher number of load cycles is required to better understand soil behaviour. It is further recommended to investigate the effect of varying load magnitude on the pile displacement accumulation.

Chapter 5

Comparison

5.1 Introduction

In order to investigate the applicability of the API for pile diameters of 2.2 m and 4.4 m, the results of the model pile tests presented in Chapter 4 will be compared with the design calculations. For this, the soil properties and initial test conditions presented in Chapter 3 will be used as input for the API method as presented in Chapter 2 and Appendix B. First the default formulation will be adopted before going to a modified version with a stress dependent expression for the soil stiffness.

5.2 Calculation assumptions

As introduced in Chapter 2, rigid piles have a centre of rotation close to $0.8L_{emb}$, i.e. $4D$ for the reference 4.4 m diameter pile with an L/D-ratio of 5. Calculations using MPile (see Appendix D) also indicate a centre of rotation of about $0.8L$. Furthermore, a linear pile deflection is assumed, i.e. the mono-pile is considered infinitely stiff. As indicated by MPile calculations (see Appendix D) this is a decent estimation, although pile bending in the order of several degrees can be seen.

The maximum lateral bearing capacity of the pile is referred to as the load cap. For a high initial stiffness a plateau is visible in the load-displacement results as shown e.g. in Appendix D.

5.3 Default API

Although the API [6] suggests in-situ soil investigation and laboratory soil tests, the use of soil parameters derived from in-situ soil investigation is not explicitly requested. It is assumed the p-y method gives a sufficiently accurate prediction of the lateral bearing capacity based on the currently available empirical relations.

The parameter k representing soil stiffness suggested by the API for medium dense sand (or sand with a peak φ equal to about 36°) equal to $4.4{\cdot}10^4$ kN/m^3. Figure 5.1 plots the lateral bearing capacity against a normalized lateral pile deflection for both experimental results and default value for k.

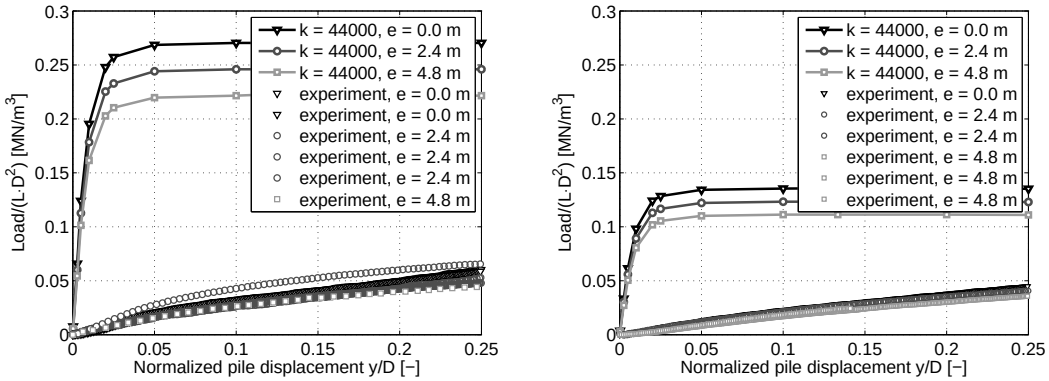

(a) $D = 2.2$ m **(b)** $D = 4.4$ m

Figure 5.1 Comparison of experimental results and lateral bearing capacity conform the API for default soil stiffness $k = 44000$ kN/m^3

A significant overestimation of initial stiffness is shown. The experimental results lack a cap for displacements up to $0.25D$. However, the API formulation reaches a limiting load within $0.1D$. To obtain a better fit of the API estimation with the experimental data, a modification of the k based on triaxial compression test results is suggested.

5.4 Modified API

The k parameter of the fine medium dense sand used for ng experiments is derived from triaxial compression tests. These triaxial compression tests have been performed at an effective stress level of 500 kPa. An overview of the executed triaxial tests is given in Appendix H. The σ_1 - σ_3 required for determining the E_{50} is 700 $\pm$ 50 kPa. The corresponding strain ε equals about 0.46%. 0.46% of the total sample height equals 0.50 mm. This leads to an E_{50} of 1500 $\pm$ 100 kPa or a corresponding k value of about 1400 kN/m^3. The stiffness of the sand for model pile tests is significantly different from the default API value. Figure 5.2 presents the results based on the modified k and shows an improvement compared to the original formulation shown in Figure 5.1.

Still an overestimation of the initial stiffness is present comparing the modified API method with the experimental results. However, the 500 kPa cell pressure at which the triaxial compression tests have been performed equates to a depth of about 31 m for a soil density of 16 kN/m^3. The mono-pile foundation only is installed to a depth of 22 m. Therefore, the $k = 1400$ kN/m^3 is not entirely representative for this mono-pile foundation. In order to further improve the still marginal performance of the modified formulation of the API, a stress dependent, or depth dependent $k(z)$ is introduced.

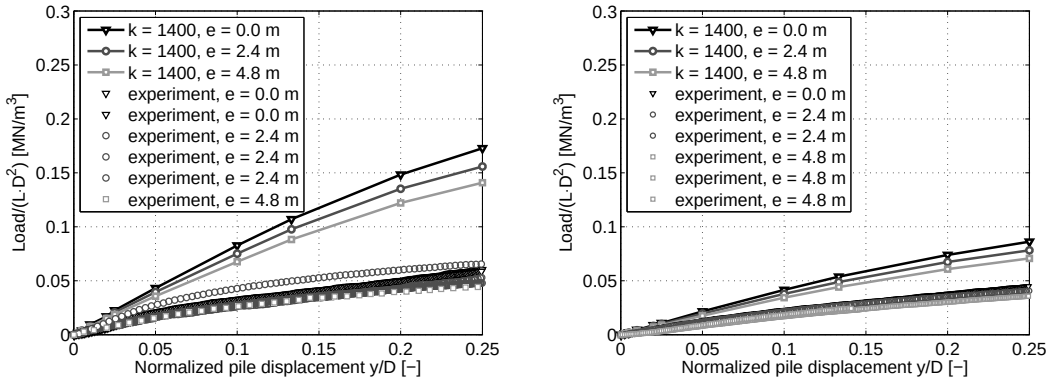

(a) $D = 2.2$ m **(b)** $D = 4.4$ m

Figure 5.2 Comparison of experimental results and lateral bearing capacity conform the API with adapted soil stiffness $k = 1400$ kN/m^3

5.5 Stress dependent formulation

Rather than selecting the E_{50} for a single stress level, the E_{50} is varied using the well known equation of [29]. Hereby, the depth dependent k as shown in Equation 5.1 is obtained. This modification has been suggested before, e.g. by [52]. For current research the stiffness as function of depth as shown in Figure 5.3 is used:

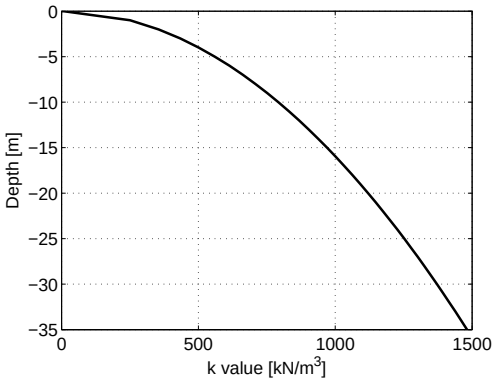

Figure 5.3 The increase of soil stiffness with increasing depth

$$k(z) = k_{500\text{kPa}} \left(\frac{z\gamma}{500\text{kPa}} \right)^n \tag{5.1}$$

Where $k(z)$ in kN/m^3 is the depth dependent soil stiffness, $k(500kPa)$ in kN/m^3 is the stiffness measured at the reference stress level of 500 kPa, z in m the depth and γ the specific weight in kN/m^3. For sand the exponent $n = 0.5$ can be taken. This modification improved the quality of the API p-y method considerably, as shown in Figure 5.4.

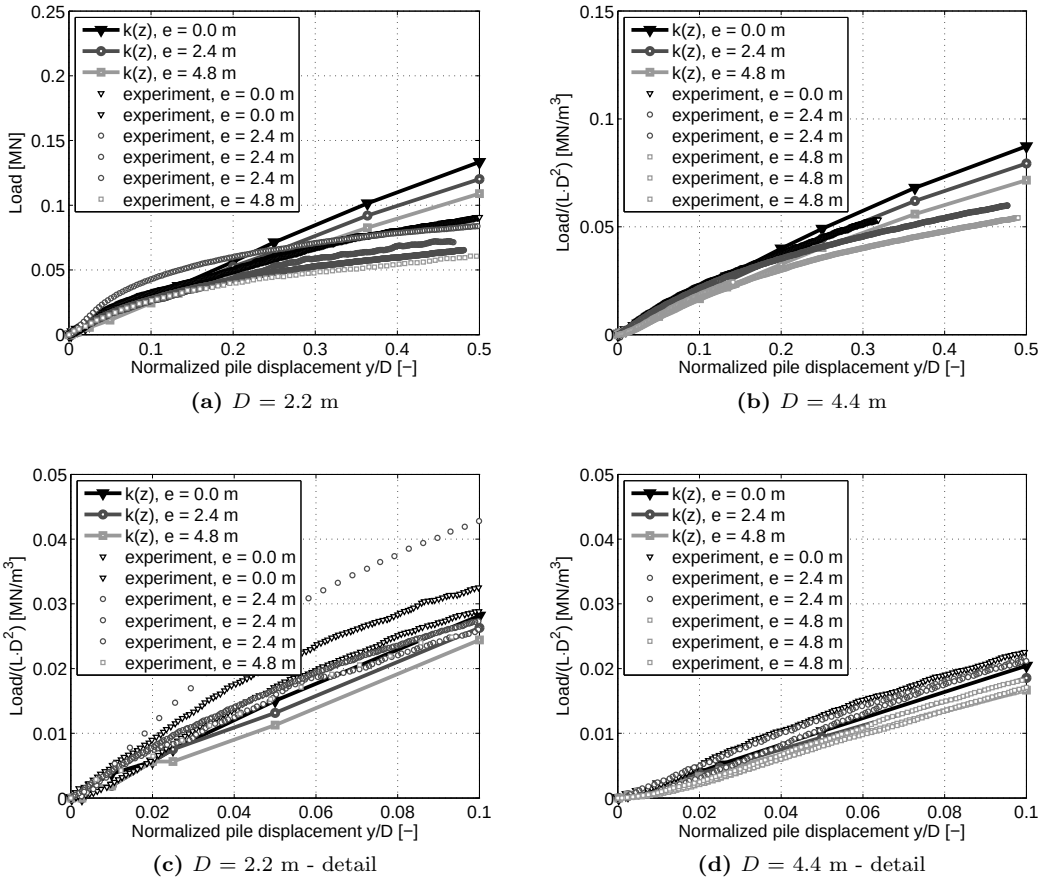

(a) $D = 2.2$ m

(b) $D = 4.4$ m

(c) $D = 2.2$ m - detail

(d) $D = 4.4$ m - detail

Figure 5.4 Comparison of experimental results and lateral bearing capacity conform the API with adapted soil stiffness k as function of depth z

A proper estimation of the experimental results is found using the stress-dependent API formulation in which soil properties are incorporated. However, for displacements $>0.25D$ still an over-estimation of experimental results is found.

5.6 Effect of adapted stiffness on the p-y curves

The p-y curves form the backbone of the lateral bearing capacity calculations as suggested by the API. Figure 5.5 reveals the effect of stiffness k modification at 5 and 11 m below soil surface level.

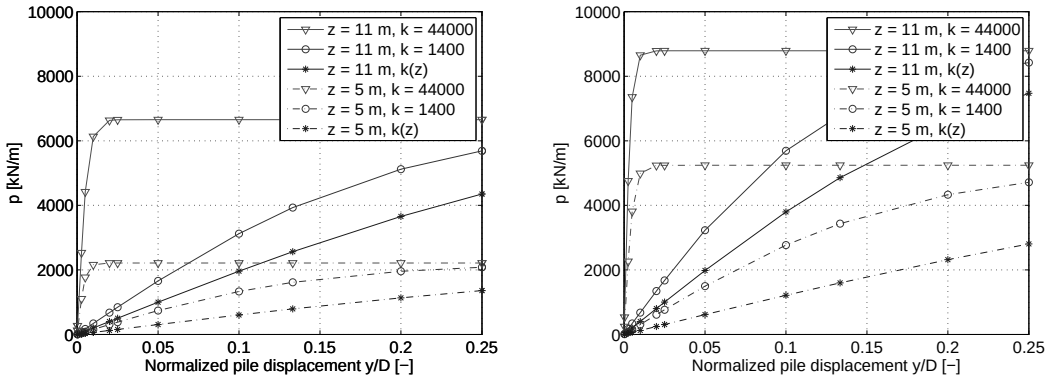

(a) $D = 2.2$ m **(b)** $D = 4.4$ m

Figure 5.5 Influence of soil stiffness k on p-y curves

5.7 Conclusions

The results of the experiments have been compared with the calculated bearing capacity from the default and modified API method. The modified API method has a correction term for the stress dependency of the soil stiffness. The initial stiffness response is largely over predicted with the default relation between initial soil density and soil strength. The results already dramatically improve if the secant stiffness E_{50} from the laboratory tests is used instead. Even better predictions are obtained if the latter stiffness is adapted to a stress dependent, i.e. depth dependent, stiffness relation of [29]. For the 2.2 m diameter pile the p-y method in current adapted form underestimates the lateral bearing capacity by up to 50% for displacements up to $0.1D$. Displacements of the 4.4 m diameter pile up to $0.1D$ can be predicted with about 25% accuracy. Differences in results between the p-y method for both 2.2 m and 4.4 m diameter piles underlines the fact that further research into the applicability of the p-y method and diameter dependency of lateral bearing capacity is needed.

Chapter 6

OWEZ Field Data Analysis

For the force controlled cyclic ng experiments, displacements of about $0.25D$ were prescribed. Mud line displacements from available OWEZ field data will be compared to soil surface displacements of model pile tests.

6.1 Field data analysis

Two OWEZ wind turbines have been equipped with measurement devices such as accelerometers, anemometers and other devices recording nacelle and rotor operational parameters. The North-South (NS) and East-West (EW) acceleration signals in the base of the tower, located 6.6 m above the transition piece, will be analysed. This analysis consists of filtering and double integration of the acceleration signal (given in m/s^2) to obtain displacements in m. This data analysis is performed using MatLab [88] and more detailed information is presented in Appendix G.

6.1.1 Assumptions

The bolted connection between tower and transition piece is able to transfer bending and torsional moments and is located 11.7 m above sea level. The grouted connection between transition piece and mono-pile foundation is assumed to be able to transfer moments as well. The accelerometer is installed about 34 m above the mud line. Since the centre of rotation is present at $4D$ below mud line level, the mud line displacement is about 0.5 times the accelerometer displacement.

6.1.2 Loading conditions

The period analysed is 20–24 November 2008. On the 20th and 21st the wave height and wind speed respectively were in the order of 5–7 m and 15–20 m/s. The other days more calm wind and sea conditions were present.

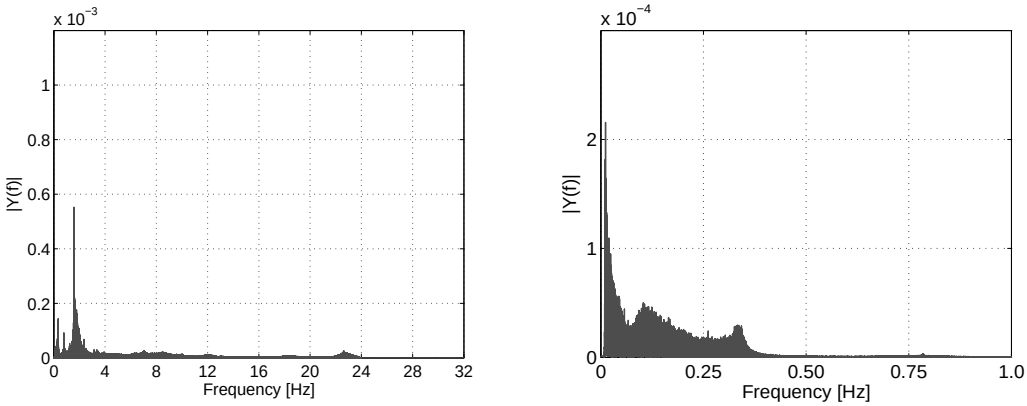

(a) Accelerations, NS **(b)** Displacements and velocities, NS

Figure 6.1 FFT spectra of NS accelerations and displacements

6.2 Results and remarks

Accelerations and velocities The acceleration data and calculated velocities are in the order of 0.1–1.0 m/s^2 and 0.05 m/s for either NS or EW loading direction.

Displacements The total maximum displacement at mud line level during the 20th and 21st of November was 9 cm from the origin, which is about $0.02D$. The information shown in Figures 6.3a and 6.3b corresponds to a height of 34 m above mud line level.

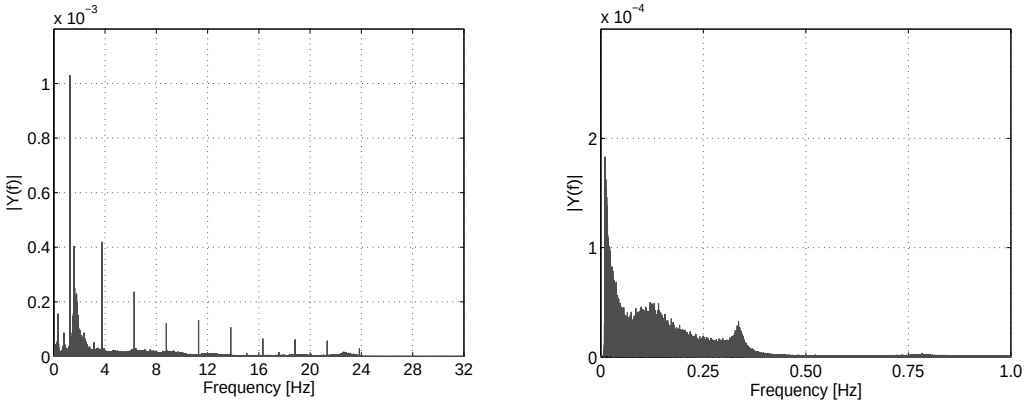

(a) Accelerations, EW **(b)** Displacements and velocities, EW

Figure 6.2 FFT spectra of EW accelerations and displacements

The *ng* model pile test displacements of up to $0.2D$ are about 10 times larger than the $0.02D$ found for field loading conditions as present on the 20th and 21st of November 2008. Higher wind speeds or higher waves can occur and therefore the lateral pile deflection at mud line can be larger, e.g. up to 0.03–$0.04D$, which still is in agreement with the maximum

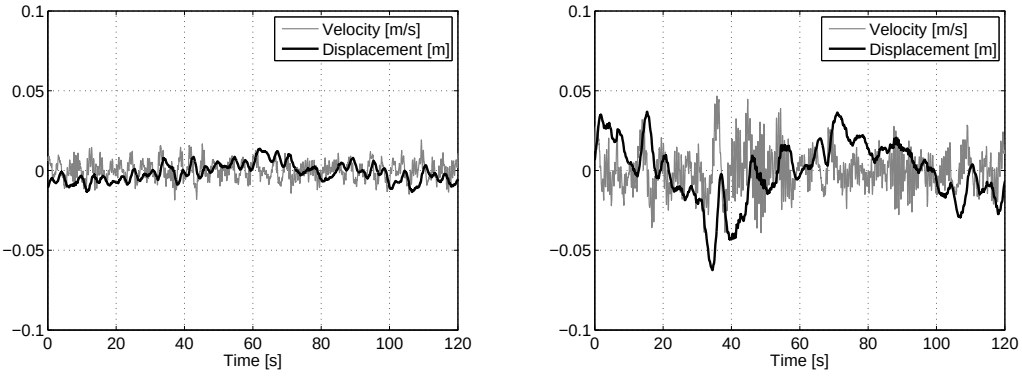

(a) NS **(b)** EW

Figure 6.3 Example of NS and EW velocities and displacements

pile rotation of 0.5° (for a 4.4 m diameter pile with an L/D-ratio of 6) as suggested by the GL [34].

The field displacements occur at a frequency of 0.01–0.4 Hz and about 0.1 and approximately 0.4 Hz are peak frequencies. Loads with a period of 3–8 s, i.e. 0.333–0.125 Hz, are caused by waves. The operational and maximum rpm are 16.1 and 18.4 respectively, which leads to 0.268 Hz and 0.301 Hz respectively. The effect of a blade temporarily shielding the tower from wind would lead to frequencies of 0.81 and 0.92 Hz respectively and is negligible compared to the total movement of the tower or foundation for the analysed period and loading conditions.

Although the currently available data does not distinguish between wind and marine loads, it is possible to determine pile displacements under different conditions. A calm sea state and <2 Bft winds will result in small pile movements and displacements. A rough sea state with high waves and high wind speeds will result in larger pile displacements. After analysing pile displacements for several loading conditions a better (extrapolated) prediction can be made for pile displacements under severe sea state conditions. This is an important field of research as small amplitude cyclic loads with a relative high frequency of about 0.3 Hz might lead to pore pressure build-up and low frequency waves of about 0.1 Hz are expected to have a much greater effect on pile displacements. It is therefore recommended to accommodate an experimental programme with the pile displacements as derived from these field data.

Chapter 7

Conclusions and Recommendations

7.1 Conclusions

In current engineering practice >2 m diameter mono-piles are designed using design standards that rely on the p-y method for lateral loading. This p-y method was derived from 0.61 m diameter 21.0 m long slender piles (L/D-ratio = 34.4) and has not been validated for rigid piles with a diameter >2 m. In order to investigate the validity of the p-y method for large diameter rigid mono-piles a new test setup for the geotechnical centrifuge has been designed. The setup is capable of laterally loading of model piles using displacement or load control. Both static and cyclic loads up to 0.1 Hz can be applied. In addition two prototype diameter mono-piles with an L/D-ratio of 5 and diameters of 2.2 m and 4.4 m have been scaled to model dimensions with according flexural stiffness whilst keeping a reasonable scaling of the pile geometry.

The new setup has been used to conduct 11 experiments which study the influence of pile diameter and load excentricity on the lateral bearing capacity and tangent and secant stiffness response by means of static and cyclic loading schemes.

The properties of the sand have been determined in laboratory tests. The minimum and maximum porosity are $n_{min} = 0.324$ and $n_{max} = 0.475$. Triaxial compression tests on dry sand and saturated sand (with a Skempton B-value of 0.95) showed a peak friction angle of 35° and a $E_{50} = 1400$ kPa. The reloading stiffness is 2200 kPa.

An increase in pile head displacement or pile rotation leads to an increase in lateral static capacity. However, no ultimate lateral bearing capacity p_{ult} was found in these experiments where pile head displacements up to $0.9D$ have been applied.

An increase in load excentricity leads to a reduction of static capacity and lower initial stiffness. A load excentricity of 4.8 m above soil level compared to 0.0 m, results in a decrease of about 20%. This reduction in capacity can be approximated by $(L_{emb} \cdot F)/(L_{emb} + e)$.

In the cyclic tests 90% of the increase in stiffness is gained in the first 20 cycles. The other 10% gain is accumulated in the remaining 480 cycles. Furthermore, the secant and tangent stiffness of the 4.4 m diameter pile are approximately 4 times higher than the

secant and tangent stiffness for the 2.2 m pile. The tangent stiffness for all load cases is about 1.5 times the secant stiffness and both reach a plateau starting in the 20^{th} cycle up to the last prescribed cycle (500).

Comparing calculated results based on the default API formulation with experimental results, a significant overestimation of the initial stiffness for both the 2.2 m and 4.4 m diameter piles is found. Substituting the default API stiffness parameter k with an E_{50} secant stiffness based on triaxial compression tests of the model sand, a less poor fit is obtained, where the height of the triaxial test sample is taken into account in order to arrive at matching dimensions with the k parameter, i.e. kN/m^3. Only after incorporating a stress dependent formulation for the stiffness parameter k does the API formulation show good agreement with the experimental results. However, further investigation into mono-pile-soil interaction is required.

OWEZ field data from a period in November 2008 have been analysed. The marine conditions in the analysed period are a wave height of 5.0–6.0 m, a wave period in the order of 6.0–8.0 s and a wind speed of about 15–18 m/s. These conditions lead to pile displacements at seabed level up to 10 cm, i.e. about $0.02D$. Displacements of the ng experiments are much larger, but also have a lower stiffness compared to the OWEZ field soil stiffness. A higher initial density therefore is recommended for further research.

7.2 Recommendations

To gain more insight into the soil-pile behaviour of large diameter mono-piles used as foundation for offshore wind turbines it is recommended to perform more advanced experiments.

The nacelle, which has a weight in the order of 300 ton, is located about 100 m above the sea floor. Due to wind and wave loading the entire structure gently sways. Experiments in which the axial load and structure geometry are better represented will deliver a better understanding of offshore wind turbine foundations.

A greater space between strongbox boundary and pile is advised as boundary effects for a laterally loaded pile cannot be considered absent using the current set-up. Either a larger strongbox or additional investigation into the boundary effects are recommended.

Waves, wind and currents load the entire structure from different directions and with varying magnitude. Experiments with a more realistic load spectrum will improve soil-pile interaction predictions for complex loading scenarios.

Improved lateral load control and for rapid load conditions a synchronisation between displacement and load is required.

In order to better quantify the soil behaviour under long term cyclic loading the number of load cycles should be increased dramatically, for instance up to 100000. Additionally, the load spectrum should be adapted to mimic field loading conditions.

Chapter 8

Acknowledgements

This Thesis is the final piece of the puzzle required to complete the study Civil Engineering & Geosciences at the Delft University of Technology. The work has been carried out at Gemeentewerken (Public Works) Rotterdam and Delft University of Technology.

During this work I have received advice from many people and I have learnt many things about many topics, from politics to aerospace engineering.

I would like to thank my committee members for answering questions and giving me feedback: Prof. Frits van Tol, Wout Broere, Jelke Dijkstra, Otto Heeres, Dirk Luger and Prof. Kees Willemse. Both Otto Heeres and Henk Brassinga made it possible to perform part of my study at Gemeentewerken Rotterdam. I had a good time with nice, interested and interesting colleagues, thanks.

The model pile tests were carried out using the TU Delft geotechnical centrifuge. I am grateful to Jelke Dijkstra, my daily supervisor, for giving me the opportunity to use this rather unique piece of equipment and for his critical thoughts and healthy dose of sarcasm.

Another thanks goes out to Nuon [63] and ECN [31], from whom I received a truly immense amount of data from two wind turbines of the OWEZ wind farm. Analysing this the data turned out to be challenging and the results are a valuable addition to this work.

Furthermore I would like to thank many friends and acquaintances for opening their minds to discuss many different subjects with me. And last, but certainly not least, my parents and brother for supporting me, regardless of the situation I am in.

April, 2011

Etienne Alderlieste

Bibliography

[1] K. Abdel-Rahman and M. Achmus, *Behaviour of Monopile and Suction Bucket Foundation Systems for Offshore Wind Energy Plants*, in 5th International Engineering Conference, Sharm El-Sheikh, Egypt, 2006.

[2] M. Achmus, K. Abdel-Rahman, and Y.-S. Kuo, *Behaviour of Large Diameter Monopiles Under Cyclic Horizontal Loading*, in ICSGE, 12th International Colloquium on Structural and Geotechnical Engineering, Cairo, Egypt, December 10–12 2007.

[3] M. Achmus, Y.-S. Kuo, and K. Abdel-Rahman, *Behavior of Monopile Foundations Under Cyclic Lateral Load*, Computers and Geotechnics, 36 (2009), pp. 725–735.

[4] Agentschap NL, Ministerie van Economische Zaken, Landbouw en Innovatie. http://regelingen.agentschapnl.nl/content/offshore-wind-energy.

[5] H. G. B. Allersma, *The University of Delft Geotechnical Centrifuge*, in International Conference Centrifuge '94, Singapore, Balkema, Aug 31–Sep 2 1994, pp. 47–52.

[6] American Petroleum Institute, *Recommended Practice for Planning, Designing and Constructing Fixed Offshore Platforms - Working Stress Design, API RP 2A-WSD*, 2000. http://www.api.org.

[7] ——, *Recommended Practice for Planning, Designing and Constructing Fixed Offshore Platforms - Working Stress Design, API RP 2A-WSD - Errata (2008)*, 2008.

[8] S. A. Ashford and T. Juirnarongrit, *Evaluation of Pile Diameter Effect on Initial Modulus of Subgrade Reaction*, Journal of Geotechnical and Geoenvironmental Engineering, 129 (2003), pp. 234–242.

[9] M. Ashour, G. Norris, and P. Pilling, *Lateral Loading of a Pile in Layered Soil Using the Strain Wedge Model*, Journal of Geotechnical and Geoenvironmental Engineering, 124 (1998), pp. 303–315.

[10] P. K. Banerjee and T. G. Davis, *The Behaviour of Axially and Laterally Loaded Single Piles Embedded in Non-Homogeneous Soils*, Géotechnique, 28 (1978), pp. 309–326.

[11] Y. O. Barton and W. D. L. Finn, *Lateral Pile Response and p-y Curves From Centrifuge Tests*, in 15th Annual Offshore Technology Conference, OTC, Houston, Texas, USA, May 1983.

[12] L. Bekken, *Lateral Behavior of Large Diameter Offshore Monopile Foundations For Wind Turbines*, Master's thesis, Delft University of Technology, Faculty of Civil Engineering and Geosciences, 2009.

[13] Belwind Offshore Energy. http://www.belwind.eu.

[14] J. L. Bijnagte and H. J. Luger, *Manual MPile - Analysis of Piles and Pile Groups, version 4.2.3.1*, 2009. Delft GeoSystems, http://www.delftgeosystems.nl.

[15] L. Brant and H. I. Ling, *Centrifuge Modeling of Piles Subjected to Lateral Loads*, in Soil Stress-Strain Behaviour: Measurement, Modeling and Analysis. Geotechical Symposium in Roma, Italy, March 2006.

[16] J. Brinch Hansen, *The Ultimate Resistance of Rigid Piles Against Transversal Forces*, (1961). Akademiet for de Tekniske Videnskaber, Geoteknisk Institut, Geotechnical Institute Denmark, Bulletin no. 12, Copenhagen.

[17] British Standard Institution, *Methods of Test for Soils for Civil Engineering Purposes. Shear Strength Tests (Total Stress), BS1377, part 7, 1990*, 1990. http://www.bsigroup.com.

[18] K. Brødbæk, M. Møller, S. Sørensen, and A. Augustesen, *Review of p-y Relationships in Cohesionless Soil*, (2009). Aalborg University, Department of Civil Engineering, DCE Technical Report No. 57.

[19] B. B. Broms, *Lateral Resistance of Piles in Cohesionless Soil*, Journal of the Soil Mechanics and Foundation Divisions, 90 (1964), pp. 123–156.

[20] N. H. Christensen, *Model Tests with Transversally Loaded Rigid Piles in Sand*, (1961). Akademiet for de Tekniske Videnskaber, Geoteknisk Institut, Danish Geotechnical Institute, Bulletin no. 12, Copenhagen.

[21] W. R. Cox, L. C. Reese, and B. R. Grubbs, *Field Testing of Laterally Loaded Piles in Sand*, in Proceedings of the 6th Offshore Technology Conference, OTC 2079, Houston, Texas, USA, May 6–8 1974.

[22] W. H. Craig, *The Seven Ages of Centrifuge Modelling*, (2001). Workshop at Monte Verita on Constitutive and Centrifuge Modelling: Two Extremes.

[23] N. N. Davidenkov, *The new Method of the Application of Models to the Study of Equilibrium of Soils*, Journal of Technical Physics, 3 (1933), pp. 31–136. Moscow, in Russian.

[24] E. T. R. Dean, *Offshore Geotechnical Engineering*, Telford, 2010. ISBN: 987-0-7277-3641-3.

[25] N. Dedić, *Analysis of Grouted Connection in Monopile Wind Turbine Foundations Subjected to Horizontal Load Transfers*, 2009.

[26] Det Norske Veritas, *Offshore Standard DNV-OS-J101, Design of Offshore Wind Turbine Structures*, October 2007. http://www.dnv.com.

[27] J. Dührkop and J. Grabe, *Monopilegründungen von Offshore-Windenergieanlagen - Zum Einfluss einer Veränderlichen Zyklischen Lastangriffsrichtung*, Bautechnik, 85 (2008), pp. 317–321.

[28] J. Dührkop, J. Grabe, B. Bienen, D. J. White, and M. F. Randolph, *Centrifuge Experiments on Laterally Loaded Piles with Wings*, in Proceedings of the 7th International Conference on Physical Modelling in Geotechnics, Zürich, 2010, pp. 919–924.

[29] J. M. Duncan and C.-Y. Chang, *Nonlinear Analysis of Stress and Strain in Soils*, Journal of the Soil Mechanics and Foundations Division, 96 (1970), pp. 1629–1653.

[30] Enercon. http://www.enercon.de.

[31] Energy Research Centre of the Netherlands, ECN. http://www.ecn.nl.

[32] C.-C. Fan and J. H. Long, *Assessment of Existing Methods for Predicting Soil Response of Laterally Loaded Piles in Sand*, Computers and Geotechnics, 32 (2005), pp. 274–289.

[33] J. Garnier, C. Gaudin, S. M. Springman, P. Culligan, D. Goodings, D. Konig, B. Kutter, R. Phillips, M. F. Randolph, and L. Thorel, *Catalogue of Scaling Laws and Similitude Questions in Geotechical Centrifuge Modelling*, International Journal of Physical Modelling in Geotechnics, 3 (2007), pp. 01–23.

[34] Germanischer Lloyd, *Guideline for the Certification of Offshore Wind Turbines*, 2005. http://www.gl-group.com.

[35] N. Gerolymos, S. Escoffier, G. Gazetas, and J. Garnier, *Numerical Modeling of Centrifuge Cyclic Lateral Pile Load Experiments*, Earthquake Engineering and Engineering Vibration, 8 (2009), pp. 61–76.

[36] J. Helm, J. Laue, and T. Triantafyllidis, *Zur Verformungsentwicklung von Oden Unter Zyklischer Beanspruchung*, Bautechnik, 77 (2000), pp. 405–415.

[37] A. Hettler, *Verschiebung Starrer und Elastischer Gr"undungskörper in Sand bei Monotoner und Zyklischer Belastung*, 1981. Ver"offentlichungen des Institutes für Bodenmechanik und Felsmechanik der Universität Fridericiana in Karlsruhe, Deutschland, Heft 90.

[38] ——, *Horizontal Belastete Pfähle mit Nichtlinearer Bettung in Körnigen Böden*, 1986. Veröffentlichungen des Institutes für Bodenmechanik und Felsmechanik der Universität Fridericiana in Karlsruhe, Deutschland, Heft 102.

[39] Japanese Geotechnical Society, *Soil Testing Standards, Test Methods for the Minimum and Maximum Densities of Sands*, 1996. In Japanse.

[40] T. Juirnarongrit and S. A. Ashford, *Effect of Pile Diameter on the Modulus of Sub-Grade Reaction*, 2005. Report no. SSRP-2001/22, Department of Structural Engineering, University of California, San Diego.

[41] R. T. Klinkvort and O. Hededal, *Centrifuge Modelling of Offshore Monopile Foundation*, in ISFOG, Frontiers in Offshore Geotechnics II, Perth, Australia, Taylor & Francis Group, November 2011, pp. 581–586.

[42] R. T. Klinkvort, C. T. Leth, and O. Hededal, *Centrifuge Modelling of a Laterally Cyclic Loaded Pile*, in The 7th International Conference on Physical Modelling in Geotechnics, 2010, pp. 959–964.

[43] S. Kumar, L. Lalvani, and M. Omar, *Nonlinear Response of Single Piles in Sand Subjected to Lateral Loads Using k_{hmax} Approach*, Geotechnical and Geological Engineering, 24 (2006), pp. 163–181.

[44] M. Laman, G. J. W. King, and E. A. Dickin, *Three-dimensional Finite Element Studies of the Moment-carrying Capacity of Short Pier Foundations in Cohesionless Soil*, Computers and Geotechnics, 25 (1999), pp. 141–155.

[45] C. LeBlanc, *Design of Offshore Wind Turbine Support Structures - Selected Topics in the Field of Geotechnical Engineering*, PhD thesis, Department of Civil Engineering, Aalborg University, Denmark, 2009.

[46] C. LeBlanc, G. T. Houlsby, and B. W. Byrne, *Response of Stiff Piles in Sand to Long-term Cyclic Lateral Loading*, Géotechnique, 60 (2010), pp. 79–90.

[47] K. L. Lee and J. A. Focht, *Cyclic testing of Soil for Ocean Wave Loading Problems*, Marine Geotechnology & Geotechnology, 1 (1976), pp. 305–325.

[48] R. W. Lentz and G. Y. Baladi, *Constitutive Equation for Permanent Strain of Sand Subjected to Cyclic Loading*, Transportation Research Record, 810 (1981), pp. 50–54.

[49] K. Lesny, *Foundations for Offshore Wind Turbines - Tools for Planning and Design*, 2010. ISBN: 978-3-86797-042-6.

[50] K. Lesny, S. G. Paikowsky, and A. Gurbuz, *Scale Effects in Lateral Load Response of Large Diameter Monopiles*, in Proceedings of Sessions of Geo-Denver, Denver, Colorado, USA, Februari 2007. Geotechnical Special Publication no. 158.

[51] K. Lesny and J. Wiemann, *Design Aspects of Monopiles in German Offshore Wind Farms*, in ISFOG, Proceedings of the International Symposium on Frontiers in Offshore Geotechnics, Perth, Australia, September 2005, pp. 383–389.

[52] K. Lesny and J. Wiemann, *Finite-element-modelling of Large Diameter Monopiles for Offshore Wind Energy Converters*, (2006). GeoCongress 2006: Geotechnical Engineering in the Information Technology Age 2006.

[53] Z. Li, S. Haigh, and M. Bolton, *Centrifuge Modelling of Mono-pile Under Cyclic Lateral Loads*, in Proceedings of the 7th International Conference on Physical Modelling in Geotechnics, Zürich, 2010, pp. 965–970.

[54] S.-S. Lin and L.-C. Liao, *Permanent Strains of Piles in Sand due to Cyclic Lateral Loads*, Journal of Geotechnical and Geoenvironmental Engineering, 125 (1999), pp. 798–802.

[55] R. Little and J.-L. Briaud, *Full Scale Cyclic Lateral Load Tests on Six Single Piles in Sand*, (1988).

[56] J. Long and G. Vanneste, *Effects of Cyclic Lateral Loads on Piles in Sand*, Journal of Geotechnical Engineering, 120 (1994), pp. 225–244.

[57] H. Matlock and L. C. Reese, *Generalized Solutions for Laterally Loaded Piles*, Journal of the Soil Mechanics and Foundation Divisions, 86 (1960), pp. 63–91.

[58] M. Miner, *Cumulative Damage in Fatigue*, Journal of Applied Mechanics, (1945).

[59] H.-B. Mühlhaus and I. Vardoulakis, *The Thickness of Shear Bands in Granular Materials*, Géotechnique, 37 (1987), pp. 271–283.

[60] J. M. Murchison and M. W. O'Neill, *Evaluation of P-Y Relationships in Cohesionless Soils*, in Analysis and Design of Pile Foundations. Proceedings of a Symposium in Conjunction with the ASCE National Convention, San Fransisco, California, USA, Oct 1–5 1984, pp. 174–191.

[61] Nederlands Normalisatie-instituut, *NEN 5117 Geotechniek - Bepaling van Schuifweerstands- en Vervormingsparameters van Grond Triaxiaalproef, 1e druk*, 1992. http://www.nen.nl.

[62] G. Norris, *Theoretically Based BEF for Laterally Loaded Pile Analysis*, in Proceedings of the 3rd International Conference on Numerical Methods in Offshore Piling, 1986, pp. 361–386.

[63] Nuon. http://www.nuon.nl.

[64] Offshore Prinses Amalia Wind Farm. http://www.prinsesamaliawindpark.eu.

[65] D. V. Okur and A. Ansal, *Stiffness Degradation of Natural Fine Grained Soils During Cyclic Loading*, Soil Dynamics and Earthquake Engineering, 27 (2007), pp. 843–854.

[66] P. Peralta and M. Achmus, *An Experimental Investigation of Piles in Sand Subjected to Cyclic Lateral Loads*, in Proceedings of the 7th International Conference on Physical Modelling in Geotechnics, Zürich, 2010, pp. 985–990.

[67] E. Phillips, *De l'Equilibre des Solides Elastiques Semblables*, Comptes Rendus de l'Académie des Sciences, Paris, 68 (1869), pp. 75–79.

[68] G. Y. Pokrovsky, *On the Application of Centrifugal Forces for Modelling Earth Works in Clay*, Journal of Technical Physics, 3 (1933), pp. 537–539. Moscow, in Russian.

[69] G. Y. Pokrovsky and I. S. Fedorov, *Studies of Soil Pressures and Soil Deformations by Means of a Centrifuge*, in ISSMFE, 1st International Symposium on Soil Mechanics and Foundation Engineering, Harvard, USA, vol. 1, 1936, p. 70.

[70] H. G. Poulos, *Behaviour of Laterally Loaded Piles - I - Single Piles*, (1971).

[71] H. G. Poulos and E. H. Davis, *Pile Foundation Analysis and Design (Series in Geotechnical Engineering)*, John Wiley & Sons, 1980. ISBN 0-471-02084-2.

[72] M. F. Randolph, *The Response of Flexible Piles to Lateral Loading*, Géotechnique, 31 (1981), pp. 247–259.

[73] ——, *Laterally Loaded Piles - Design Methods and Recent Developments*, (2010). Presentation given as part State-of-the-Art Design of Pile Foundations at Deltares, Delft, the Netherlands.

[74] L. C. Reese, W. R. Cox, and F. Kooper, *Analysis of Laterally-Loaded Piles in Sands*, in Proceedings of the 6th Annual Offshore Technology Conference, OTC 2080, Houston, Texas, USA, 1974.

[75] L. C. Reese and H. Matlock, *Non-dimensional Solutions for Laterally Loaded Piles With Soil Modulus Assumed to be Proportional to Depth*, (1956). Special Publication no. 29.

[76] L. C. Reese and W. F. van Impe, *Single Piles and Pile Grounds Under Lateral Loading*, Balkema, 2001. ISBN: 90 5809 340 90.

[77] P. W. Rowe and W. H. Craig, *Studies of Offshore Caissons Founded on Oosterschede Sand*, in Design and Construction of Offshore Structure, London, Institution of Civil Engineers, 1976, pp. 49–55.

[78] P. Schaumann and C. Böker, *Can Jackets and Tripods Compete with Monopiles*, in Copenhagen Offshore Wind, 26–28 October 2005.

[79] F. Schnaid and G. T. Houlsby, *An Assessment of Chamber Size Effects in the Calibration of In-Situ Tests in Sand*, Géotechnique, 41 (1991), pp. 437–445.

[80] A. N. Schofield, *Cambridge Geotechnical Centrifuge Operations*, Géotechnique, 30 (1980), pp. 227–268.

[81] S. M. Springman (ed.), *Proceedings of the Workshop on Constitutive and Centrifuge Modelling: Two Extremes*, Balkema, The Netherlands, July 2001. ISBN: 90 5809 361 1.

[82] H. E. Stewart, *Permanent Strains from Cyclic Variable Loading Amplitude Loadings*, Journal of Geotechnical Engineering, 112 (1986), pp. 646–660.

[83] H. G. Stuit, *Sand in the Geotechnical Centrifuge*, PhD thesis, Delft University of Technology, Faculty of Civil Engineering, 1995.

[84] A. S. J. Suiker, *Static and Cyclic Loading Experiments on Non-Cohesive Granular Materials*, (1999). Report no. 1-99-DUT-1, Delft University of Technology, Faculty of Civil Engineering.

[85] A. S. J. Suiker, E. T. Selig, and R. Frenkel, *Static and Cyclic Triaxial Testing of Ballast and Subballast*, Journal of Geotechnical and Geoenvironmental Engineering, 131 (2005), pp. 771–782.

[86] R. Taylor (ed.), *Geotechnical Centrifuge Technology*, Blackie, 1995. ISBN 0-7514-0032-7.

[87] K. Terzaghi, *Evaluation of Coefficient of Subgrade Reaction*, Géotechnique, 5 (1955), pp. 297–326.

[88] The MathWorks, *Manual for* MatLab*, r2008b, r2009b*, 2009.

[89] The Wind Power - Wind Turbines and Wind Farms Database. http://www.thewindpower.net/index_en.php.

[90] A. F. Tol, van, *Foundation Engineering and Underground Construction*, 2006. Delft University of Technology, Course CT5330.

[91] A. Verruijt, *Soil Mechanics*, 2001. Delft University of Technology, Course CT2090.

[92] ——, *Offshore Soil Mechanics*, 2006. Delft University of Technology, Course OE4624.

[93] T. Wichtmann, A. Niemunis, and T. Triantafyllidis, *Strain Accumulation in Sand due to Cyclic Loading: Drained Triaxial Tests*, Soil Dynamics and Earthquake Engineering, 25 (2005), pp. 967–979.

[94] ——, *Strain Accumulation in Sand due to Drained Cyclic Loading: on the Effect of Monotonic and Cyclic Preloading (Miner's Rule)*, Soil Dynamics and Earthquake Engineering, 30 (2010), pp. 736–745.

[95] J. Wiemann, K. Lesny, and W. Richwien, *Evaluation of Pile Diameter Effects on Soil-Pile Stiffness*, (2004). DEWEK, Dokumentation der 7th German Wind Energy Konference.

[96] J. Wilkes, J. Moccia, N. Fichaux, J. Guillet, and P. Wilczek, *The European Offshore Wind Industrie - Key Trends and Statistics 2009*, (2010). EWEA, European Wind Energy Association.

[97] Wind Energy Facts. http://www.wind-energy-the-facts.org.

[98] Windmolen Park Egmond aan Zee (OWEZ). http://www.noordzeewind.nl.

[99] D. M. Wood, *Geotechnical Modelling, Applied Geotechnics, Volume 1*, Spon Press, 2005. ISBN: 0-419-23730-5.

Appendices

Appendix A

OWEZ CPT results and borehole logs

This Appendix contains borehole logs and CPT results of a North Sea location used for the OWEZ wind farm. The mono-pile foundation used at this site is introduced in Chapter 1 and further analysed in Chapter 3.

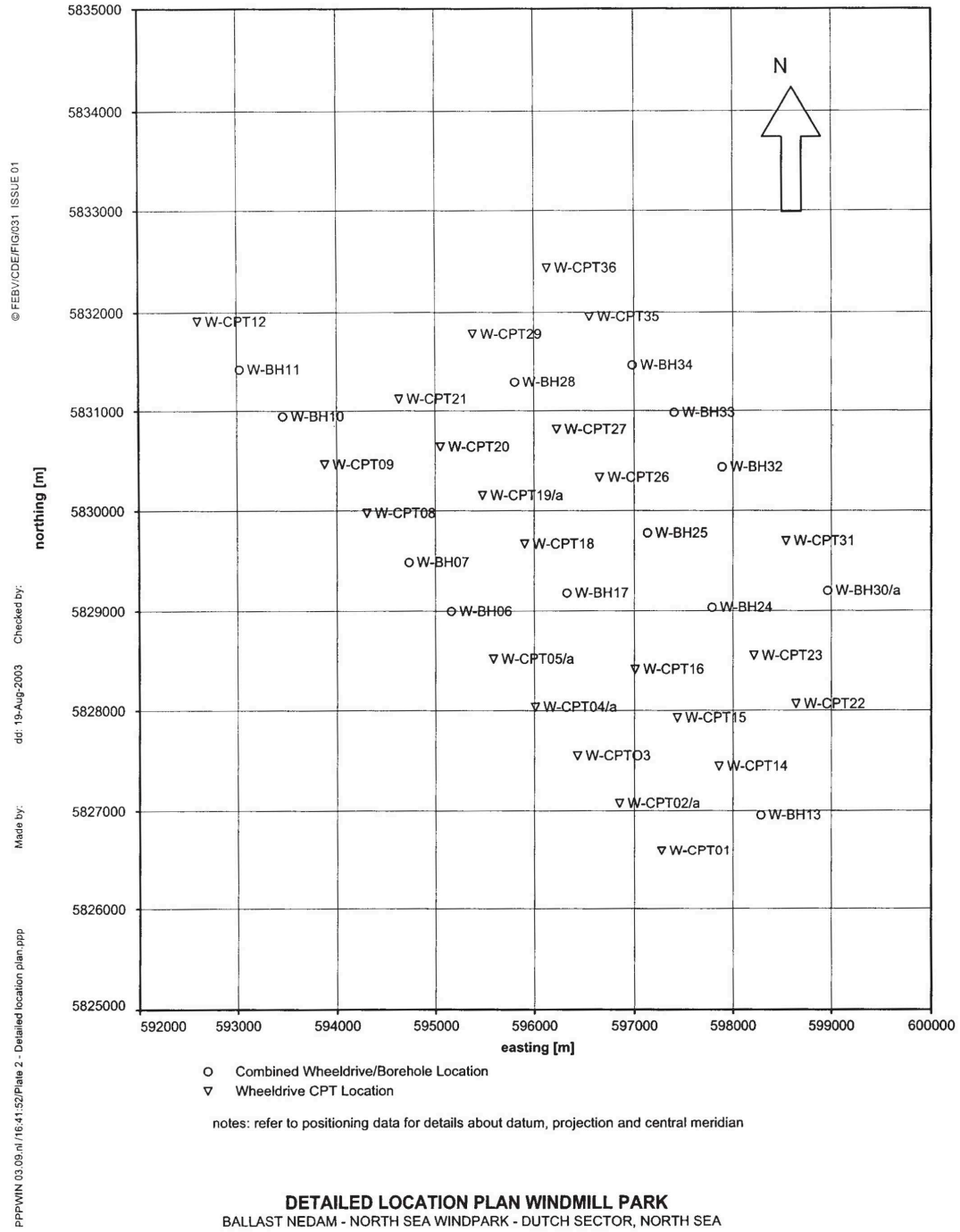
FUGRO
© FEBV/CDE/FIG/031 ISSUE 01
PPPWIN 03.09.ni /16:41:52/Plate 2 - Detailed location plan.ppp
Made by:
dd: 19-Aug-2003
Checked by:
N
northing [m]
5835000
5834000
5833000
5832000
5831000
5830000
5829000
5828000
5827000
5826000
5825000
592000
593000
594000
595000
596000
597000
598000
599000
600000
easting [m]
W-CPT36
W-CPT12
W-CPT35
W-CPT29
W-BH11
W-BH34
W-BH28
W-CPT21
W-BH10
W-BH33
W-CPT27
W-CPT20
W-CPT09
W-BH32
W-CPT26
W-CPT19/a
W-CPT08
W-BH25
W-CPT31
W-CPT18
W-BH07
W-BH17
W-BH30/a
W-BH06
W-BH24
W-CPT05/a
W-CPT23
W-CPT16
W-CPT04/a
W-CPT22
W-CPT15
W-CPT03
W-CPT14
W-CPT02/a
W-BH13
W-CPT01
Combined Wheeldrive/Borehole Location
Wheeldrive CPT Location
notes: refer to positioning data for details about datum, projection and central meridian
DETAILED LOCATION PLAN WINDMILL PARK
BALLAST NEDAM - NORTH SEA WINDPARK - DUTCH SECTOR, NORTH SEA
Report No: N4322/01
Plate 2

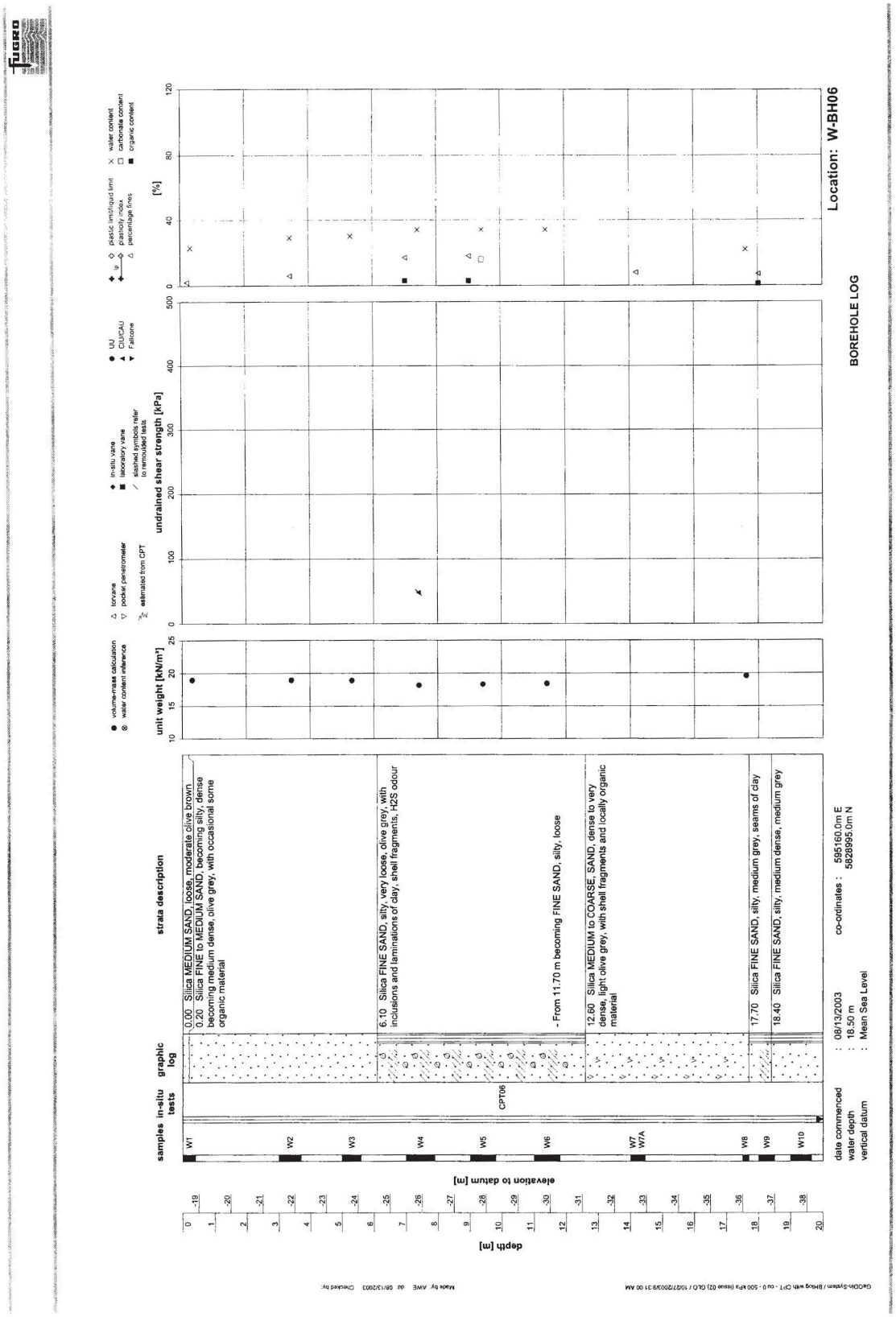
FUGRO
BOREHOLE LOG
Location: W-BH06
Report No.: N4322/01
Plate B1
strata description
graphic log
samples
in-situ tests
unit weight [kN/m³]
undrained shear strength [kPa]
[%]
depth [m]
elevation to datum [m]
0.00 Silica MEDIUM SAND, loose, moderate olive brown
0.20 Silica FINE to MEDIUM SAND, becoming silty, dense becoming medium dense, olive grey, with occasional some organic material
6.10 Silica FINE SAND, silty very loose, olive grey, with inclusions and laminations of clay, shell fragments, H2S odour
- From 11.70 m becoming FINE SAND, silty, loose
12.60 Silica MEDIUM to COARSE, SAND, dense to very dense, light olive grey, with shell fragments and locally organic material
17.70 Silica FINE SAND, silty, medium grey, seams of clay
18.40 Silica FINE SAND, silty, medium dense, medium grey
CPT06
W1
W2
W3
W4
W5
W6
W7
W7A
W8
W9
W10
date commenced : 08/13/2003
water depth : 18.50 m
vertical datum : Mean Sea Level
co-ordinates : 595160.0m E
5828995.0m N

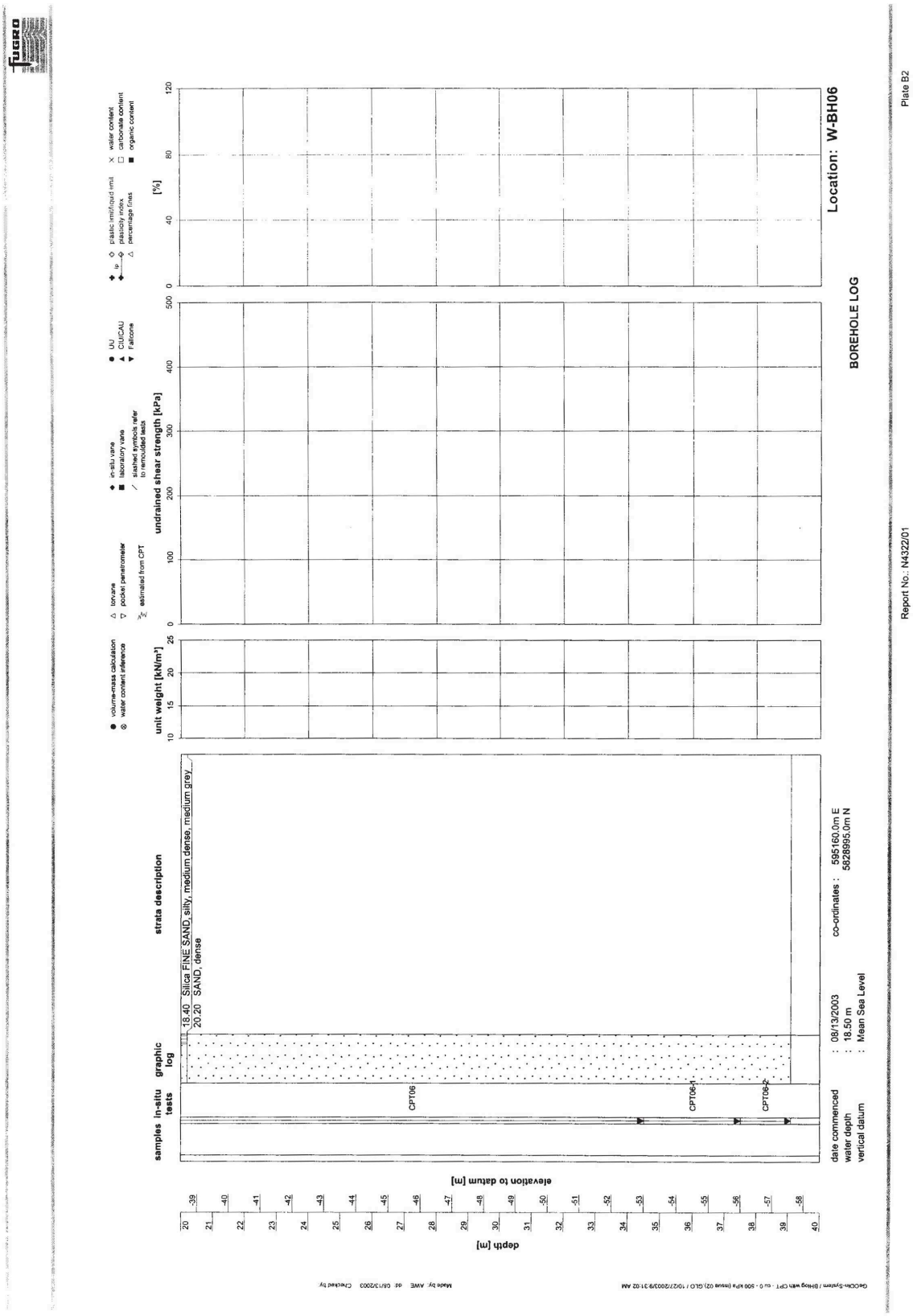
FUGRO
Location: W-BH06
BOREHOLE LOG
Plate B2
Report No.: N4322/01
samples
in-situ tests
graphic log
strata description
18.40 Silica FINE SAND, silty, medium dense, medium grey
20.20 SAND, dense
CPT06
CPT06-1
CPT06-2
date commenced : 08/13/2003
water depth : 18.50 m
vertical datum : Mean Sea Level
co-ordinates : 595160.0m E
5828995.0m N
unit weight [kN/m³]
undrained shear strength [kPa]
[%]
elevation to datum [m]
depth [m]

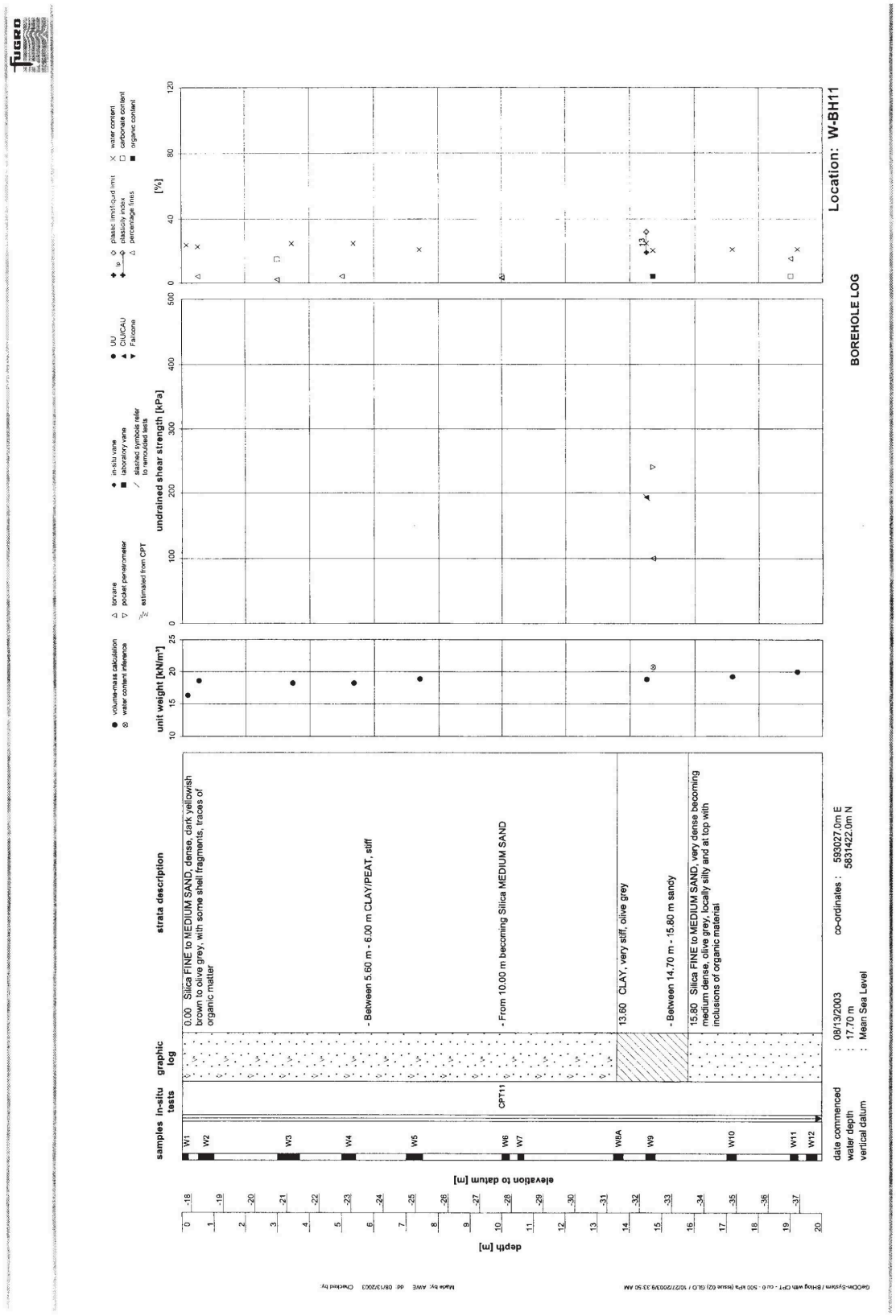
TUGRO
BOREHOLE LOG
Location: W-BH11
Plate B3
Report No.: N4322/01
samples
in-situ tests
graphic log
strata description
unit weight [kN/m³]
undrained shear strength [kPa]
[%]
depth [m]
elevation to datum [m]
0.00 Silica FINE to MEDIUM SAND, dense, dark yellowish brown to olive grey, with some shell fragments, traces of organic matter
- Between 5.60 m - 6.00 m CLAY/PEAT, stiff
- From 10.00 m becoming Silica MEDIUM SAND
13.60 CLAY, very stiff, olive grey
- Between 14.70 m - 15.80 m sandy
15.80 Silica FINE to MEDIUM SAND, very dense becoming medium dense, olive grey, locally silty and at top with inclusions of organic material
CPT11
W1
W2
W3
W4
W5
W6
W7
W8A
W9
W10
W11
W12
date commenced : 08/13/2003
water depth : 17.70 m
vertical datum : Mean Sea Level
co-ordinates : 593027.0m E
5831422.0m N

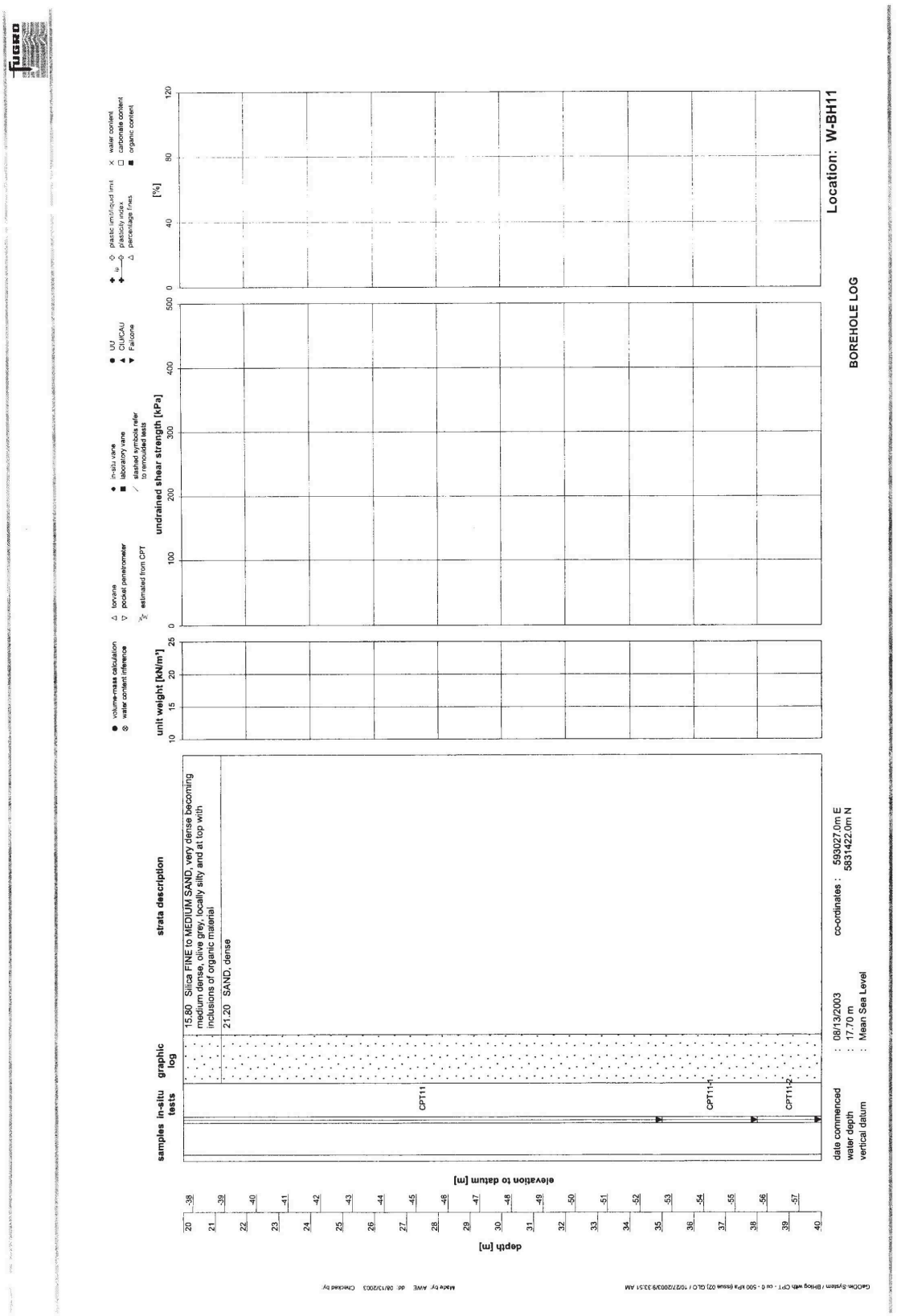
FUGRO
BOREHOLE LOG
Location: W-BH11
Report No.: N4322/01
Plate B4
strata description
15.80 Silica FINE to MEDIUM SAND, very dense becoming medium dense, olive grey, locally silty and at top with inclusions of organic material
21.20 SAND, dense
CPT11
CPT11-1
CPT11-2
data commenced : 08/13/2003
water depth : 17.70 m
vertical datum : Mean Sea Level
co-ordinates : 593027.0m E
5831422.0m N
unit weight [kN/m³]
undrained shear strength [kPa]
[%]
depth [m]
elevation to datum [m]

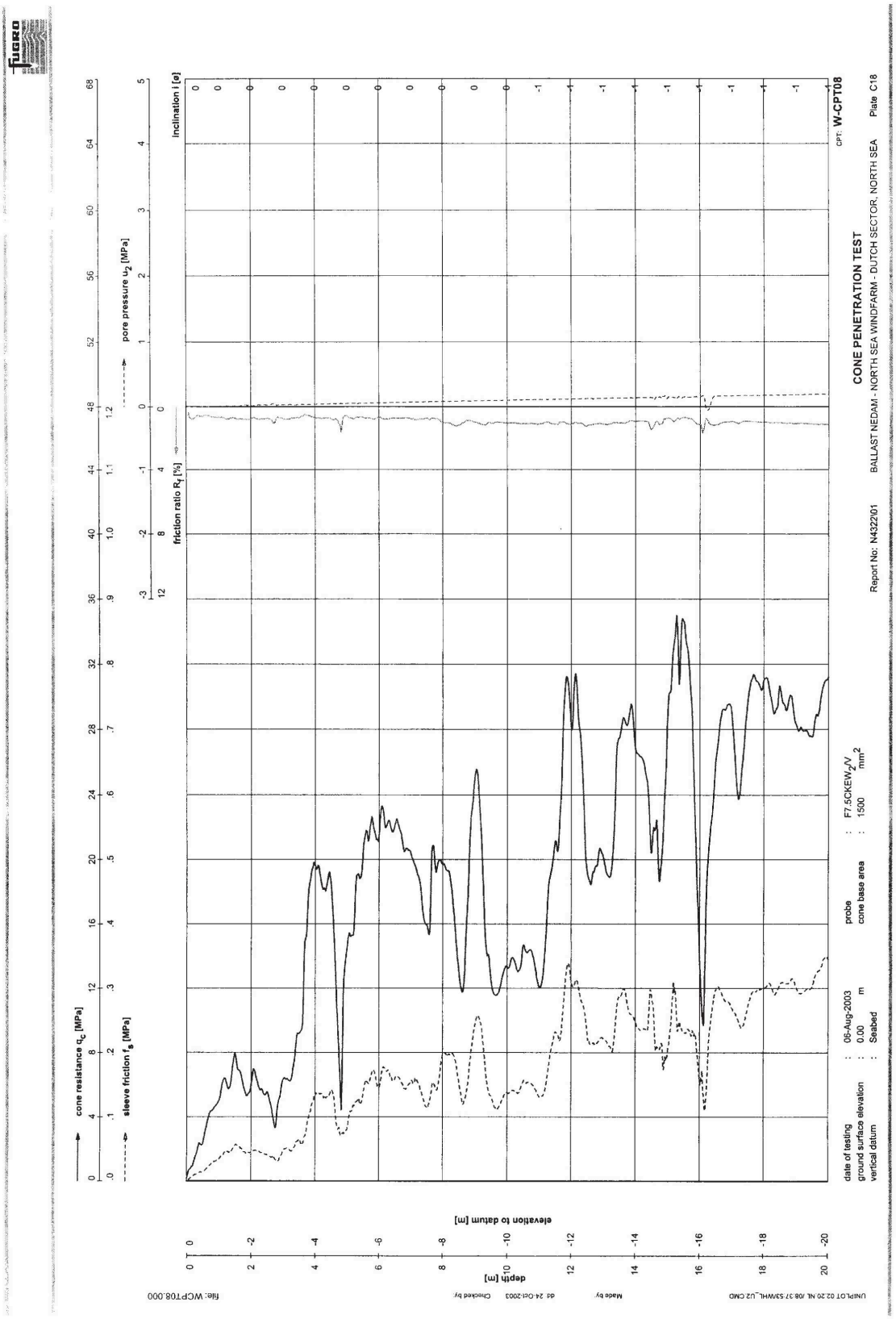
TUGRO
CONE PENETRATION TEST
CPT: W-CPT08
Report No: N4322/01
BALLAST NEDAM - NORTH SEA WINDFARM - DUTCH SECTOR, NORTH SEA
Plate C18
cone resistance q_c [MPa]
sleeve friction f_s [MPa]
pore pressure u_2 [MPa]
friction ratio R_f [%]
inclination i [o]
elevation to datum [m]
depth [m]
date of testing : 06-Aug-2003
ground surface elevation : 0.00 m
vertical datum : Seabed
probe : F7.5CKEW2/V
cone base area : 1500 mm2
Made by
dd. 24-Oct-2003
Checked by
file: WCPT08.000
UNIPLOT 02.20 NL /08:37:53/WHL_U2 CMD

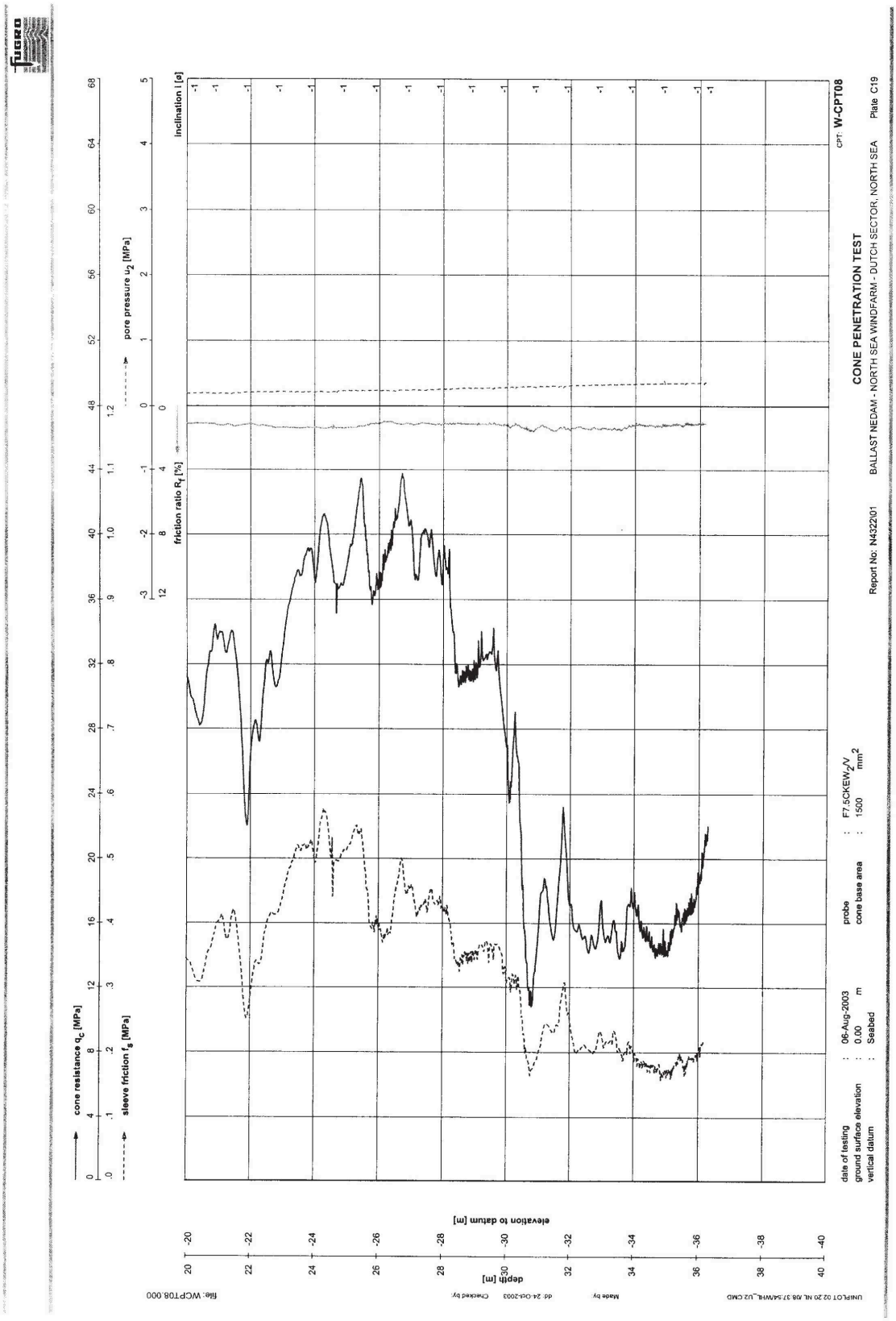
CONE PENETRATION TEST
CPT: W-CPT08
Report No: N4322/01
BALLAST NEDAM - NORTH SEA WINDFARM - DUTCH SECTOR, NORTH SEA
Plate C19
cone resistance q_c [MPa]
sleeve friction f_s [MPa]
friction ratio R_f [%]
pore pressure u_2 [MPa]
inclination i [°]
elevation to datum [m]
depth [m]
date of testing : 06-Aug-2003
ground surface elevation : 0.00 m
vertical datum : Seabed
probe : F7.5CKEW-2-V
cone base area : 1500 mm2
File: WCPT08.000
Checked by:
dd: 24-Oct-2003
Made by:
UNIPLOT 02.20 NL M8.37-SAWHL-U2.CMD

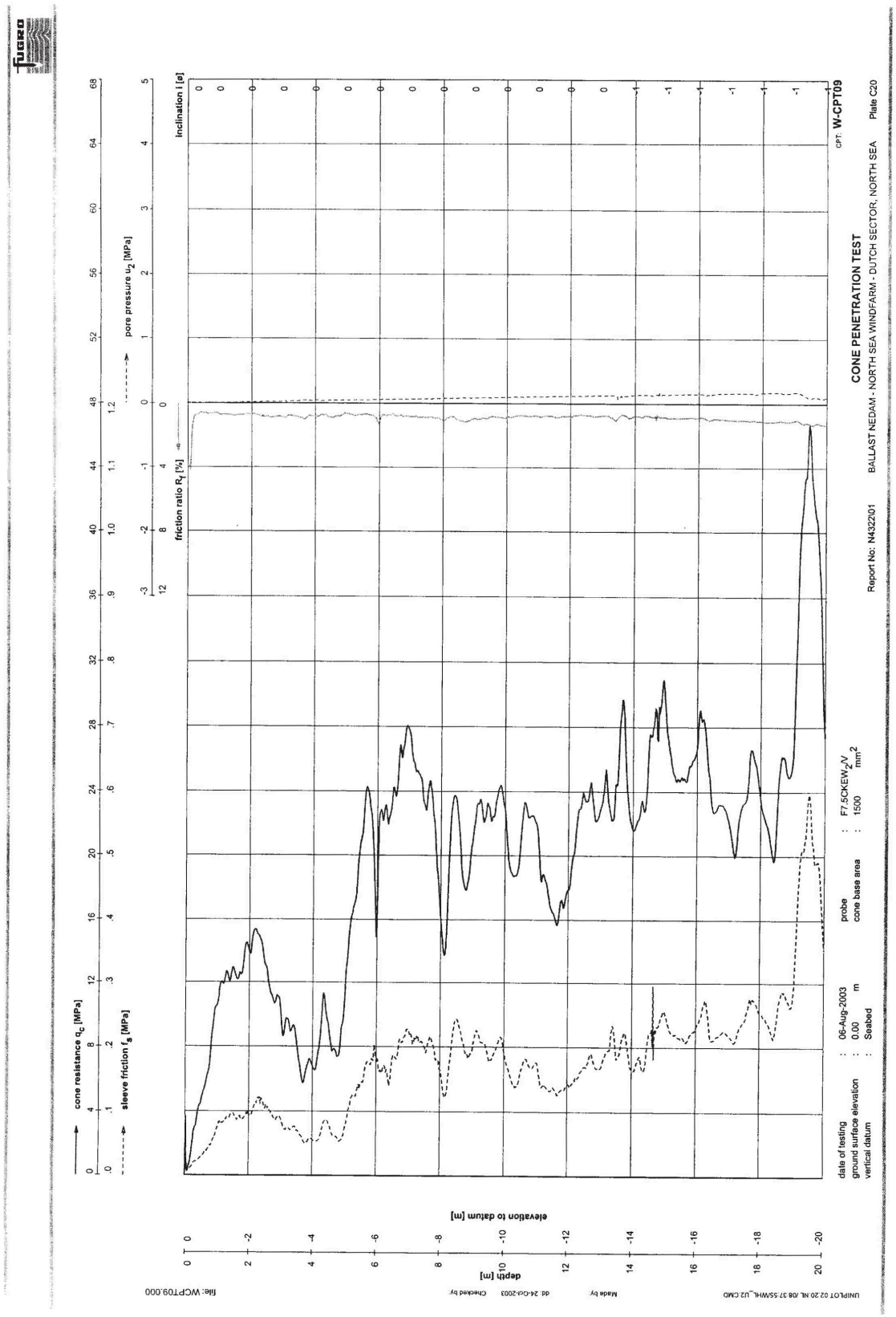
FUGRO
CPT: W-CPT09
CONE PENETRATION TEST
Report No: N432201
BALLAST NEDAM - NORTH SEA WINDFARM - DUTCH SECTOR, NORTH SEA
Plate C20
cone resistance q_c [MPa]
sleeve friction f_s [MPa]
friction ratio R_f [%]
pore pressure u_2 [MPa]
Inclination i [o]
elevation to datum [m]
depth [m]
date of testing : 06-Aug-2003
ground surface elevation : 0.00 m
vertical datum : Seabed
probe : F7.5CKEW-2-V
cone base area : 1500 mm2
Made by:
dd: 24-Oct-2003
Checked by:
File: WCPT09.000
UNIPLOT 02.20 NL /08.37.55/WHL_U2.CMD

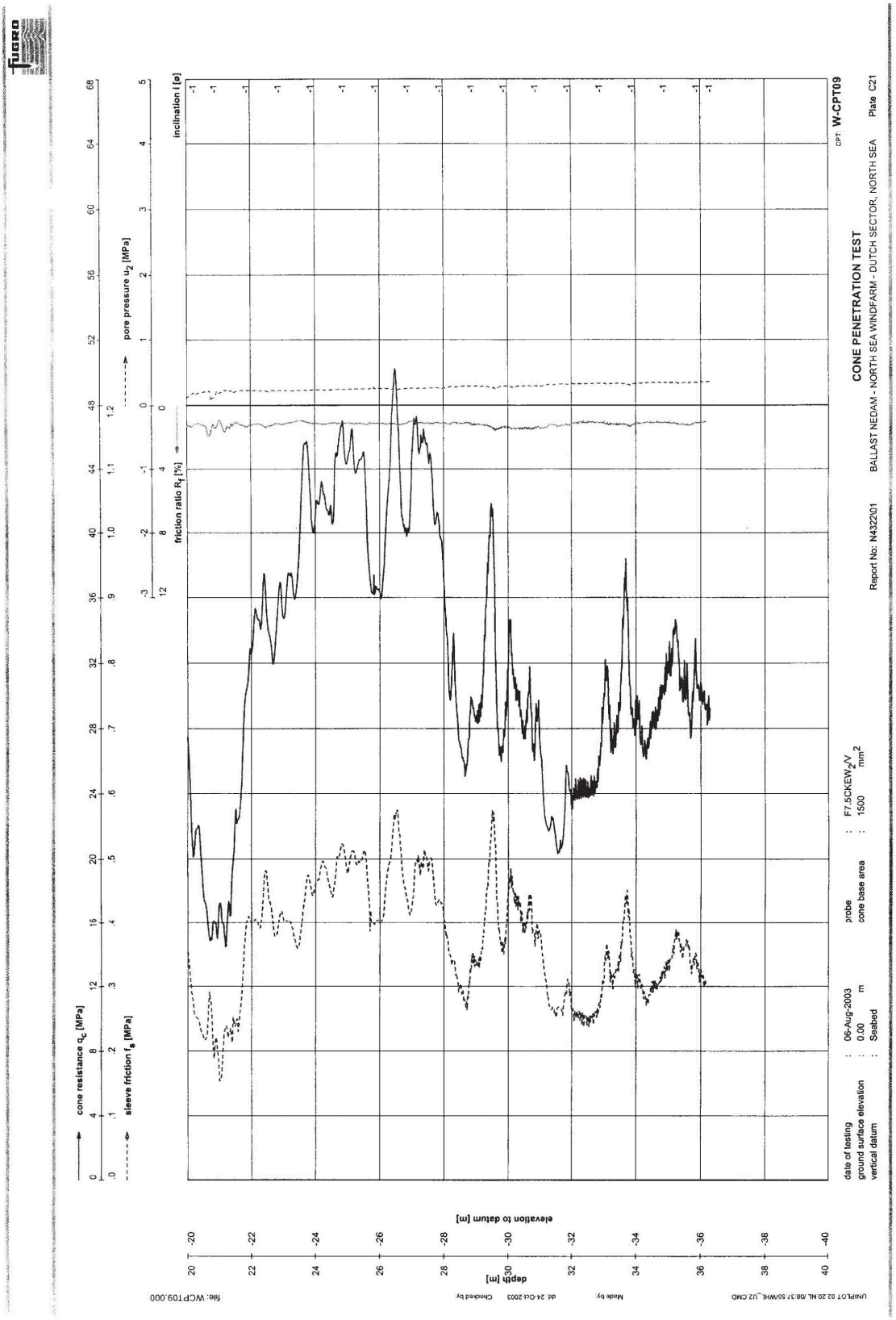
FUGRO
CONE PENETRATION TEST
CPT W-CPT09
Report No: N4322101
BALLAST NEDAM - NORTH SEA WINDFARM - DUTCH SECTOR, NORTH SEA
Plate C21
cone resistance q_c [MPa]
sleeve friction f_s [MPa]
friction ratio R_f [%]
pore pressure u_2 [MPa]
inclination [o]
date of testing : 06-Aug-2003
ground surface elevation : 0.00 m
vertical datum : Seabed
probe : F7.5CKEW2V
cone base area : 1500 mm2
elevation to datum [m]
depth [m]
Made by:
dd. 24-Oct-2003 Checked by:
file: WCPT09.000

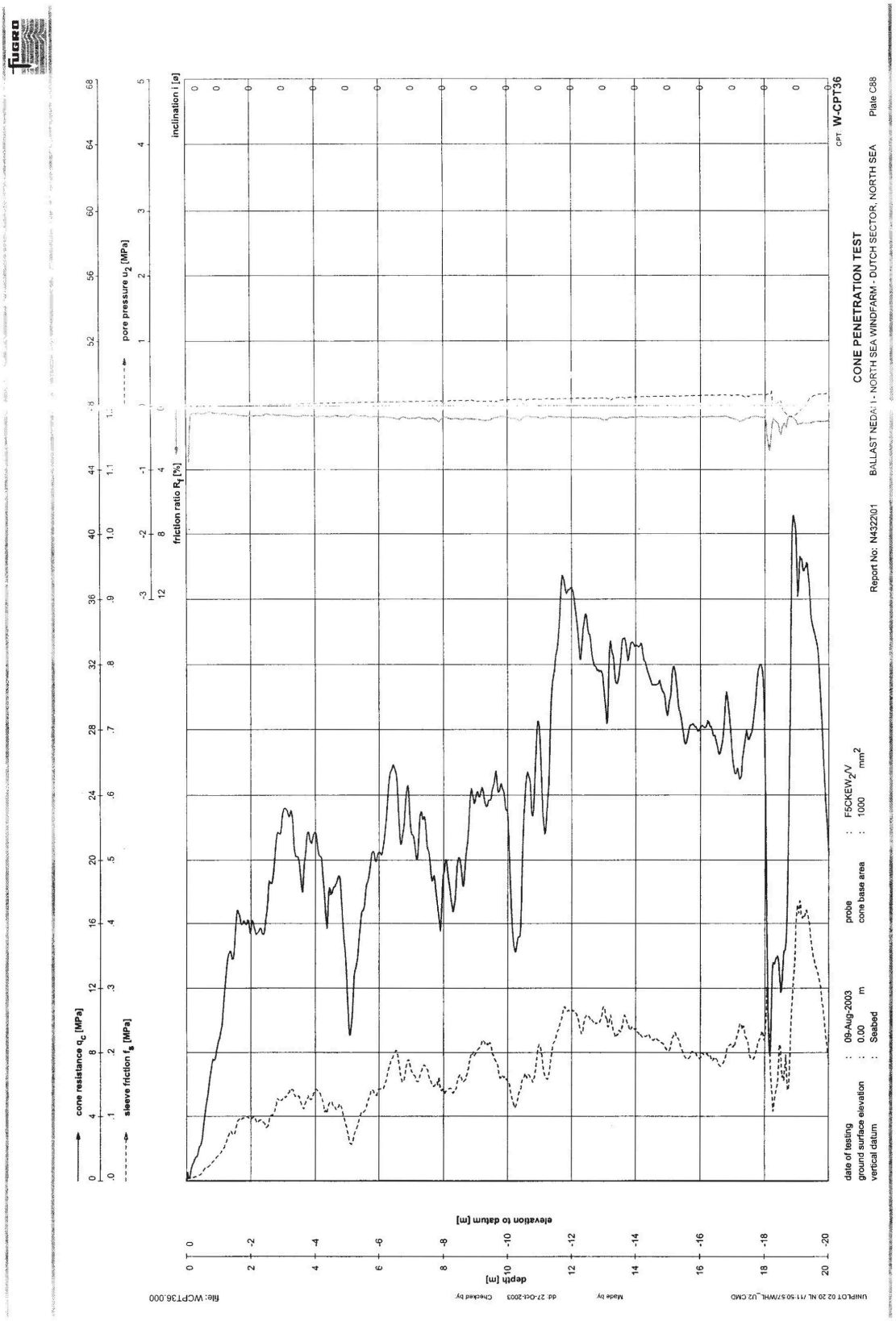
CONE PENETRATION TEST
CPT: W-CPT36
Report No: N4322101
BALLAST NEDAM - NORTH SEA WINDFARM - DUTCH SECTOR, NORTH SEA
Plate C88
cone resistance q_c [MPa]
sleeve friction f_s [MPa]
pore pressure u_2 [MPa]
friction ratio R_f [%]
inclination i [o]
elevation to datum [m]
depth [m]
date of testing : 09-Aug-2003
ground surface elevation : 0.00 m
vertical datum : Seabed
probe : F5CKEW-2-V
cone base area : 1000 mm2
File: WCPT36.000

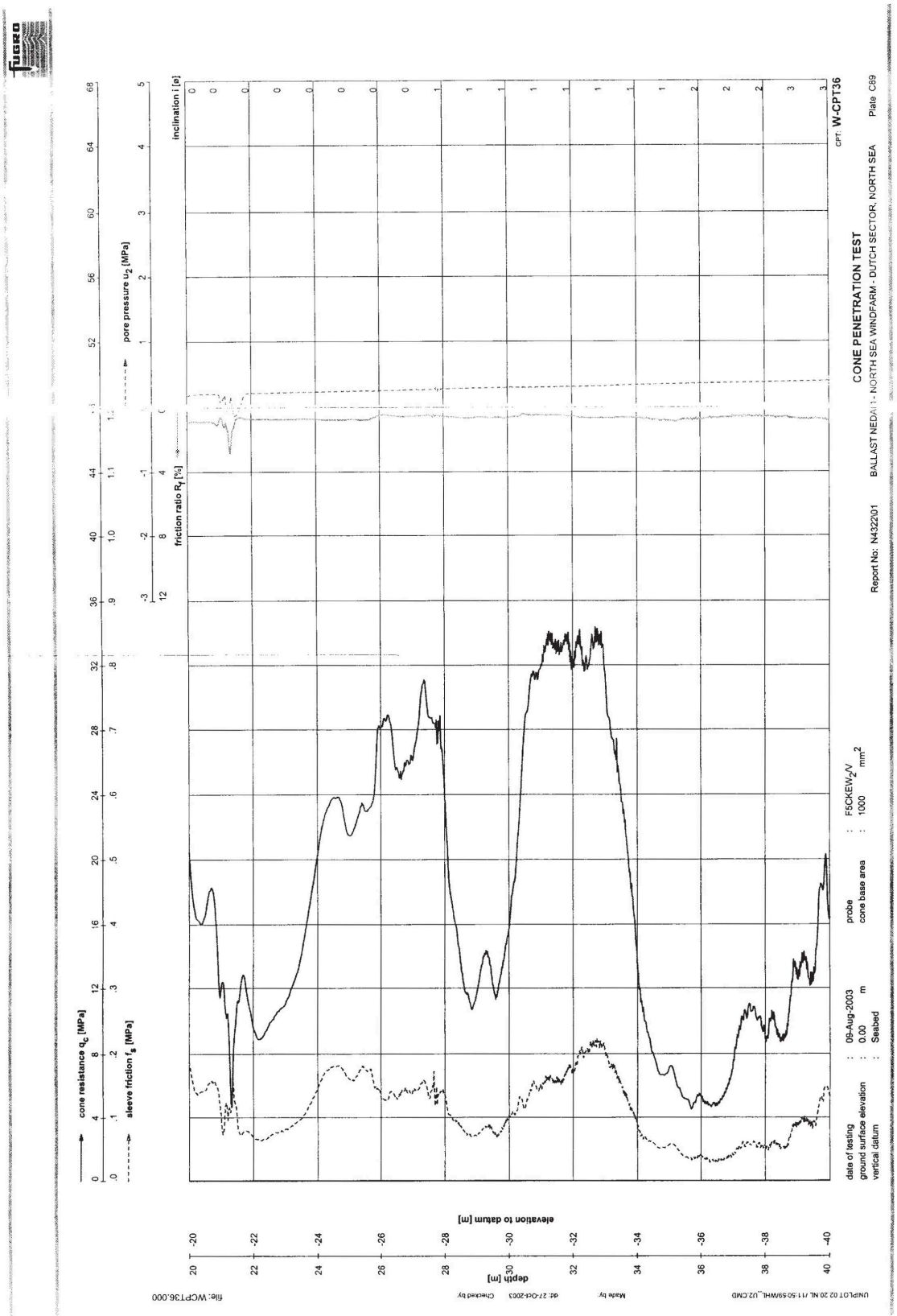
FUGRO
CONE PENETRATION TEST
CPT: W-CPT36
Report No.: N4322/01
BALLAST NEDAM - NORTH SEA WINDFARM - DUTCH SECTOR, NORTH SEA
Plate C69
cone resistance q_c [MPa]
sleeve friction f_s [MPa]
friction ratio R_f [%]
pore pressure u_2 [MPa]
inclination [°]
depth [m]
elevation to datum [m]
date of testing : 09-Aug-2003
ground surface elevation : 0.00 m
vertical datum : Seabed
probe : F5CKEW-2-N
cone base area : 1000 mm²
File: WCPT36.000

Appendix B

Effect of diameter and loading type on p-y method parameters

This Appendix presents several plots in which the diameter D influence is plotted against depth z. In Chapter 2 the parameters depending on the diameter D and depth z, A(z), p_{us}(z) and p_{ud}(z), which form the basis for p-y curves, are presented. Figures B.2 and B.3 show that at a depth greater than 12 m below soil surface there is no difference between static loading and cyclic loading.

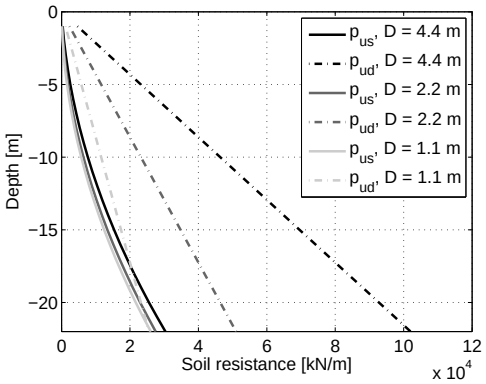

Figure B.1 p_{us} and p_{ud} as function of D plotted against depth (z)

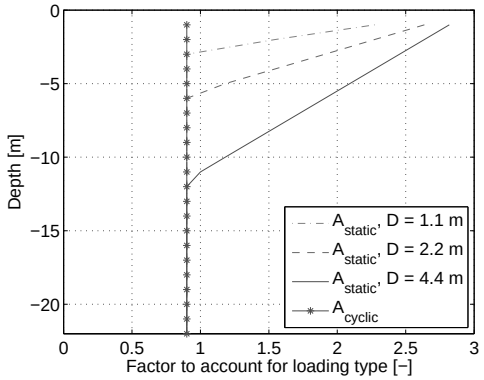

Figure B.2 Factor A to account for loading type plotted against depth (z)

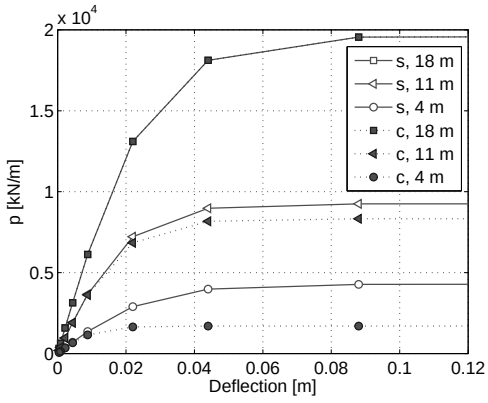

Figure B.3 Differences between static and cyclic p-y curves at different depth (z)

Appendix C

$q_C(z)$ used for MPile calculations

Based on the CPTs as shown in Appendix A an estimated soil profile q_c is created. The $q_{c,1}$, $q_{c,2}$ and $q_{c,3}$ refer to CPTs W-CPT08, W-CPT09 and W-CPT36 respectively. The q_c values is used for MPile calculations for North Sea (OWEZ) conditions. The results of these calculations are the cap plots shown as Figures 3.1b and 3.1a.

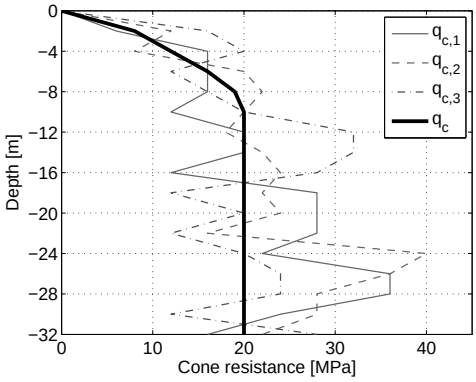

Figure C.1 Estimated CPT values for North Sea sand at the OWEZ wind farm

Appendix D

Results for MPile calculations

This Appendix presents an overview of MPile calculations performed to indicate the lateral p_{ult} of 2.2 m and 4.4 m diameter mono-piles. In Chapter 3 different topics concerning a laterally loaded large diameter mono-pile in sand are covered.

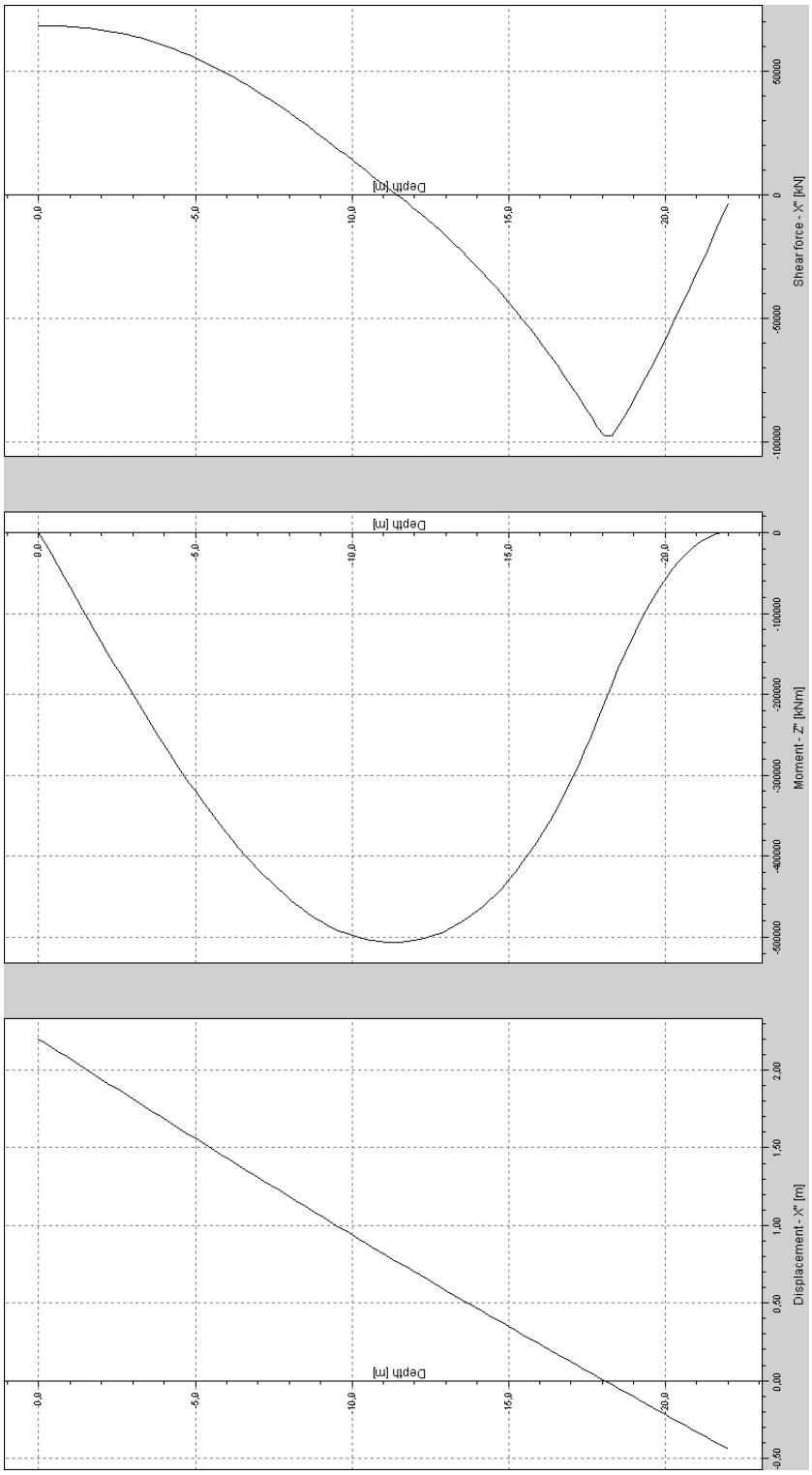

Figure D.1 Ultimate pile deflection, moments and shear forces of laterally loaded 4.4 m monopile with a load excentricity e of 0.0 m

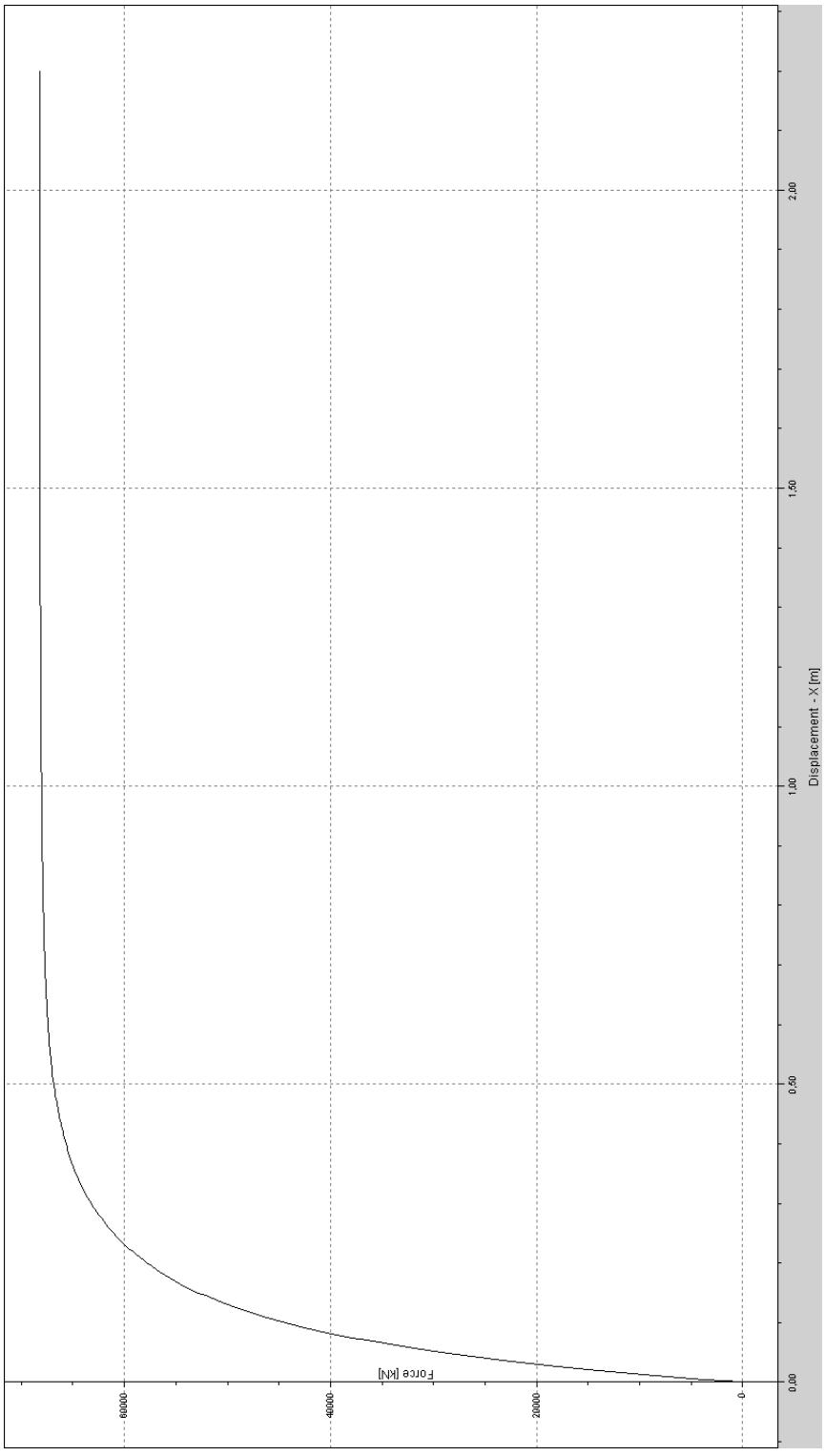

Figure D.2 Ultimate load cap of 4.4 m mono-pile with a load excentricity e of 0.0 m

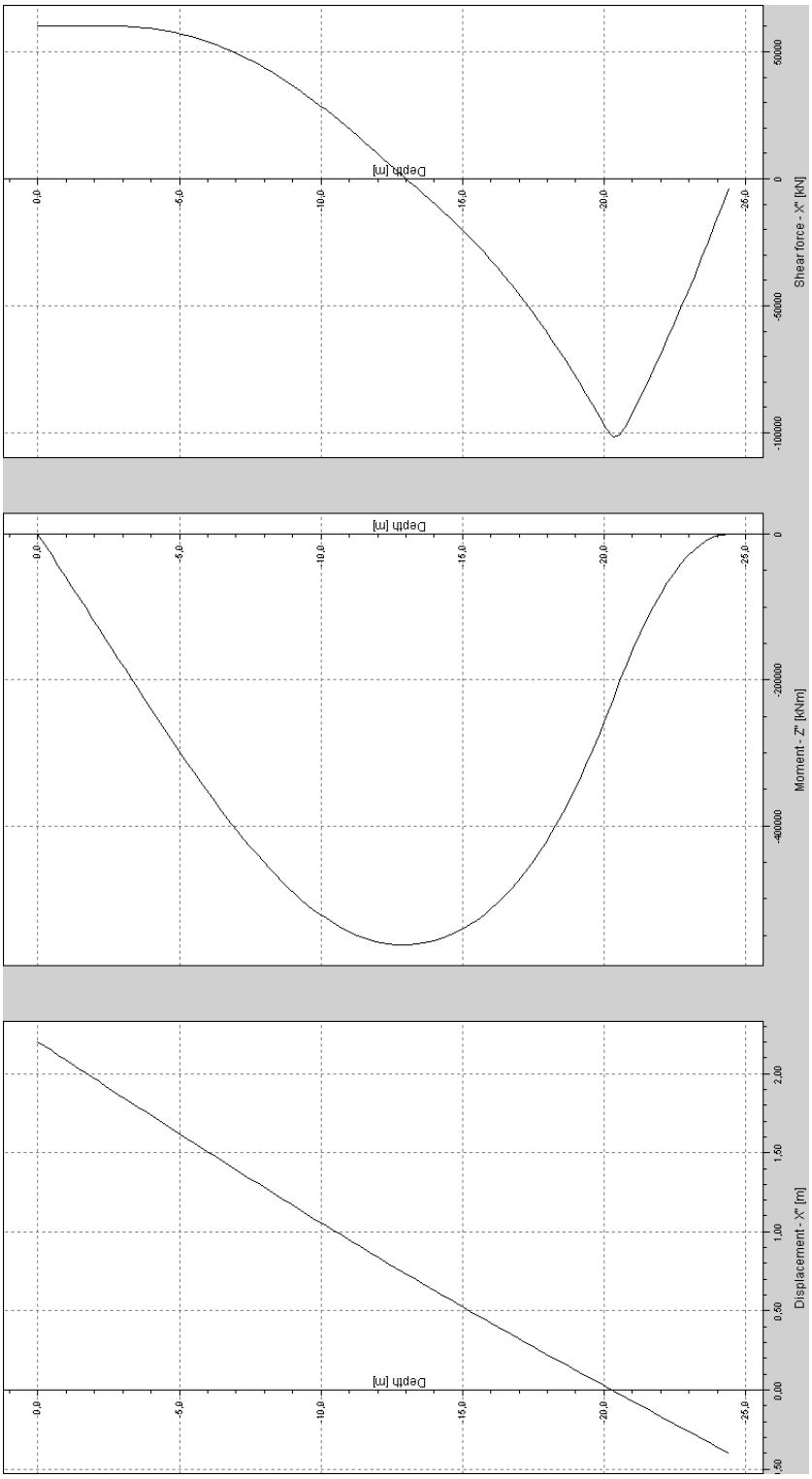

Figure D.3 Ultimate pile deflection, moments and shear forces of laterally loaded 4.4 m monopile with a load excentricity e of 2.4 m

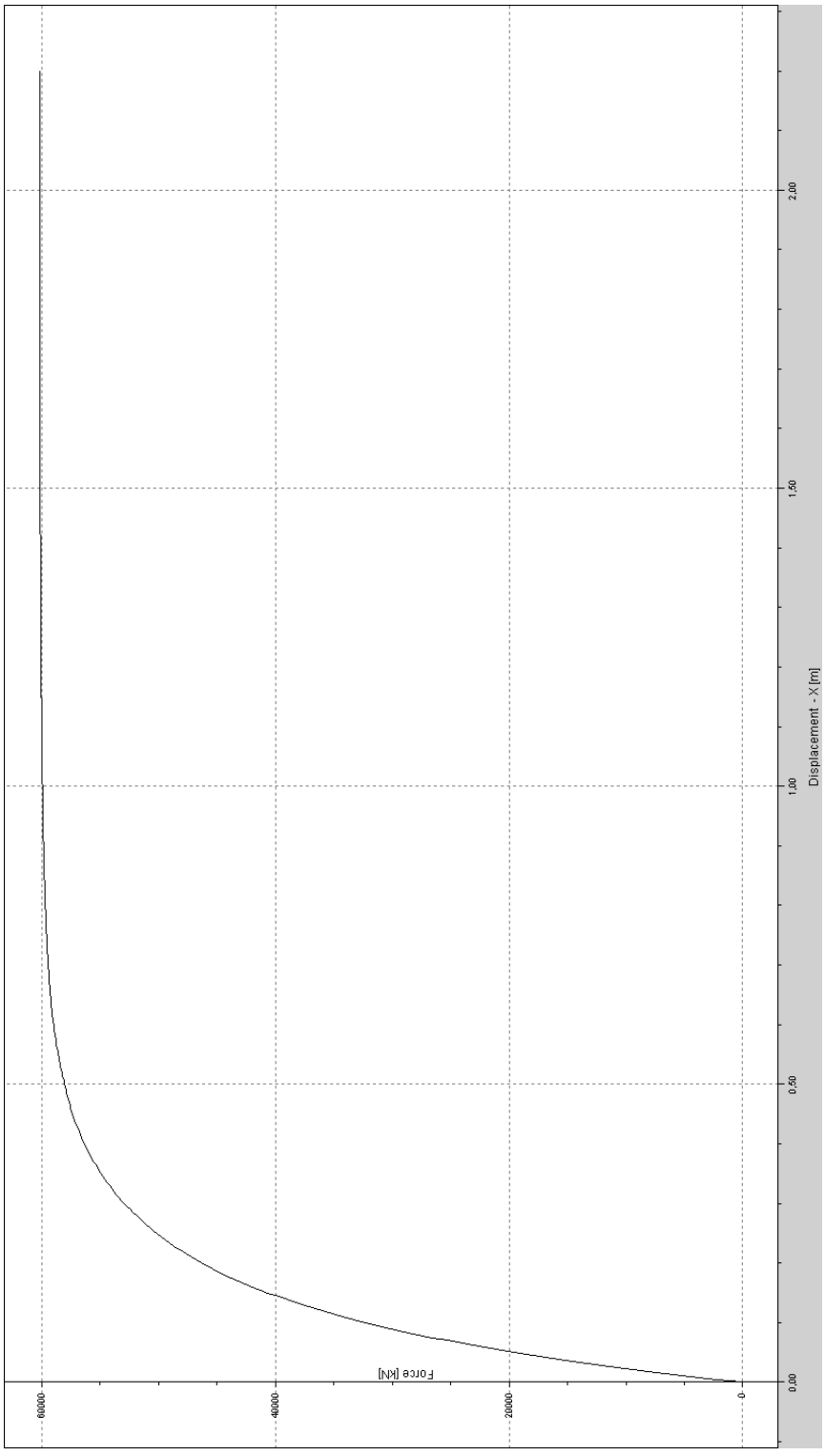

Figure D.4 Ultimate load cap of 4.4 m mono-pile with a load excentricity e of 2.4 m

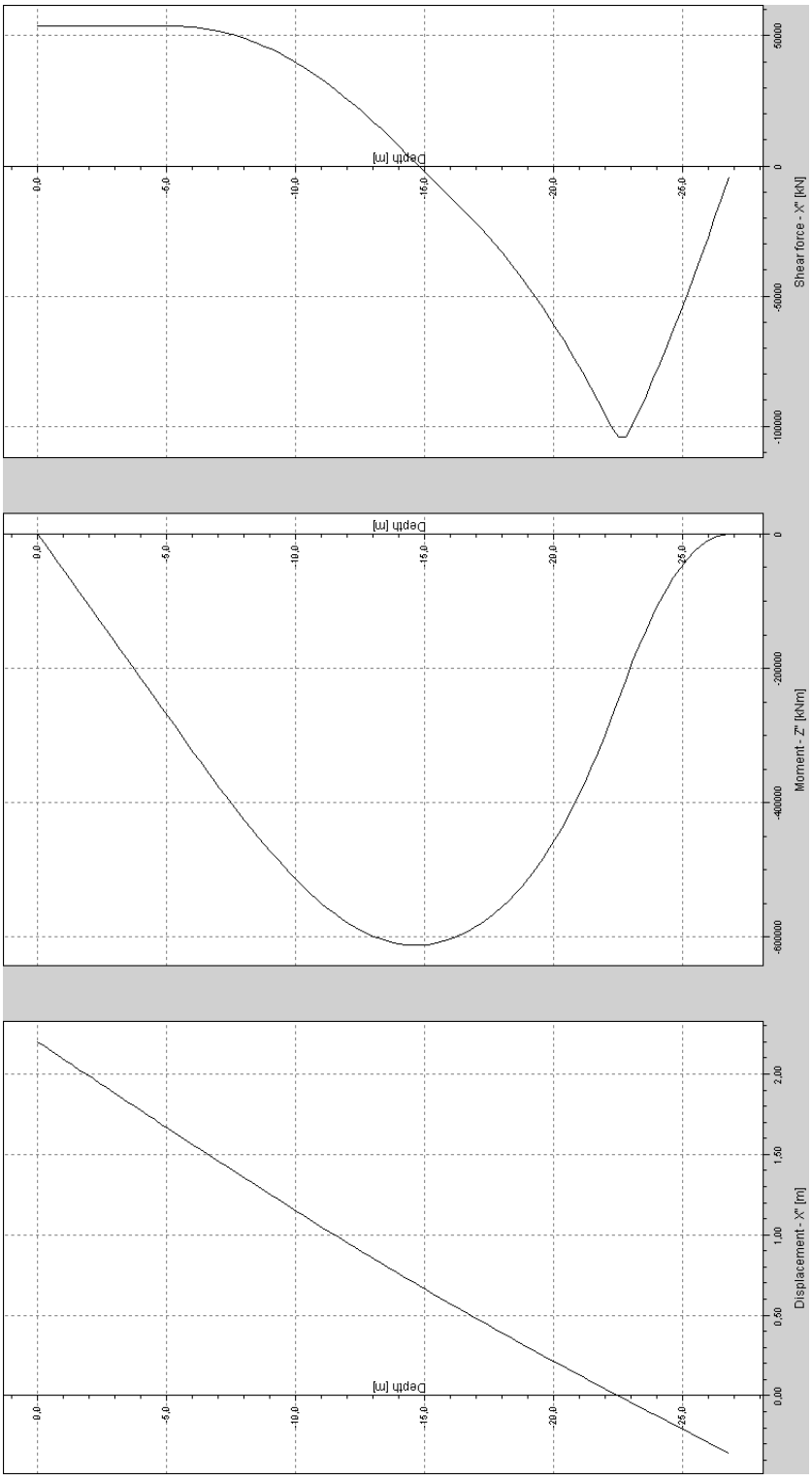

Figure D.5 Ultimate pile deflection, moments and shear forces of laterally loaded 4.4 m monopile with a load excentricity e of 4.8 m

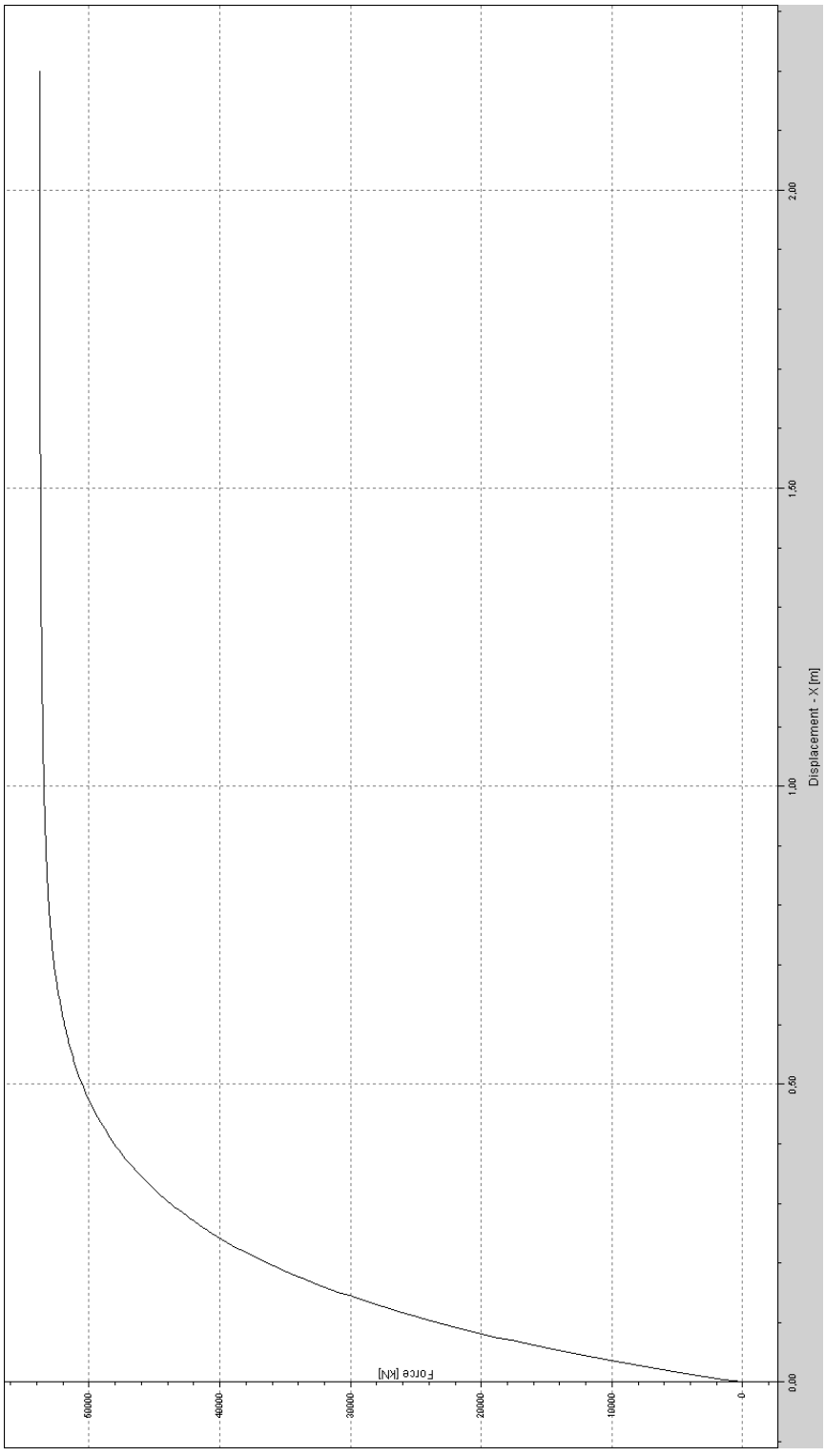

Figure D.6 Ultimate load cap of 4.4 m mono-pile with a load excentricity e of 4.8 m

Appendix E

Model piles

Figure E.1 gives details of the 2 model piles used for the *ng* experiments. In Chapter 3 the testing programme is introduced and Chapter 4 contains the test results.

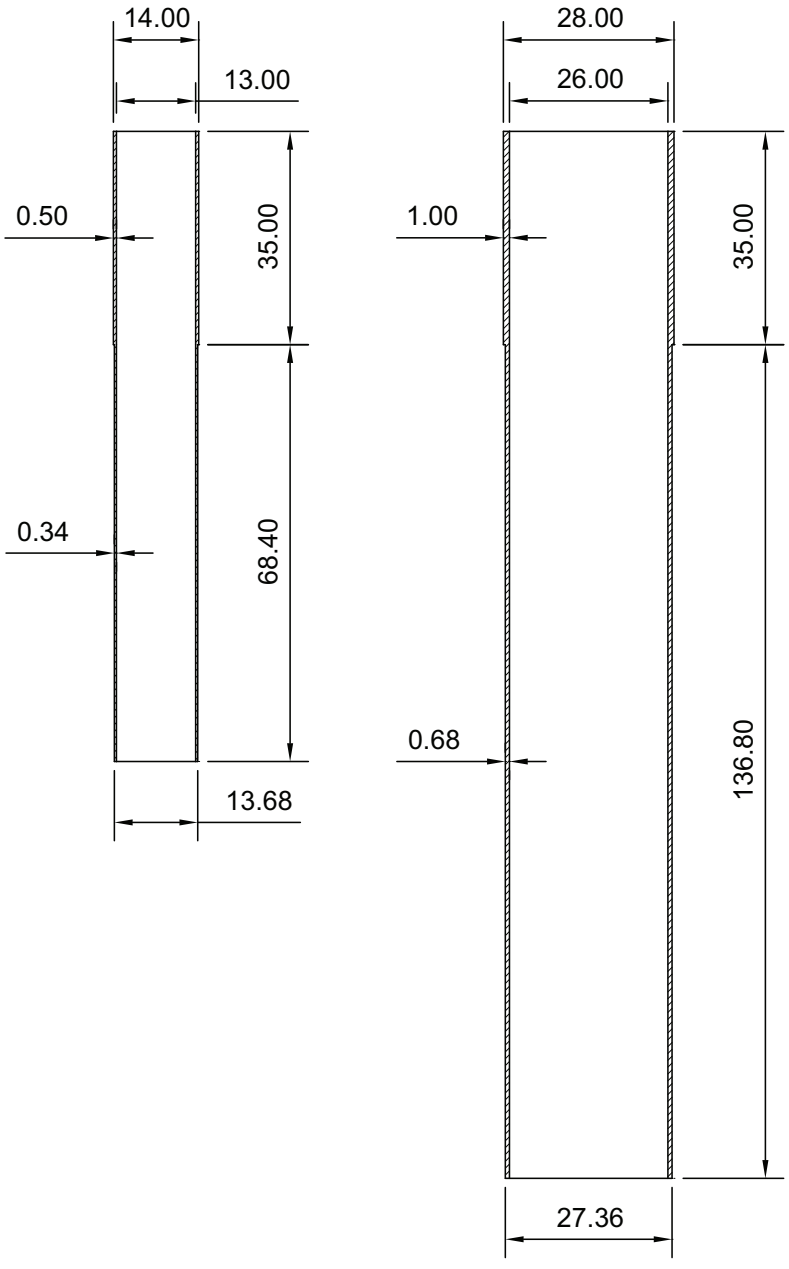

Figure E.1 Cross-section of the two model piles, dimensions in mm

Appendix F

Pycnometer results

The specific density of the sand particles that have been used for centrifuge testing is examined using a *QuantaChrome Ultrapycnometer 1000*. Thereafter, the test series and results are shown in Table F.1. In Chapter 3 additional soil tests are discussed. The average density is determined using the mean of the last 3 measurements for both series and equal to 2.6457 Mg/m^3. The (room) temperature at which the tests were performed was 23.4°C.

Table F.1 Pycnometer test results

	Series 1 [Mg/m^3]	Series 2 [Mg/m^3]	
	2.6479	2.6527	
	2.6471	2.6504	
	2.6471	2.6493	
	2.6468	2.6481	
	2.6461	2.6475	
	2.6464	2.6470	
	2.6457	2.6464	
	2.6453	2.6458	
	2.6458	2.6460	
	2.6456	2.6456	
Standard deviation	0.0002	0.0002	[g/cc]
Coefficient of variation	0.0079	0.0072	[%]

Appendix G

Field data analysis details

This Appendix contains the steps performed analysing the field data using MatLab [88]. Results are presented in Chapter 6.

OWEZ data Two wind turbines of the Offshore Wind farm Egmond aan Zee have been instrumented with accelerometers, anemometers, a thermometer and several devices measuring nacelle and rotor related information. All recorded data is stored in a single file for each 10-minute period.

The aim of this analysis is to derive pile displacements at mud line or seabed level during strong wind or storm conditions. To achieve this, the 64 Hz North-South (NS) and East-West (EW) acceleration data of the tower is used. Since the available data could not be processed at once, each 10-minute periode file is analysed individually first, storing the minimum, maximum and mean of each file in a new vector. This vector has been examined and 20–24 November 2008 is chosen is reference period. The following steps were performed to find the corresponding displacements.

- Open the consecutive 10-minute period files from 20–24 November 2008, extract the acceleration information and store this data in a single vector. Accelerations in NS and EW direction are treated separately.

- A periodic moving window technique with a 50% overlap (see Figure G.1) is applied and the NS and EW signals are filtered using a low pass filter. The window size was 512, i.e. 8 seconds.

  This periodic Hanning technique relies on analysing subsequent parts of the total data file. A 50% overlap is used which results in an amplification factor of 1 for the entire data range except both ends. By choosing a relatively small window size compared to the total vector length (i.e. $22{\cdot}10^6$) the disturbed data is kept to a minimum. 512 data points in this case make up a negligible percentage.

  Although frequencies in excess of 10 Hz are not likely to be expected offshore or from small magnitude, a small peak in the frequency spectrum was found around 23 Hz. Signals >24 Hz are filtered out by a stable low pass filter.

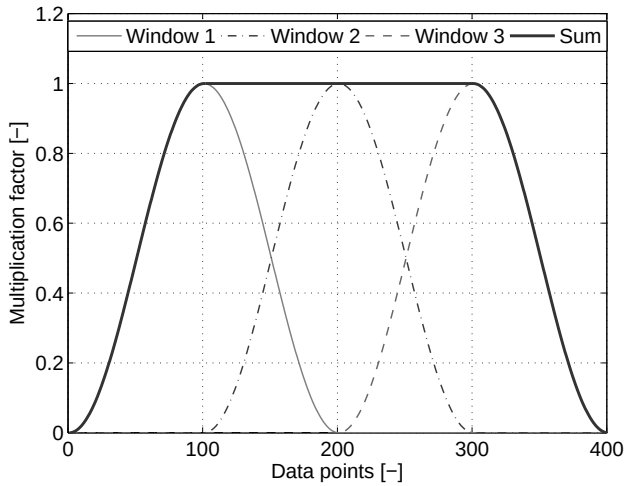

Figure G.1 Principle of splitting and re-assembling data using consecutive 50% overlapping windows

The average of the signal was positive, in the order of 0.08 m/s^2. Although a positive mean of a signal does not make double integration impossible, the obtained displacements would not make sense, i.e. displacements of several dozen metres are deemed impossible by commom sense. Therefore, the mean of the signal was subtracted before integration, which also is a common applied filtering technique.

Having applied a low pass filter and mean subtraction for each 512 long sub signal, the entire signal is re-assembled.

- The re-assembed signal is integrated once to get velocities in m/s and a 5-point smoothing is applied.
- The second integration step is performed and displacements in m are the result.
- A stable high pass filter is applied with a pass frequency of about 0.03 Hz.
- The displacement signal is analysed and the dominant frequencies are determined using a fast fourier transform (FFT).

Appendix H

Triaxial test results

This Appendix contains results of performed triaxial tests including Mohr circles and plots of ε versus the deviatoric stress (σ_1 - σ_3). Tests have been performed with different conditions, although mainly with a cell pressure of 500 kPa. In Chapter 3 the soil properties are discussed. The legends of Figures H.1 and H.2 refer to this Table H.1, which shows test conditions.

In the following table the σ_3' is the effective cell pressure. The porosity and void ratio are represented by n and e respectively. The h and w refer to the sample height and the sample weight. *Rate* indicates the rate at which the deformation is applied. Finally, *Avg.* and *SD* are used to represent the average and standard deviation respectively for several relevant parameters.

Table H.1 Overview of triaxial tests and test conditions

Test	Condition	I_d [%]	B-value [-]	σ_3' [kPa]	n [-]	e [-]	h [mm]	w [g]	Rate [mm/min]
a	dry	60	-	100	0.395	0.652	108.4	344.1	1.0
b	drained	59	0.93	400	0.395	0.654	108.5	334.0	0.5
c	dry	68	-	500	0.386	0.629	110.1	344.1	1.0
d	dry	66	-	500	0.388	0.632	110.4	344.0	1.0
e	dry	67	-	500	0.387	0.631	107.0	334.1	0.5
f	dry	58	-	500	0.396	0.657	108.7	334.1	1.0
g	dry	58	-	500	0.397	0.658	108.8	334.1	0.5
h	dry	65	-	500	0.389	0.637	107.4	334.1	0.75
i	dry	62	-	500	0.392	0.645	107.9	334.0	5.0
j	dry	69	-	500	0.385	0.625	106.6	334.0	5.0
k	dry	78	-	500	0.375	0.601	105.0	334.0	5.0
l	drained	53	0.93	500	0.402	0.671	109.6	333.9	0.5
m	drained	56	0.98	500	0.399	0.663	109.1	334.0	0.2
n	drained	53	0.95	500	0.402	0.672	109.7	334.1	0.4
o	drained	66	0.96	500	0.389	0.636	107.3	344.0	0.5
Avg.		62.5			0.392	0.644	108.3		
SD		6.8			0.007	0.019	1.5		

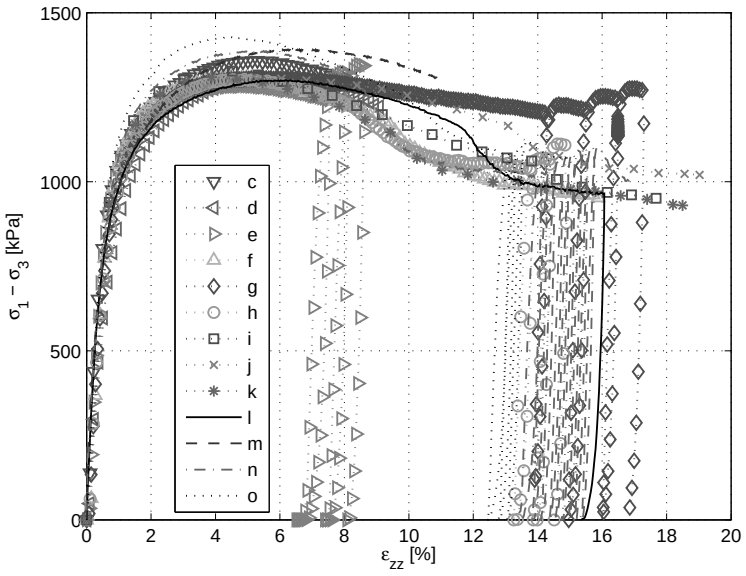

Figure H.1 Stress-strain curve with a cell pressure of 500 kPa

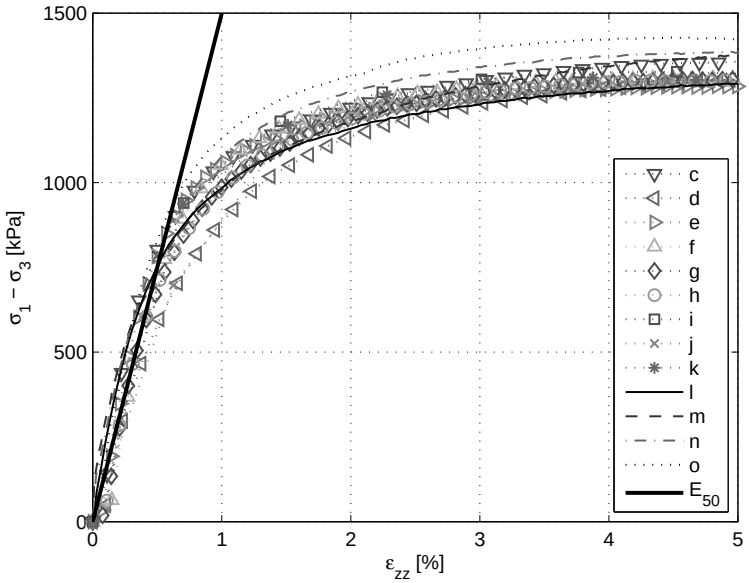

Figure H.2 Stress-strain curve with a cell pressure of 500 kPa, 0–5% strain

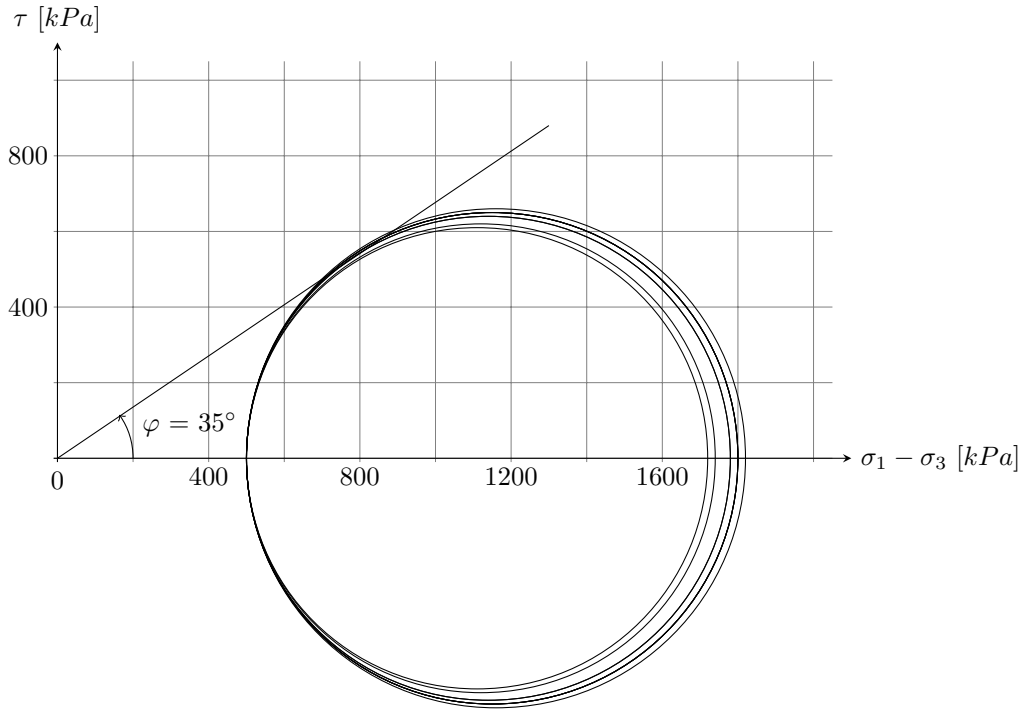

Figure H.3 Mohr circles